COPPE
Instituto Alberto Luiz Coimbra de Pós-Graduação e Pesquisa de Engenharia
UFRJ

PERFORMANCE ANALYSIS OF DETERMINISTIC, MIN-MAX AND MULTI-STAGE NMPC APPLIED TO A SUBSEA GAS COMPRESSION SYSTEM

Otávio Fonseca Ivo

Dissertação de Mestrado apresentada ao Programa de Pós-graduação em Engenharia Química, COPPE, da Universidade Federal do Rio de Janeiro, como parte dos requisitos necessários à obtenção do título de Mestre em Engenharia Química.

Orientadores: Argimiro Resende Secchi
Maurício Bezerra de Souza Jr.

Rio de Janeiro
Outubro de 2018

PERFORMANCE ANALYSIS OF DETERMINISTIC, MIN-MAX AND MULTI-STAGE NMPC APPLIED TO A SUBSEA GAS COMPRESSION SYSTEM

Otávio Fonseca Ivo

DISSERTAÇÃO SUBMETIDA AO CORPO DOCENTE DO INSTITUTO ALBERTO LUIZ COIMBRA DE PÓS-GRADUAÇÃO E PESQUISA DE ENGENHARIA (COPPE) DA UNIVERSIDADE FEDERAL DO RIO DE JANEIRO COMO PARTE DOS REQUISITOS NECESSÁRIOS PARA A OBTENÇÃO DO GRAU DE MESTRE EM CIÊNCIAS EM ENGENHARIA QUÍMICA.

Examinada por:

Prof. Argimiro Resende Secchi, Ph.D.

Prof. Maurício Bezerra de Souza Jr., Ph.D.

Eng. Mario César Mello Massa de Campos, Ph.D.

Prof. Bruno Didier Olivier Capron, Ph.D.

RIO DE JANEIRO, RJ – BRASIL
OUTUBRO DE 2018

Ivo, Otávio Fonseca

Performance Analysis of deterministic, min-max and multi-stage NMPC Applied to a Subsea Gas Compression System/Otávio Fonseca Ivo. – Rio de Janeiro: UFRJ/COPPE, 2018.

XXII, 91 p.: il.; 29, 7cm.

Orientadores: Argimiro Resende Secchi

Maurício Bezerra de Souza Jr.

Dissertação (mestrado) – UFRJ/COPPE/Programa de Engenharia Química, 2018.

Referências Bibliográficas: p. 83 – 91.

1. Multi-stage control. 2. Robust Control. 3. Nonlinear Model Predictive Control. I. Secchi, Argimiro Resende *et al.* II. Universidade Federal do Rio de Janeiro, COPPE, Programa de Engenharia Química. III. Título.

Resumo da Dissertação apresentada à COPPE/UFRJ como parte dos requisitos necessários para a obtenção do grau de Mestre em Ciências (M.Sc.)

ANÁLISE DE PERFORMANCE DE NMPC DETERMINÍSTICO, MIN-MAX E MULTI-ESTÁGIO APLICADO A UM SISTEMA SUBSEA DE COMPRESSÃO DE GÁS

Otávio Fonseca Ivo

Outubro/2018

Orientadores: Argimiro Resende Secchi
Maurício Bezerra de Souza Jr.

Programa: Engenharia Química

Recentemente, tecnologias *subsea* têm se tornado mais confiáveis. Novos projetos foram elaborados e, nos próximos anos, um grande volume de investimentos é esperado na área. No entanto, instalações *subsea* têm se tornado cada vez mais complexas e controladores capazes de tomar decisões de forma inteligente são necessários para redução de custos e aumento da confiabilidade. No entanto, devido à presença de incertezas em operações *subsea*, novos controladores capazes de operar em um ambiente incerto devem ser desenvolvidos. No Mar do Norte, uma tecnologia promissora de compressão *subsea* de gás começou recentemente a operar. No campo de Asgard, o projeto do sistema de compressão foi baseado em instalações *topside*. Devido a isso, estratégias anti-surge são necessárias para que o sistema possa operar sem maiores problemas frente à presença de perturbações e incertezas. Caso a operação entre em surge, o sistema de compressão pode ser afetado ocasionando a quebra do compressor. Devido a isso, foram avaliados o desempenho e a robustez de um sistema de compressão *subsea* quando controlado por um NMPC determinístico, offline min-max e multi-estágio. Indicadores que levam em consideração o desempenho do controle de set-point, violação de restrições, produção de gás, consumo energético e eficiência na produção foram utilizados para avaliação dos controladores. O NMPC determinístico foi a solução mais eficiente, no entanto violações nas restrições foram detectadas. Apesar do controlador min-max conseguir impedir que restrições sejam violadas, ele teve um desempenho conservativo. Já o controlador NMPC multi-estágio também conseguiu lidar com a restrição do processo, apresentando um desempenho menos conservativo que a solução NMPC offline min-max.

Abstract of Dissertation presented to COPPE/UFRJ as a partial fulfillment of the requirements for the degree of Master of Science (M.Sc.)

PERFORMANCE ANALYSIS OF DETERMINISTIC, MIN-MAX AND MULTI-STAGE NMPC APPLIED TO A SUBSEA GAS COMPRESSION SYSTEM

Otávio Fonseca Ivo

October/2018

Advisors: Argimiro Resende Secchi
Maurício Bezerra de Souza Jr.

Department: Chemical Engineering

In recent years, subsea technologies have become more reliable. New projects emerged and an increase of investment in the area is expected in the following years. However, subsea installations are becoming more complex and smart decision making controllers are necessary to reduce operational costs and increase process reliability. Besides, the presence of uncertainties makes the development of controllers that can handle operation in an uncertain environment imperative. A prominent subsea technology is the subsea compression, which has been recently delivered in the North Sea. Åsgard field compression system design was based on topside design. Therefore, surge avoidance strategy is necessary in order to operate without major issues in presence of disturbances and uncertainties. If surge occurs, compression system operation is strongly affected, leading even to compressors breakage. Thus, in this work, Nonlinear Model Predictive Controls (NMPC), such as deterministic, offline min-max and multi-stage were employed to a subsea compression system to evaluate controllers performance and closed-loop robustness in an environment with unknown disturbances affecting upstream pressure. For performance assessment, indicators that consider set-point tracking, constraint violation, gas production, energy consumption, and production efficiency were employed. Deterministic NMPC was the most efficient controller, but constraint violation was detected. Although offline min-max operation managed to handle constraint violation, it proved to be overly conservative. Multi-stage NMPC controller was able to also handle constraint violation, while being less conservative than offline min-max NMPC.

Contents

List of Figures

List of Tables

List of Symbols

A	Duct cross sectional area $[m^2]$, p. 33
$CSPC$	Compression system power consumption index, p. 78
EP	Efficient production index, p. 78
F_γ	Specific heat ratio factor, p. 30
H	Actual head $[J/kg]$, p. 35
H_p	Polytropic head $[J/kg]$, p. 35
I_s	Surge index, p. 21
K_v	Flow coefficient $[kg/s]$, p. 30
L	Duct length $[m]$, p. 33
MFP	Mass flow production index, p. 78
M_w	Fluid molecular weight $[kg/mol]$, p. 30
N	Prediction horizon, p. 5
N_R	Robust horizon, p. 13
N_Δ	Total amount of realizations, p. 9
P	Pressure $[Pa]$, p. 30
P_W	Terminal cost weight matrix, p. 16
Q	Heat removed from the inlet fluid $[W]$, p. 31
Q_W	Stage cost state weight positive semidefinite matrix, p. 6
R	Ideal gas constant $[J/mol.K]$, p. 31
R_W	Stage cost input weight positive semidefinite matrix, p. 6

S_t	Total amount of scenarios, p. 11
T	Temperature $[K]$, p. 30
V	Volume $[m^3]$, p. 31
$V_N(\cdot)$	Finite horizon objective function, p. 7
$V_N^0(\cdot)$	Finite horizon objective function at optimum, p. 7
$V_\infty(\cdot)$	Infinite horizon objective function, p. 6
$V_\infty^0(\cdot)$	Infinite horizon objective function at optimum, p. 6
$V_{N_s}(\cdot)$	Finite horizon objective function of scenario s, p. 42
$V_{\mathcal{S}}(\cdot)$	Multi-stage objective function, p. 13
$V_{\mathcal{S}}^0(\cdot)$	Multi-stage objective function at optimum, p. 13
W	Power $[W]$, p. 35
W_W	Stage cost input weight matrix, p. 41
Y	Expansion factor, p. 30
Z	Compressibility factor, p. 29
$\Delta\tilde{\mathbf{u}}_{k,s}$	Control actions changes at stage k, scenario s, p. 42
$\Delta\tilde{\mathbf{u}}_k$	Control action change vector at stage k, p. 41
Δt	Sampling interval $[s]$, p. 43
Δ	Realization, p. 9
$\Phi_N(\cdot)$	Feedback min-max objective function, p. 10
$\Phi_N^0(\cdot)$	Feedback min-max objective function at optimum, p. 10
$\Psi_c(\cdot)$	Compressor characteristic, p. 33
α_W	Slack variable weight, p. 41
β	Polytropic volume exponent, p. 33
δ_{ssl}	Safe surge line margin, p. 22
$\ell_s(\cdot)$	Stage cost of the s-th scenario, p. 13

$\ell(\cdot)$	Stage cost function, p. 5
η_p	Polytropic efficiency, p. 33
γ	Adiabatic index or specific heat ratio factor, p. 30
$\mathbb{N}$	Natural numbers, p. 6
$\mathbb{E}(P^{so})$	Expected value of the source pressure, p. 39
$\mathbb{N}^+$	Natural positive numbers, p. 5
$\mathbb{R}$	Real numbers, p. 4
$\mathbb{R}_0^+$	Non-negative real numbers, p. 5
$\mathbb{U} \subseteq \mathbb{R}^m$	Control constraint set, p. 4
$\mathbb{W} \subseteq \mathbb{R}^p$	Uncertainty compact set, p. 9
$\mathbb{X} \subseteq \mathbb{R}^n$	State constraint set, p. 4
$\tilde{\mathbf{u}}_{k,s}$	Control action vector at stage k, scenario s, p. 42
$\tilde{\mathbf{w}}_{\Delta(k,s)}$	Uncertainty vector with realization $\Delta(k,s)$, p. 42
$\tilde{\mathbf{x}}^{\mathbf{u}}_{k,c,s}$	Predicted or open-loop trajectory at stage k, collocation c, scenario s, p. 42
$\tilde{\mathbf{z}}^{\mathbf{u}}_{k,c,s}$	Predicted or open-loop algebraic variable at stage k, collocation c, scenario s, p. 42
$\mathbf{f}_c$	Continuous differential equation vector, p. 37
$\mathbf{g}_c$	Continuous algebraic equation vector, p. 37
$\mathbf{u}$	Virtual plant control action vector, p. 37
$\mathbf{u}_0$	Virtual plant initial control action vector, p. 44
$\mathbf{u}_N$	Finite control sequence, p. 7
$\mathbf{u}_\infty$	Infinite control sequence, p. 6
$\mathbf{w}$	Virtual plant uncertainty vector, p. 37
$\mathbf{w}_0$	Virtual plant initial uncertainty vector, p. 44
$\mathbf{x}$	Virtual plant state vector, p. 37

$\mathbf{x}^{\mathbf{u}}_{\Delta}(x_0)$	Predicted or open-loop trajectory associated with realization Δ, p. 9
$\mathbf{x}_0$	virtual plant initial state vector, p. 44
$\mathbf{z}$	Virtual plant algebraic variable vector, p. 37
$\mathbf{F}$	Discretized system, p. 41
$\tilde{\mathbf{u}}$	Discretized control action vector, p. 18
$\tilde{\mathbf{u}}_k$	Control action vector at stage k, p. 41
$\tilde{\mathbf{w}}^{\mathbf{u}}_{\Delta^0}$	Open-loop uncertainty vector associated with the worst realization Δ^0, p. 41
$\tilde{\mathbf{w}}^{\mathbf{u}}_{\mathbb{E}}$	Open-loop uncertainty vector associated with the expected realization, p. 41
$\tilde{\mathbf{x}}$	Discretized states vector, p. 18
$\tilde{\mathbf{x}}^{\mathbf{u}}_{k,c}$	Predicted or open-loop state vector at stage k, collocation c, p. 41
$\tilde{\mathbf{z}}$	Discretized algebraic variable vector, p. 18
$\tilde{\mathbf{z}}^{\mathbf{u}}_{k,c}$	Predicted or open-loop algebraic variable vector at stage k, collocation c, p. 41
$\mathbf{a}$	Slack variable vector, p. 41
$\mathbf{u}$	Control sequence, p. 5
$\mathbf{u}^0_N(x_0)$	Finite horizon optimal control sequence, p. 8
$\mathbf{u}^0_\infty(x_0)$	Infinite optimal control sequence, p. 6
$\mathbf{w}_{S_s}$	Uncertainty trajectory of the scenario s, p. 13
$\mathbf{w}_{\mathcal{W}}$	Uncertainty ensemble, p. 9
$\mathbf{x}^{\mathbf{u}}(x_0)$	Predicted or open-loop trajectory, p. 5
$\mathbf{x}^{\mu_N}(x_0)$	Finite horizon closed-loop trajectory, p. 8
$\mathbf{x}^{\mu_\infty}(x_0)$	Infinite horizon closed-loop trajectory, p. 6
$\mathcal{U}_N$	Set of admissible finite horizon control sequences, p. 7

$\mathcal{U}_\Delta$	Set of admissible traditional min-max control sequences, p. 10
$\mathcal{U}_\Phi$	Set of admissible feedback min-max control sequences, p. 10
$\mathcal{U}_\infty$	Set of admissible infinite horizon control sequences, p. 6
$\mathcal{U}_\mathcal{S}$	Set of admissible multi-stage control sequences, p. 13
$\mathcal{C}$	Collocation points set, p. 18
$\mathcal{K}$	Stage set, p. 18
$\mathcal{S}$	Scenario set, p. 13
$\mathcal{W}$	Realization set, p. 9
N_d	Number of collocation points, p. 18
$\mu_N(x_0)$	Finite horizon feedback law, p. 8
ω_s	Weight associated with each scenario or scenario likelihood, p. 13
ϕ^v	Valve opening percentage, p. 30
$\phi_N^0(\cdot)$	Min-max objective function at optimum, p. 10
ϕ^{rev}	Recycle valve opening percentage, p. 39
$\phi_{k,s}^{rev}$	Valve opening percentage at stage k, scenario s, p. 42
$\phi_N(\cdot)$	Min-max objective function, p. 10
ϕ_k^{rev}	Valve opening percentage at stage k, p. 41
ρ	Density $[m^3/kg]$, p. 33
$\sigma_{P^{so}}$	Standard deviation of the source pressure, p. 39
$\theta(\cdot)$	Heaviside function, p. 54
$a_{k,s}$	Slack variable at stage k, scenario s, p. 42
a_k	Slack variable at stage k, p. 41
c_p	Specific heat capacity at constant pressure $[J/K.kg]$, p. 29
c_v	Specific heat capacity at constant volume $[J/K.kg]$, p. 29
dP	Pressure boost $[bar]$, p. 26

f	Discrete time control system, p. 4
f_Δ	Discrete time control system associated with realization Δ, p. 9
f_c	Continuous time control system or continuous differential equations, p. 4
h	Enthalphy [J/kg], p. 33
m	Mass flow $[kg/s]$, p. 30
q	Volumetric flow rate $[m^3/s]$, p. 21
r	Angular speed or rotation $[Hz]$, p. 33
r_p^{co}	Compressor rotation percentage, p. 36
t	Time $[s]$, p. 4
t_0	Initial condition sampling time $[s]$, p. 5
t_k	Time sample $[s]$, p. 5
t_f	Final time of simulation $[s]$, p. 77
u	Control action vector, p. 4
u_0^0	First optimal control action, p. 8
$u_{\infty,k}^0(x_0)$	Optimal infinite horizon control action vector at stage k, p. 6
u_k^j	Control action vector at stage k, position j, p. 12
u_*	Control action at equilibrium or set-point, p. 6
$u_{\Delta,k}$	Control action vector at stage k associated with realization Δ, p. 10
$u_{k,s}$	Control action vector at stage k, scenario s, p. 13
u_k	Control action vector at stage k, p. 5
w	Uncertainty vector, p. 9
$w_k^{\Delta(j)}$	Uncertainty vector associated with realization $\Delta(j)$ at stage k, p. 12

$w^{\mathbf{u}}_{\Delta,k}$ Open-loop uncertainty vector at stage k associated with realization Δ, p. 10

$w^{\mathbf{u}}_{\Delta(k,s)}$ Open-loop uncertainty vector associated with realization $\Delta(k,s)$, p. 13

w_{Δ} Uncertainty vector associated with realization Δ, p. 9

x System state vector, p. 4

$x(t_k)$ Current estimated system state vector, p. 8

$x(t_{k+1})$ Newly estimated system state vector, p. 8

x^+ System state vector at next time instant, p. 4

$x^{\mathbf{u},j}_{k+1}(x_0)$ Predicted or open-loop state vector at stage $k+1$, position j, p. 12

$x^{\mathbf{u},p(j)}_{k}(x_0)$ Predicted or open-loop state vector that parents $x^{\mathbf{u},j}_{k+1}(x_0)$, p. 12

$x^{\mathbf{u}}_{\Delta,k}(x_0)$ Predicted or open-loop system state vector at stage k associated with realization Δ, p. 10

$x^{\mathbf{u}}_{k,s}(x_0)$ Predicted or open-loop system state vector at stage k, scenario s, p. 13

$x^{\mathbf{u}}_{k}(x_0)$ Predicted or open-loop system state vector at stage k, p. 5

$x^{\mu_N}_{k}(x_0)$ Finite horizon closed-loop trajectory at stage k, p. 8

$x^{\mu_\infty}_{k}(x_0)$ Infinite horizon closed-loop state vector at stage k, p. 6

x_* State at equilibrium or set-point, p. 6

x_0 Initial condition of a trajectory, p. 5

x_T Pressure diferential ratio factor, p. 30

IE_s Integral of the surge index error, p. 77

ISE_p Integral square of the scrubber pressure error, p. 77

List of Abbreviations

CVP	Control Vector Parameterization, p. 18
DAEs	Differential-Algebraic Equations, p. 18
FPSO	Floating Production Storage and Offloading, p. 25
LMF	Liquid Mass Fraction, p. 27
LVF	Liquid Volume Fraction, p. 24
MPC	Model Predictive Control, p. 2
NLP	Nonlinear Programming, p. 2
NMPC	Nonlinear Model Predictive Control, p. 2
OCP_N	Finite Horizon Optimal Control Problem, p. 7
OCP_Δ	Traditional Min-Max Optimal Control Problem, p. 10
OCP_Φ	Feedback Min-max Optimal Control Problem, p. 10
OCP_∞	Infinite Horizon Optimal Control Problem, p. 6
$\text{OCP}_\mathcal{S}$	Multi-stage Optimal Control Problem, p. 13
QP	Quadratic Programming, p. 2
ROV	Remoted Operated Vehicles, p. 28
SI	International System of Units, p. 29
VSD	Variable Speed Driver, p. 29

List of Subscripts and Superscripts

co	Compressor identification, p. 33
d	Discharge identification, p. 33
hx	Cooler identification, p. 31
in	Inlet identification, p. 30
lb	Lower bound, p. 41
lb	Upper bound, p. 41
mix	Mixer identification, p. 30
out	Outlet identification, p. 30
p	Plenum identification, p. 33
rev	Recycle valve identification, p. 33
sc	Scrubber identification, p. 31
siv	Sink valve identification, p. 33
sl	Surge line identification, p. 21
ssl	Safe surge line identification, p. 21
v	Valve identification, p. 30

Chapter 1

Introduction

In modern process industries, control and process optimization are key factors for improving plant performance while meeting productivity, quality, safety and environmental objectives. A particular challenging subject is subsea operation as new fields are being developed in deep and ultra-deep waters at remote locations with extreme meteorological and oceanographic (metocean) conditions.

Subsea technologies are becoming increasingly accepted as a solution to accelerate reserves, maximize production and reduce costs. This is indicated by an increase in the number of subsea processing projects that have been recently considered during project development. It is estimated that oil industry will expend more than 5 billion dollars in subsea related projects for the next decade (KONDAPI *et al.*, 2017).

According to WU *et al.* (2016), several advantages can be obtained from subsea processing, such as:

(i) Accelerated production during field lifespan;

(ii) Production enabler in previously uneconomical fields;

(iii) Hydrocarbon processing enabler from fields with extreme conditions;

(iv) Flow backpressure reduction;

(v) Flow assurance increase.

To deliver all these advantages, subsea installations are becoming more complex with one to several separation modules, pumping and/or boosting systems. Also, harsh deepwater environment makes it harder to access and stabilize subsea systems for repair, increasing intervention duration and, consequently, its cost (FANAILOO & ANDREASSEN, 2008). Therefore, it is necessary to increase extensively the usage of advanced control, capable of smart decision making and monitoring solutions.

The decision making procedure distinguishes MPC methods from conventional control strategies. In MPC, an open-loop optimal control problem is solved *on-line* for the current process state. As a result, an optimal control sequence is obtained and the first control action is implemented in the plant. This formulation brings flexibility as it enables explicit process and operational constraints handling (CAMACHO & BORDONS, 2007), which can play a major role for achieving autonomous operation in subsea environment. In conventional control strategies, a control law is computed *offline*, which can be difficult or even impossible to obtain for some systems (MAYNE & RAWLINGS, 2000).

In process industry, notably in downstream industries (e.g. refining and petrochemical), MPC technology quickly became popular (QIN & BADGWELL, 1997). There were several potential reasons for this. The development of identification technology allowed linear empirical models to be obtained from process test data, which, if carefully identified, can be sufficiently accurate in the neighbourhood of a single operating point. MPC techniques using linear models are considered to be well-established for processes with slow dynamics. Previously, it was believed that MPC could not handle more complex systems, such as nonlinear, hybrid, or very fast processes. However, some advancements were made in those fields (BEMPORAD, 2006).

The term Nonlinear Model Predictive Control (NMPC) is applied to predictive controllers that use nonlinear dynamic models and/or nonlinear constraints. The usage of NMPC is justified in those areas where nonlinearities are relevant and market demands require frequent changes in operation regime. Although the number of NMPC applications is still limited (QIN & BADGWELL, 2000), it has a great potential (BINDLISH, 2015; PLUYMERS *et al.*, 2008). By changing the linear model to a nonlinear model, the optimal control problem changes from a convex Quadratic Programming (QP) to a non-convex Nonlinear Programming (NLP) .

In a subsea facility, control methods need to deal with uncertainties that may arise from (KRISHNAMOORTHY *et al.*, 2016):

(i) Structural uncertainty, due to a lack of knowledge or model simplification.

(ii) Parametric uncertainty, due to parameter estimation with old or incomplete data.

(iii) Measurement uncertainty, due measurement noise, badly calibrated systems or state estimators.

(iv) Disturbance uncertainty, due to unaccounted disturbances that may occur, such as slugs.

Deterministic NMPC can be robustly stable for processes that suffer from small additive disturbances when certain restrict conditions are met (MARRUEDO *et al.*, 2002). However, in the presence of uncertainty, stability is not guaranteed. Moreover, process constraints might be violated with severe operational consequences. Therefore, an NMPC framework which deals with uncertainty must be taken in consideration.

Robust NMPC is concerned with control of uncertain systems associated with hard constraints. Its main objective is to obtain a robust solution which guarantees that hard constraints are satisfied for all uncertainty realizations (BEN-TAL & NEMIROVSKI, 1999). Most robust approaches are based on min-max schemes, which have performance issues as optimal solutions may differ substantially from the actual system optimal value. One prominent approach, known as multi-stage, has been recently developed and may improve robust NMPC performance since multi-objective optimization is used to take into account several scenarios while attaining hard constraint satisfaction (LUCIA *et al.*, 2013).

Subsea gas compression technology has gained great attention in recent years from oil and gas industries. In Åsgard, two subsea dry compression trains were installed with anti-surge control system. Surge must be avoided at all cost since it can cause damage to compressors. In the present work, deterministic, min-max and multi-stage NMPC were implemented in a dry gas compression station. The main objective is to evaluate each controller performance when uncertainty is present. The main objective is to unravel decision making procedure of these controllers, while performance evaluation is performed.

This work is structured in the following way: theory and literature review are covered in Chapter 2. The main topics approached encompass the development of deterministic NMPC and robust NMPC, with feasibility, stability and performance discussion. Also, some strategies for centrifugal compressor control are shown. As for Chapter 3, subsea gas compression is discussed with a focus in single phase compression. Moreover, it can be found the models that were used to simulate the virtual plant. In the Chapter 4, the proposed problem is described, with its initial conditions, and controllers formulation and tuning. Results of the virtual plant open-loop simulations, controllers predicted trajectories and closed-loop performance are discussed. Finally, in Chapters 5 the conclusions for this work are summarized, with future research being suggested in Chapter 6.

Chapter 2

Theory and Literature Review

In this chapter, a broad review about the topics explored in the present work and the state-of-art of nonlinear model predictive control are presented. This discussion mainly focuses on presenting controllers' deterministic and robust formulations; control feasibility and stability; and numerical implementation of the optimal control problem.

2.1 Deterministic Nonlinear Model Predictive Control

In this section, several NMPC formulations for a deterministic problem are presented. This case is relatively simple as it arises from the fact that dynamic states are known. Also, no unknown disturbances and model errors are considered, which implies a lack of uncertainty that, in principle, makes feedback unnecessary. Consider the following class of nonlinear systems, which are described by ordinary differential equations such as Equation 2.1.

$$\dot{x}(t) = f_c(x(t), u(t)) \tag{2.1}$$

where $f_c : \mathbb{R}^n \times \mathbb{R}^m \to \mathbb{R}^n$ is the continuous time control system; $x \in \mathbb{X}$ is the system state vector; and $u \in \mathbb{U}$ is the control action vector. Both $\mathbb{X}$ and $\mathbb{U}$ are defined below.

Definition 2.1.1 (State and control constraint sets) *The state set $\mathbb{X}$ is a closed subset of $\mathbb{R}^n$ and the control set $\mathbb{U}$ is a compact subset of $\mathbb{R}^m$.*

The continuous system in Equation 2.1 can be rewritten as an analogous discrete system, which follows in Equation 2.2.

$$x^+ = f(x, u) \tag{2.2}$$

where $f : \mathbb{R}^n \times \mathbb{R}^m \to \mathbb{R}^n$ is the discrete time control system; $x^+ \in \mathbb{X}$ is the system state vector at next time instant. To predict the discrete system behaviour, Equation 2.2 must be iterated. Therefore, given an initial condition $x_0 \in \mathbb{X}$ obtained at sampling time t_0 and any control sequence $\mathbf{u} := \{u_k \mid k \in [0, 1, ..., N-1]\}$, one can calculate the open-loop prediction trajectory, which is given by Equation 2.3.

$$x_0^{\mathbf{u}}(x_0) = x_0, \quad x_{k+1}^{\mathbf{u}}(x_0) = f(x_k^{\mathbf{u}}(x_0), u_k), \quad \forall k \in [0, 1, ..., N-1] \tag{2.3}$$

where $\mathbf{x}^{\mathbf{u}}(x_0) := \{x_k^{\mathbf{u}}(x_0) \mid k \in [0, 1, ..., N-1]\}$ is the predicted or open-loop trajectory; $x_0 \in \mathbb{X}$ is the initial condition of a trajectory; $x_k^{\mathbf{u}}(x_0) \in \mathbb{X}$ is the predicted or open-loop system state vector at stage k; $u_k \in \mathbb{U}$ is the control action vector at stage k; and $N \in \mathbb{N}^+$ is the prediction horizon. With a proper model to predict the system's behaviour, an NMPC algorithm must be formulated to accomplish several tasks. QIN & BADGWELL (1997) enumerated these objectives in order of importance:

1. prevent violation of output and input constraints.

2. drive the controlled variables to their reference values.

3. drive the manipulated variables to their reference values using the remaining degree of freedom.

4. prevent excessive movement of manipulated variables.

5. when signals and actuators fail, control as much of the plant as possible.

For a deterministic open-loop optimal control problem, the first objective can be achieved by introducing state and control constraints sets in the optimal control problem. The idea behind introducing these sets is to maintain the trajectories inside the set $\mathbb{X}$ and the corresponding control action vector to lie inside the set $\mathbb{U}$. However, since the system is continuous and is being predicted as a discrete system, state constraints $\mathbb{X}$ can be mildly violated during inter-sampling times, $t \neq t_k$. This should be taken into account while designing the controller.

The stage cost function is usually crafted to accomplish the second, third and fourth objectives. In general, it penalizes deviations between open-loop states and control actions regarding their respective reference values, as well as large changes in control actions. Considering this, the stage cost function is chosen to be of the form $\ell : \mathbb{R}^n \times \mathbb{R}^m \to \mathbb{R}_0^+$. A stage cost function commonly used in NMPC literature is shown in Equation 2.4. According to GRÜNE & PANNEK (2011) large changes in control actions are not penalized as they are more common in linear MPC literature. However, for industrial application, control actions should be penalized as major

changes are undesirable.

$$\ell(x_k^{\mathbf{u}}, u_k) = \|x_k^{\mathbf{u}}\|_{x_*}{}^T Q_W \|x_k^{\mathbf{u}}\|_{x_*} + \|u_k\|_{u_*}{}^T R_W \|u_k\|_{u_*} \tag{2.4}$$

where x_* is the state at equilibrium or set-point; u_* is the control action at equilibrium; Q_W is the stage cost state weight positive semidefinite matrix; and R_W is the stage cost input weight positive semidefinite matrix. The notation $\|\cdot\|$ is defined in Equation 2.5.

$$\|x\|_{x_*} := x - x_* \tag{2.5}$$

Given the stage cost in Equation 2.4 and the discrete open-loop model in Equation 2.3, the first nominal NMPC formulation is introduced. KEERTHI & GILBERT (1988) proposed an infinite horizon optimal control problem (OCP_∞) and proved the closed-loop stability of the discrete non-linear system. The OCP_∞ formulation is posed in Equation 2.6.

$$\begin{aligned} V_\infty^0(x_0) = \min_{\mathbf{u}_\infty} \quad & \{V_\infty(x_0, \mathbf{u}_\infty) := \sum_{k=0}^{\infty} \ell(x_k^{\mathbf{u}}(x_0), u_k) | \mathbf{u}_\infty \in \mathcal{U}_\infty\} \\ \text{s.t.} \quad & x_{k+1}^{\mathbf{u}}(x_0) = f(x_k^{\mathbf{u}}(x_0), u_k) \\ & x_0^{\mathbf{u}}(x_0) = x_0 \\ & u_k \in \mathbb{U}, \quad x_k^{\mathbf{u}} \in \mathbb{X} \end{aligned} \tag{2.6}$$

where $V_\infty^0(\cdot) : \mathbb{R}^n \to \mathbb{R}_0^+$ is the infinite horizon objective function at optimum; $V_\infty(\cdot) : \mathbb{R}^n \times \mathbb{R}^m \to \mathbb{R}_0^+$ is the infinite horizon objective function; $\mathbf{u}_\infty$ is the infinite control sequence; and $\mathcal{U}_\infty$ is the set of admissible infinite horizon control sequences. Both variables are defined in Equations 2.7 and 2.8.

$$\mathbf{u}_\infty := \{u_k \mid k \in \mathbb{N}\} \tag{2.7}$$

$$\mathcal{U}_\infty := \{u_k \in \mathbb{U}, k \in \mathbb{N} \,|\, x_k^{\mathbf{u}}(x_0) \in \mathbb{X}\} \tag{2.8}$$

When the OCP_∞ is solved, one obtains an optimal value function of the form $V_\infty^0(x_0)$ and an infinite optimal control sequence of the form present at Equation 2.9.

$$\mathbf{u}_\infty^0(x_0) := \left\{u_k^0(x_0) \mid k \in \mathbb{N}\right\} \tag{2.9}$$

where $\mathbf{u}_\infty^0(x_0)$ is the infinite optimal control sequence; and $u_k^0(x_0)$ is the optimal control action at stage k.

The closed-loop system under the infinite optimal control sequence is given in Equation 2.10.

$$x_{k+1}^{\mu_\infty}(x_0) = f(x_k^{\mu_\infty}(x_0), u_k^0(x_0)) \tag{2.10}$$

where $\mathbf{x}^{\mu_\infty}(x_0) := \{x_k^{\mu_\infty}(x_0) \mid k \in [0, 1, ..., N-1]\}$ is the infinite horizon closed-loop trajectory; $x_k^{\mu_\infty}(x_0)$ is the infinite horizon closed-loop state vector at stage k; and $u_{\infty,k}^0(x_0) \in \mathbb{U}$ is the optimal infinite horizon control action vector at stage k.

It is important to distinguish between open-loop $\mathbf{x}^{\mathbf{u}}(x_0)$ and infinite horizon closed-loop $\mathbf{x}^{\mu_\infty}(x_0)$ trajectories. For the deterministic OCP_∞, both predicted and actual states are exactly the same leading to an optimal control law with excellent closed-loop properties. However, several impediments arise from the usage of this approach as feedback is usually necessary due to uncertainty, rather than open-loop control. The idea of an optimal feedback control, namely a receding horizon approach, can be found on LEE & MARKUS (1968).

> "One technique for obtaining a feedback controller synthesis is to measure the current control process state and then compute very rapidly the open-loop control function. The first portion of this function is then used during a short time interval after which a new measurement of the process state is made and a new open-loop control function is computed for this new measurement. The procedure is then repeated."

In this observation, an "open-loop control function" must be computed quickly, which is not possible for the OCP_∞. The semi-infinite time interval present in Equation 2.6 poses numerical challenges. Therefore, for an on-line implementation, OCP_∞ may be replaced by a similar problem that shares important structural aspects while being easier to solve (RAWLINGS & MAYNE, 2015). The modified optimal open-loop infinite horizon problem OCP_∞ can be posed as a time invariant open-loop fixed horizon optimal control problem (OCP_N) shown in Equation 2.11.

$$\begin{aligned} V_N^0(x_0) = \min_{\mathbf{u}_N} \quad & \{V_N(x_0, \mathbf{u}_N) = \sum_{k=0}^{N-1} \ell\left(x_k^{\mathbf{u}}(x_0), u_k\right) \mid \mathbf{u}_N \in \mathcal{U}_N\} \\ \text{s.t.} \quad & x_{k+1}^{\mathbf{u}}(x_0) = f(x_k^{\mathbf{u}}(x_0), u_k) \\ & x_0^{\mathbf{u}}(x_0) = x_0 \\ & u_k \in \mathbb{U}, \quad x_k^{\mathbf{u}} \in \mathbb{X} \end{aligned} \tag{2.11}$$

where $V_N^0(\cdot) : \mathbb{R}^n \to \mathbb{R}_0^+$ is the finite horizon objective function at optimum; $V_N(\cdot) : \mathbb{R}^n \times \mathbb{R}^m \to \mathbb{R}_0^+$ is the finite horizon objective function; $\mathbf{u}_N$ is the finite control sequence; and $\mathcal{U}_N$ is the set of admissible finite horizon control sequences. Both variables are defined in Equations 2.12 and 2.13.

$$\mathbf{u}_N := \{u_k \mid k \in [0, 1, ..., N-1]\} \tag{2.12}$$

$$\mathcal{U}_N := \{u_k \in \mathbb{U}, k \in [0, 1, ..., N-1] \mid x_k^{\mathbf{u}}(x_0) \in \mathbb{X}\} \tag{2.13}$$

It is relatively easy to obtain a solution for OCP_N. Therefore, the receding horizon strategy employing OCP_N is described: during each sampling time, t_k, the current estimated system state vector $x(t_k)$ is given as initial condition of a trajectory x_0 for OCP_N. This yields a solution in the form of a finite horizon optimal control sequence $\mathbf{u}_N^0(x_0) = \{u_k^0(x_0) \mid k \in [0, 1, ..., N-1]\}$. Despite having an optimal control sequence, only the first element of the finite horizon optimal control action u_0^0 is implemented in the system. For the next sample, the optimal control problem is solved again with a newly estimated system state vector $x(t_{k+1})$, leading to an optimal control sequence $\mathbf{u}_N^0(x_0) = \{u_k^0(x_0) \mid k \in [0, 1, ..., N-1]\}$. Again, the first element of the finite horizon optimal control action u_0^0 is implemented in the plant. This procedure is repeated at each sampling time as long as the process is operating.

Receding horizon is of great importance, since it yields a feedback notion based on current states (MAYNE & MICHALSKA, 1990). This is advantageous, as feedback can compensate for disturbances, modelling errors, and other forms of uncertainty. Therefore, by applying only the first element of the optimal control sequence to the system, there is an implicit NMPC feedback law which is shown Equation 2.14.

$$u_0^0(x_0) = \mu_N(x_0) \tag{2.14}$$

where $\mu_N : \mathbb{R}^n \to \mathbb{R}^m$ is the finite horizon feedback law. Usage of the finite horizon feedback law to the system results in the finite horizon closed-loop system as given in Equation 2.15.

$$x_{k+1}^{\mu_N}(x_0) = f(x_k^{\mu_N}(x_0), u_0^0(x_0)) \tag{2.15}$$

where $\mathbf{x}^{\mu_N}(x_0) := \{x_k^{\mu_N}(x_0) \mid k \in [0, 1, ..., N-1]\}$ is the finite horizon closed-loop trajectory; and $x_k^{\mu_N}(x_0)$ is the finite horizon closed-loop state vector at stage k.

For the OPC_N, the predicted states may differ considerably from the actual states, even for nominal problems due to the usage of a finite horizon. Depending on parameters design such as the prediction horizon N, and the weight matrices Q_W and R_W, the closed-loop trajectory may be unstable (JOHANSEN, 2011). It is important to highlight that implementation of the NMPC feedback law from Equation 2.14 does not necessary lead to recursive feasibility and system stability (MAYNE, 2014).

2.2 Robust Non-linear Model Predictive Control

The deterministic NMPC formulations presented in this work are based in a few assumptions. First, the controlled system is perfectly modeled. Second, all disturbances that might affect the system are known. This is clearly unrealistic in practical applications as the control law obtained from a deterministic approach ig-

nores the effect of possible future changes in disturbance and model mismatch, which can lead to a poor closed-loop performance as well as possible constraint violation (RAWLINGS *et al.*, 1994).

The idea of a robust NMPC is to calculate a solution which is feasible for every uncertainty realization. Therefore, the optimal control problem is altered to take uncertainty directly into account. Usually, these formulations are based on a min-max approach (ALLGÖWER *et al.*, 2004), where the maximized objective function over all uncertainty is minimized.

Consider a non-linear discrete time system with additive disturbance, such as Equation 2.16.

$$x^+ = f(x, u, w) \tag{2.16}$$

where $f : \mathbb{R}^n \times \mathbb{R}^m \times \mathbb{R}^p \to \mathbb{R}^n$ is the discrete time control system; $x^+ \in \mathbb{X}$ is the system state vector at next time instant; $x \in \mathbb{X}$ is the system state vector; $u \in \mathbb{U}$ is the control action vector; and $w \in \mathbb{W}$ is the uncertainty vector.

In general, prior knowledge of uncertainty is limited to a compact convex set $\mathbb{W}$. This means that an infinite number of uncertainty realizations must be taken into account at the optimal control problem, leading to an infinite dimension optimization. Implementation of this approach seems only practical if the uncertainty set is discretized into a number of finite realizations. Therefore, the ensemble of each uncertainty realization vector is defined in Equation 2.17.

$$\mathbf{w}_{\mathcal{W}} = \{w_\Delta \,|\, \Delta \in \mathcal{W}\} \tag{2.17}$$

where $\mathbf{w}_{\mathcal{W}}$ is the uncertainty ensemble; w_Δ is the uncertainty vector associated with realization Δ; $\mathcal{W} = [1, 2, ..., N_\Delta]$ is the realization set; and N_Δ is the total amount of realizations. Given initial conditions($x_0 \in \mathbb{X}$) obtained at sampling time t_k, the uncertainty vector associated with realization Δ (w_Δ) and a control sequence ($\mathbf{u}$), it is possible to predict the open-loop trajectory associated with realization Δ, which is given in Equation 2.18.

$$\begin{aligned} &x^{\mathbf{u}}_{k+1}(x_0) = f_\Delta(x^{\mathbf{u}}_k(x_0), u_k),\ \forall k \in [0, 1, ..., N-1]\,, \\ &x^{\mathbf{u}}_0(x_0) = x_0 \end{aligned} \tag{2.18}$$

where $f_\Delta : \mathbb{R}^n \times \mathbb{R}^m \to \mathbb{R}^n$ is the discrete time control system associated with realization Δ; $\mathbf{x}^{\mathbf{u}}_\Delta(x_0) := \{x^{\mathbf{u}}_k(x_0) \mid k \in [0, 1, ..., N-1]\}$ is the predicted or open-loop trajectory associated with realization Δ; $x^{\mathbf{u}}_k(x_0) \in \mathbb{X}$ is the predicted or open-loop system state vector at stage k; $x_0 \in \mathbb{X}$ is the initial condition of a trajectory; $u_k \in \mathbb{U}$ is the control action vector at stage k; and $N \in \mathbb{N}^+$ is the prediction horizon.

The traditional min-max optimal control problem (OCP_Δ) is posed in Equation

2.19.

$$
\begin{aligned}
\phi_N^0(x_0) = \min_{\mathbf{u}} \max_{\Delta \in \mathcal{W}} \{ \phi_N(x_0, \mathbf{u}) = \sum_{k=0}^{N-1} \ell\left(x_k^{\mathbf{u}}(x_0), u_k\right) \mid \mathbf{u} \in \mathcal{U}_\Delta \} \\
\text{s.t.} \quad & x_{k+1}^{\mathbf{u}}(x_0) = f_\Delta(x_k^{\mathbf{u}}(x_0), u_k), \\
& x_0^{\mathbf{u}}(x_0) = x_0, \\
& x_k^{\mathbf{u}} \in \mathbb{X}, \\
& u_k \in \mathbb{U}
\end{aligned}
\tag{2.19}
$$

where $\phi_N^0(\cdot) : \mathbb{R}^n \to \mathbb{R}_0^+$ is the min-max objective function at optimum; $\phi_N(\cdot) : \mathbb{R}^n \times \mathbb{R}^m \to \mathbb{R}_0^+$ is the min-max objective function; $\mathbf{u}$ is the control sequence; and $\mathcal{U}_\Delta$ is the set of admissible min-max control sequences.

The closed-loop implementation of the optimal control problem shown in Equation 2.19 provides good performance for the worst-case scenario. However, as a single control profile is optimized over all possible uncertainty realizations it has a major flaw due to the lack of feedback. This leads OCP_Δ formulation to perform poorly by being unnecessarily conservative and even infeasible for more common scenarios, such as the nominal (ALLGÖWER *et al.*, 2004). Hence, there is a *price of robustness* which must be payed. Several authors proposed different approaches to deal with these issues (BEN-TAL & NEMIROVSKI, 1999; BERTSIMAS & SIM, 2004; DARLINGTON *et al.*, 2000).

SCOKAERT & MAYNE (1998) introduced the notion of feedback inside the min-max formulation by allowing a different control sequence for each extreme realization of the uncertainty. This partially solves the problems of conservativeness and feasibility because feedback notion is also considered inside the optimization problem and not only by the receding horizon approach. The feedback min-max optimal control problem (OCP_Φ) is stated on Equation 2.20.

$$
\begin{aligned}
\Phi_N^0(x_0) = \min_{\mathbf{u}_\Phi} \max_{\Delta \in \mathcal{W}} \{ \Phi_N(x_0, \mathbf{u}_\Phi) = \sum_{k=0}^{N-1} \ell\left(x_{\Delta,k}^{\mathbf{u}}(x_0), u_{\delta,k}\right) \mid \mathbf{u}_\Phi \in \mathcal{U}_\Phi \} \\
\text{s.t.} \quad & x_{\Delta,k+1}^{\mathbf{u}}(x_0) = f(x_{\Delta,k}^{\mathbf{u}}(x_0), u_{\Delta,k}, w_{\Delta,k}), && \forall \Delta \in \mathcal{W}, \\
& x_{\Delta,0}^{\mathbf{u}}(x_0) = x_0, && \forall \Delta \in \mathcal{W}, \\
& x_{\Delta,k}^{\mathbf{u}} \in \mathbb{X}, && \forall \Delta \in \mathcal{W}, \\
& u_{\Delta,k} \in \mathbb{U}, && \forall \Delta \in \mathcal{W}, \\
& x_{\Delta_1,k}^{\mathbf{u}} = x_{\Delta_2,k}^{\mathbf{u}} \Rightarrow u_{\Delta_1,k} = u_{\Delta_2,k}, && \forall \Delta_1, \Delta_2 \in \mathcal{W};
\end{aligned}
\tag{2.20}
$$

where $\Phi_N^0(\cdot) : \mathbb{R}^n \to \mathbb{R}_0^+$ is the feedback min-max objective function at optimum; $\Phi_N(\cdot) : \mathbb{R}^n \to \mathbb{R}_0^+$ is the feedback min-max objective function; $x_{\Delta,k}^{\mathbf{u}}(x_0) \in \mathbb{X}$ is the

predicted or open-loop system state vector at stage k associated with realization Δ; $u_{\Delta,k} \in \mathbb{U}$ is the control action vector at stage k associated with realization Δ; $w^{\mathbf{u}}_{\Delta,k} \in \mathbb{U}$ is the open-loop uncertainty vector at stage k associated with realization Δ; $\mathbf{u}_\Phi$ is the feedback min-max control sequences; and $\mathcal{U}_\Phi$ is the set of admissible feedback min-max control sequences. Both variables are defined in Equations 2.21 and 2.22.

$$\mathbf{u}_\Phi := \{u_{\Delta,k} \mid \Delta \in \mathcal{W}, k \in \mathbb{N}\} \tag{2.21}$$

$$\mathcal{U}_\Phi := \{u_{\Delta,k} \in \mathbb{U}, \Delta \in \mathcal{W}, k \in [0, 1, ..., N-1] \mid x^{\mathbf{u}}_{\Delta,k}(x_0) \in \mathbb{X}\} \tag{2.22}$$

When a different control sequence for each extreme realization of the uncertainty is considered, the freedom of control sequences must be restricted. Therefore, the constraint $x^{\mathbf{u}}_{\Delta_1,k} = x^{\mathbf{u}}_{\Delta_2,k} \Rightarrow u_{\Delta_1,k} = u_{\Delta_2,k}$ was added to enforce a single control action for each state. Because feedback is taken into account inside OCP_Φ, this formulation can be classified as a closed-loop approach. It is known that robust closed-loop approaches reduces the controller conservativeness (SCOKAERT & MAYNE, 1998). Also, in a closed-loop framework, a solution is less likely to be infeasible than in an open-loop framework (SCOKAERT & MAYNE, 1998). Therefore, feedback min-max is capable of reducing conservativeness while increasing feasibility and robustness. Despite having these qualities, feedback min-max approach needs a high computational effort, which is a hindrance. The main reason is that the number of extreme realizations grows combinatorially with the prediction horizon. Therefore, this method is only recommended for small horizons.

A multi-stage NMPC approach has been proposed in LUCIA *et al.* (2013). Instead of considering only extreme realizations of the uncertainty, it is assumed that a tree of discrete scenarios, such as the one in Figure 2.1, represents the dynamic state behaviour under uncertainty influence. For simplicity, an uniform scenario tree will be considered for the rest of this section, i.e., all nodes generate the same number of branches.

This scenario tree representation is a well-known approach used in the field of stochastic programming. The branching starts from the initial condition x_0 of the controlled system, referenced as root, continuing until the end of the prediction horizon, known as leafs. Each root-leaf path is called a scenario. The s-th scenario is comprised of the root node x_0, and several other states x^j_k, control actions u^j_k and uncertainty realizations $w^{\Delta(j)}_k$. For a particular prediction horizon and an uniform scenario tree, the total number of scenarios can be calculated by Equation 2.23.

$$S_t = {N_w}^N \tag{2.23}$$

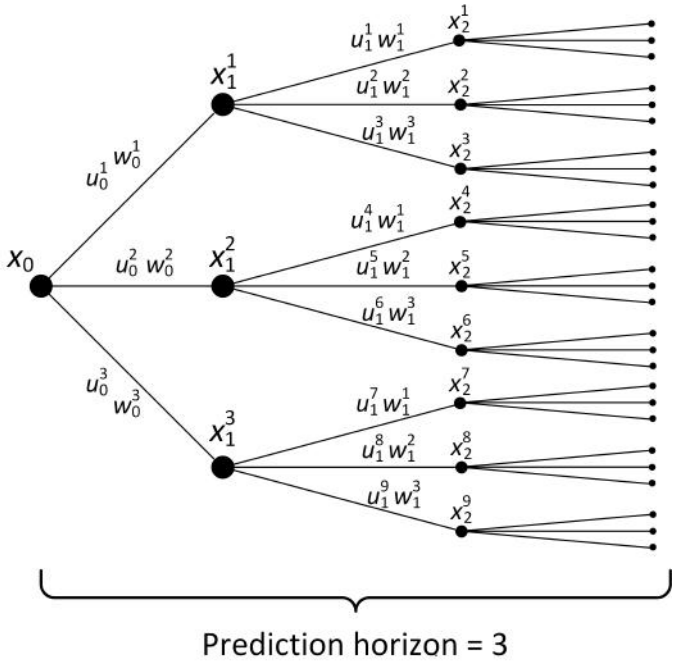

Figure 2.1: Uniform scenario tree representation for a multi-stage NMPC with prediction horizon set to 3 and 3 uncertainty combinations, leading to 27 scenarios. Adapted from LUCIA *et al.* (2013).

where S_t is the total amount of scenarios; and N is the prediction horizon.

Similarly to feedback min-max, multi-stage NMPC also takes explicitly feedback notion inside the optimal control problem. Due to that, optimized control actions at later stages can be regarded as recourse decision variables, as each future decisions can compensate for bad effects that might advent from previous decisions made at early stages (LUCIA *et al.*, 2013). In Equation 2.24, the mathematical formulation of an open-loop scenario tree is represented for a discrete time non-linear system.

$$\begin{aligned} &x_{k+1}^{\mathbf{u},j}(x_0) = f(x_k^{\mathbf{u},p(j)}(x_0), u_k^j, w_k^{r(j)}), \quad \forall k \in \{0,1,...,N-1\} \\ &x_0^{\mathbf{u},j}(x_0) = x_0 \end{aligned} \tag{2.24}$$

where $x_{k+1}^{\mathbf{u},j}(x_0) \in \mathbb{X}$ is the predicted or open-loop state vector at position j at stage $k+1$; $x_k^{\mathbf{u},p(j)}(x_0) \in \mathbb{X}$ is the predicted or open-loop state vector that parents $x_{k+1}^{\mathbf{u},j}(x_0)$; $u_k^j \in \mathbb{U}$ is the control action vector at stage k, position j; $w^{\Delta(j)}$ is the uncertainty vector associated with realization $\Delta(j)$ at stage k; and $N \in \mathbb{N}^+$ is the prediction horizon. As an example, the predicted open-loop state at position 5 and stage 2 ($x_2^{\mathbf{u},5}(x_0)$) shown in Figure 2.1 is given in Equation 2.25.

$$x_2^{\mathbf{u},5}(x_0) = f(x_1^{\mathbf{u},2}(x_0), u_1^5, w_1^2) \tag{2.25}$$

To avoid exponential growth of the scenario tree LUCIA *et al.* (2013) suggest that

the far future does not need to be rigorously represented as the near future. Also, due to receding horizon implementation, new information are obtained from the controlled process, while control actions are recalculated. Therefore, tree branching may be interrupted after a certain number of stages $N_R < N$, which is called robust horizon. The number of scenarios is now calculated as Equation 2.26

$$S_t = {N_w}^{N_R} \tag{2.26}$$

where N_R is the robust horizon.

The multi-stage optimal control problem ($\text{OCP}_{\mathcal{S}}$) optimizes over all scenarios. To simplify the notation adopted by LUCIA *et al.* (2013), it is considered that each particular scenario $s \in \mathcal{S} = \{1, 2, ..., S_t\}$ is comprised by an uncertainty trajectory, which is introduced in Equation 2.27

$$\mathbf{w}_{S_s} = \{w_{\Delta(k,s)} \mid \forall k \in [0, 1, ..., N-1]\}, \forall s \in \mathcal{S} \tag{2.27}$$

where $\mathbf{w}_{S_s}$ is the uncertainty trajectory of the scenario s; and $w_{\Delta(k,s)}$ is the open-loop uncertainty vector associated with realization $\Delta(k, s)$.

With the introduced notation, an open-loop trajectory and an illustration for the scenario tree with a robust horizon is shown in Equation 2.28 and Figure 2.2, respectively.

$$\begin{aligned} &x^{\mathbf{u}}_{k+1,s}(x_0) = f(x^{\mathbf{u}}_{k,s}(x_0), u_{k,s}, w^{\mathbf{u}}_{\Delta(s,k)}), \quad \forall k \in \{0, 1, ..., N-1\}, \forall s \in \mathcal{S} \\ &x^{\mathbf{u}}_{0,s}(x_0) = x_0, \qquad \forall s \in \mathcal{S} \end{aligned} \tag{2.28}$$

where $x^{\mathbf{u}}_{k,s}(x_0)$ is the predicted or open-loop system state vector at stage k, scenario s; and $u_{k,s}$ is the control action vector at stage k, scenario s. With the ability of predicting each scenario behavior, it is possible to tune the confidence on each particular scenario by the introduction of weights. Therefore, the optimal control problem ($\text{OCP}_{\mathcal{S}}$) is posed in Equation 2.29.

$$\begin{aligned} V^0_{\mathcal{S}}(x_0) = \min_{\mathbf{u}} \{ & V_{\mathcal{S}}(x_0, \mathbf{u}) = \sum_{s=1}^{S_t} \left[\sum_{k=0}^{N-1} \omega_s \ell_s \left(x^{\mathbf{u}}_{k,s}(x_0), u_{k,s} \right) \right] \mid \mathbf{u} \in \mathcal{U}_{\mathcal{S}} \} \\ \text{s.t.} \quad & x^{\mathbf{u}}_{k+1,s}(x_0) = f(x^{\mathbf{u}}_{k,s}(x_0), u_{k,s}, w_{\Delta(k,s)}), \\ & x^{\mathbf{u}}_{0,s}(x_0) = x_0, \\ & x^{\mathbf{u}}_{k,s} \in \mathbb{X}, \\ & u_{k,s} \in \mathbb{U}, \\ & x^{\mathbf{u}}_{k,s_1} = x^{\mathbf{u}}_{k,s_2} \Rightarrow u_{k,s_1} = u_{k,s_2} \end{aligned} \tag{2.29}$$

where $V^0_{\mathcal{S}}(\cdot) : \mathbb{R}^n \to \mathbb{R}^+_0$ is the multi-stage objective function at optimum; $V_{\mathcal{S}}(\cdot)$:

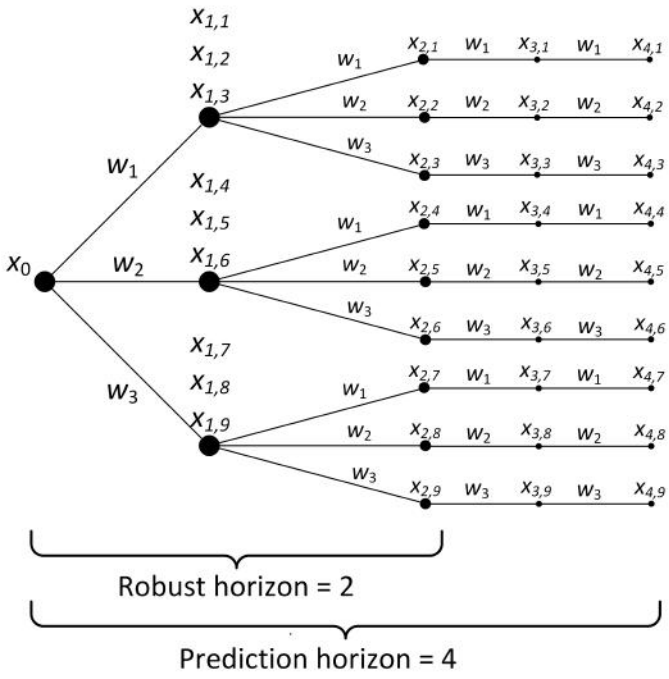

Figure 2.2: Uniform scenario tree representation for a multi-stage NMPC with robust horizon set to 2, prediction horizon set to 4, and 3 uncertainty combinations, leading to 9 scenarios. Adapted from LUCIA *et al.* (2014b).

$\mathbb{R}^n \to \mathbb{R}_0^+$ is the multi-stage objective function; ω_s is the weight associated with each scenario or scenario likelihood; $\ell_s(\cdot) : \mathbb{R}^n \times \mathbb{R}^m \to \mathbb{R}_0^+$ is the stage cost of the s-th scenario; and $\mathcal{U}_\mathcal{S}$ is the set of admissible multi-stage control sequences.

Non-anticipative constraints are present in the multi-stage optimal control problem. They are used to enforce a single control action if different scenarios has the same state at stage k. Therefore, using Figure 2.2 as a reference, non-anticipative constraints at stage $k = 1$ would behave as show in Equation 2.30

$$x_{1,4}^{\mathbf{u}} = x_{1,5}^{\mathbf{u}} = x_{1,6}^{\mathbf{u}} \Rightarrow u_{1,4} = u_{1,5} = u_{1,6} \tag{2.30}$$

Some works have been recently developed to explore multi-stage optimization. A theoretical study was published by LUCIA *et al.* (2014a), where a batch polymerization reactor was optimized with a multi-stage economic NMPC that used a model provided by BASF SE. In KRISHNAMOORTHY *et al.* (2016), multi-stage NMPC was applied to a daily production optimization problem involving a two-well gas-lift system. As for VERHEYLEWEGHEN & JÄSCHKE (2016), a multi-stage NMPC was used to increase remaining useful life of a subsea gas compressor by inserting an equipment degradation model in the NMPC framework. An interesting work by TOMASGARD *et al.* (2016) applied multi-stage optimization in the energy market to cope with short-term and long-term decision making when market uncertainties

are present.

2.3 Feasibility, Stability and Performance

According to MORARI & H. LEE (1999), there are three issues that need to be addressed for a NMPC. First, when is the optimal control problem feasible? Second, when does the implemented control actions lead to a system which is closed-loop stable? Third, what closed-loop performance results from repeated solution of the specified open-loop optimal control problem? Constraints play a major role in problem feasibility. For the controlled system, input saturation constraints cannot be exceeded, while constraints involving states can be violated. Nevertheless, the violation of states constraints will have undesirable consequences for the process.

In an optimal control problem, state constraints are characterized as hard constraints. Disturbances in the controlled system may occur leading to a violation of the open-loop trajectory. A consequence is that the optimal control solution is infeasible. Slack variables may be introduced to soften hard constraints by adding a penalty term in the objective function (VADA *et al.*, 1999; ZHENG & MORARI, 1995). Another issue may arise if the periodic solution of the optimal control problem inadvertently drives the closed-loop system out of the feasible region. Therefore, the designed control needs to be robust in the sense of performance when uncertainties are present.

Receding horizon approach uses the recent state information and solves periodically an open-loop optimization problem. By applying only the first optimal control action in the controlled system, closed-loop instability might occur. To deal with that, some ingredients should be added to the optimal control problem. Since non-linear models are used in the formulation, Lyapunov stability theory is needed. Several proposals in the literature were made to modify the open-loop optimal control problem in order to stabilize the closed-loop system (MAYNE & RAWLINGS, 2000). For simplicity it will be assumed that the NMPC objective is to achieve the set-point $x_* = 0$. Some of these approaches are mentioned below.

Terminal equality constraints. KEERTHI & GILBERT (1988) proposed the addition of the following ingredients:

$$\mathbb{X}_f = \{0\}\,, \tag{2.31a}$$

$$V_f(0) = 0. \tag{2.31b}$$

This choice leads to stability of the deterministic closed-loop if the optimal control problem has a solution at the first sampling time t_0 (KEERTHI & GILBERT, 1988). However, the usage of these constraints has some issues as the open-loop

optimization is forced to reach the origin in a finite time. This may result in feasibility problems for a short prediction horizon N. Terminal constraints can increase the optimization computational cost, which may lead to an optimal control problem that takes more than one sample period to be solved (ALLGÖWER *et al.*, 2004). In Figure 2.3, two feasible and one infeasible open-loop trajectories predicted by a NMPC with terminal equality constraints are shown.

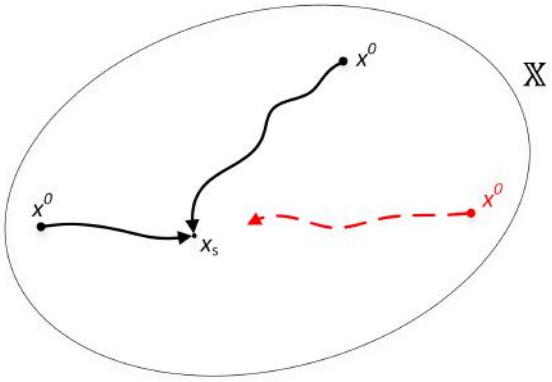

Figure 2.3: An illustration of possible open-loop predicted trajectories under NMPC formulated with terminal equality constraint for a feasible (solid) and an infeasible (dotted) optimal control problem.

Terminal cost. Another proposal was made by BITMEAD *et al.* (1990) with the addition of a terminal cost function. Nevertheless, these changes will only lead to a stable closed-loop if the prediction horizon is considered sufficiently large. The ingredient required for this formulation can be seen below:

$$\mathbb{X}_f = \mathbb{X} \subseteq \mathbb{R}^n, \tag{2.32a}$$

$$V_f(0) = \frac{1}{2}\|\mathbf{x}\|^2 P_W. \tag{2.32b}$$

where Equation 2.32b is the terminal cost. It is also possible to see in Equation 2.32a that the terminal constraint is not used. According to MAYNE & RAWLINGS (2000), it is generally necessary to have a terminal constraint if a non-linear optimal controller is employed. Possible open-loop predicted trajectories for obtained by a NMPC formulated with terminal cost are shown in Figure 2.4.

Terminal constraint set. This concept was introduced by MICHALSKA & MAYNE (1993) for a MPC with variable horizon N. Later, fixed horizon versions were studied by CHISCI *et al.* (1996) and SCOKAERT *et al.* (1999). In this methodology, a terminal set region $\mathbb{X}_f$ is considered. The objective of the optimal control problem is to drive the states close enough to its set-point, entering the region $\mathbb{X}_f$. Once the states are inside $\mathbb{X}_f$, a local stabilizing controller is used to ensure that the states never leave it and eventually goes asymptotically to the set-point. Due to the usage of a local stabilizing controller, this approach is sometimes

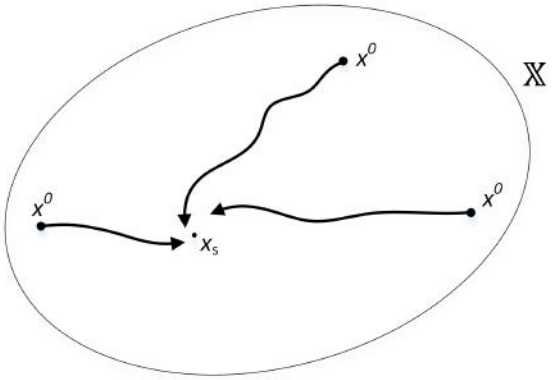

Figure 2.4: An illustration of possible open-loop predicted trajectories under NMPC formulated with terminal cost.

called the *dual-mode* MPC. Ingredients for the terminal constraint set approach are highlighted below:

$$\mathbb{X}_f \subset \mathbb{X} \subseteq \mathbb{R}^n. \tag{2.33a}$$

$$\tilde{\mathbf{u}} = \kappa(\tilde{\mathbf{x}}). \tag{2.33b}$$

where the terminal constraint set is represented by Equation 2.33a and Equation 2.33b is a local stabilizing controller. Figure 2.5 shows possible open-loop predicted trajectories by a NMPC with terminal constraint region and local stabilizing controller.

Terminal cost and constraint set. This version employs both a terminal cost $V_f(\cdot)$ and a terminal constraint set $\mathbb{X}_f$ in its formulation. It is considered to have a superior performance when compared with terminal constraint and terminal constraint set strategies. Moreover, this approach handles a much wider range of problems than terminal cost MPC.

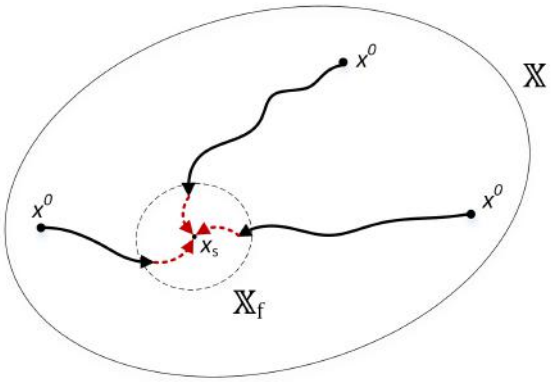

Figure 2.5: An illustration of possible open-loop predicted trajectories under NMPC formulated with a terminal constraint region and a local stabilizing controller.

2.4 Methods for Optimal Control

The NMPC optimization problem must be solved by using numerical methods based on NLP solvers. These methods can be separated into two groups, known as the *sequential* and the *simultaneous* strategies (BIEGLER, 2012).

In *sequential methods* only the control variables are discretized and the resulting NLP is solved with *Control Vector Parameterization* (CVP) methods. This approach undergoes the necessity of repeating *Differential-Algebraic Equations* (DAEs) numerical integration and are not guaranteed to handle open loop unstable systems. It became quite popular after the development of good NLP solvers based on the Sequential Quadratic Programming (SQP) (SPANGELO & EGELAND, 1994).

Optimization with multiple shooting is an intermediate approach that connects sequential and simultaneous methods. In this method, the time domain is partitioned into smaller time elements or intervals $[t_k, t_{k+1}, t_{k+2}, ..., t_{k+N-1}]$. For each interval, the DAE system is numerically integrated, which means that it is integrated from t_k to t_{k+1}, from t_{k+1} to t_{k+2}, and so on. Equality constraints are added in the NLP formulation to bridge two consecutive time intervals, guaranteeing continuity.

The *simultaneous* approach has similarities with the method previously discussed in the sense that time domain is partitioned into smaller time domains. However, the DAE system is discretized using *collocation* method, each interval has a number of collocation points so that:

$$\tilde{\mathbf{x}} = \{\tilde{\mathbf{x}}_{k,c} \mid k \in \mathcal{K},\ c \in \mathcal{C}\}, \tag{2.34a}$$

$$\tilde{\mathbf{z}} = \{\tilde{\mathbf{z}}_{k,c} \mid k \in \mathcal{K},\ c \in \mathcal{C}_{\neq 0}\}, \tag{2.34b}$$

$$\tilde{\mathbf{u}} = \{\tilde{\mathbf{u}}_k \mid k \in \mathcal{K} \backslash N\} \tag{2.34c}$$

where $\mathcal{K} = [0, 1, ..., N]$ is the stage set; $\mathcal{C} = [0, 1, ..., N_d]$ is the number of collocation points set; $\tilde{\mathbf{u}}$ is the discretized control action vector; $\mathcal{K}$, $\mathcal{C}$ and $\tilde{\mathbf{u}}$ are piecewise constant; $\tilde{\mathbf{z}}$ is the discretized algebraic variable vector; and $\tilde{\mathbf{x}}$ is the discretized state vector. The vectors can be represented as follows:

$$\tilde{\mathbf{x}} = \begin{bmatrix} \tilde{\mathbf{x}}_{0,0}^T & \tilde{\mathbf{x}}_{0,1}^T & ... & \tilde{\mathbf{x}}_{k,d-1}^T & \tilde{\mathbf{x}}_{k,d}^T & \tilde{\mathbf{x}}_{k,0}^T & ... & \tilde{\mathbf{x}}_{N,d}^T \end{bmatrix}^T, \tag{2.35a}$$

$$\tilde{\mathbf{z}} = \begin{bmatrix} \tilde{\mathbf{z}}_{0,1}^T & \tilde{\mathbf{z}}_{0,2}^T & ... & \tilde{\mathbf{z}}_{k,d-1}^T & \tilde{\mathbf{z}}_{k,d}^T & \tilde{\mathbf{z}}_{k,1}^T & ... & \tilde{\mathbf{z}}_{N,d}^T \end{bmatrix}^T, \tag{2.35b}$$

$$\tilde{\mathbf{u}} = \begin{bmatrix} \tilde{\mathbf{u}}_0^T & \tilde{\mathbf{u}}_1^T & \tilde{\mathbf{u}}_2^T & ... & \tilde{\mathbf{u}}_{N-1}^T \end{bmatrix}^T. \tag{2.35c}$$

To ensure continuity of the states between two consecutive time intervals, equal-

ity constraints (shooting gap) must be added to the NLP formulation.

$$\tilde{\mathbf{x}}_{k,d} = \tilde{\mathbf{x}}_{k+1,0} \quad \forall k \in \mathcal{K} \backslash N \tag{2.36}$$

The simultaneous approach procedure results into a large-scale NLP without the need for numerical integration and must be addressed by large-scale NLP solvers. For a better understanding, Figure 2.6 displays a schematic representation of a third order collocation using Radau scheme.

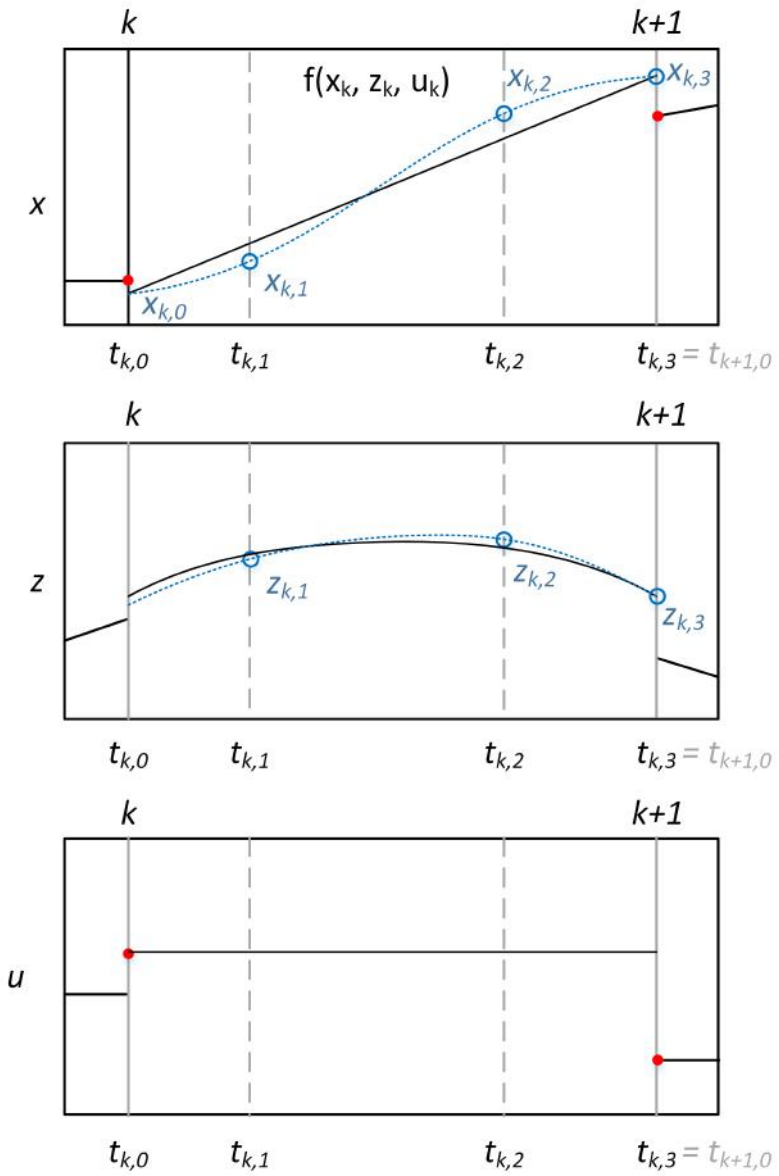

Figure 2.6: Schematic representation of a third order direct collocation using Radau scheme showing the polynomial approximation of a dynamic state, an algebraic variable and an input in the interval $[k, k+1]$. The control input $\mathbf{u}$ is piecewise constant over the interval $[k, k+1]$. Adapted from KRISHNAMOORTHY *et al.* (2016).

2.5 Centrifugal Compressor Control System

FERGUSON (1963) describes compressors as machines that raise the pressure of a specified mass flow of gas by a prescribed amount using the minimal power input. To achieve that, a centrifugal compressor adds kinetic energy to the fluid by accelerating it. Afterwards, a diffuser decelerates the fluid converting its kinetic energy into potential energy and, consequently, raising its pressure (GRAVDAHL & EGELAND, 1999b).

Useful operational range of a centrifugal compressor is limited. Chocking may occur for high mass flow rate as sonic velocity is achieved by the fluid. Whereas, for low mass flow rate, surge and rotation stall destabilize compressor operation. Despite surge and rotation stall being two distinctive phenomena, there is a relation between them.

Surge is a highly unwanted phenomena characterized by a limit cycle in the compressor characteristic causing fluid pressure to rise and flow to undergo through severe amplitude oscillations. It affects the system by introducing thermal and mechanical loads, oscillations, and reduced pressure ratio and efficiency, leading to poor performance or even compressor damage (YOON *et al.*, 2013). Rotating stall is a flow regime in which one or more stall cells are located between the compressor blades. These cells can cover small parts of a span and some blades. In a more severe situation, it can cover the full span and extend to more than 180 degrees of the compressor annulus. Affected blades are considered to be severely stalled, meaning that fluid rotational speed is lower than rotor speed. Also, in these locations there is negligible net through-flow, with some areas containing local reverse flow (GREITZER, 1980). Therefore, for the overall compressor system, rotating stall can be considered a local instability, while surge a more global.

Exact location where change of stability properties occur in centrifugal compressor is unknown. However, based on the compressor characteristic curve, it is known that surge transition starts near local maximum of pressure ratio versus mass/volumetric flow, with a certain positive slope (GRAVDAHL & EGELAND, 1999b).

In Figure 2.7 a compressor map is shown. A region, referred as operation zone, is located at the right side of the surge line. If the compressor is operating at this part of the map, flow is nominally steady and axisymmetric, apart from the blade to blade pressure variations and small scale unsteadiness associated with the moving pressure and velocity field of the impellers. Another region, referred as surge zone, is located at the left side of the surge line. Operation in this particular region implies unstable flow, which may be caused due to surge, rotating stall or a combination of both (GREITZER, 1980).

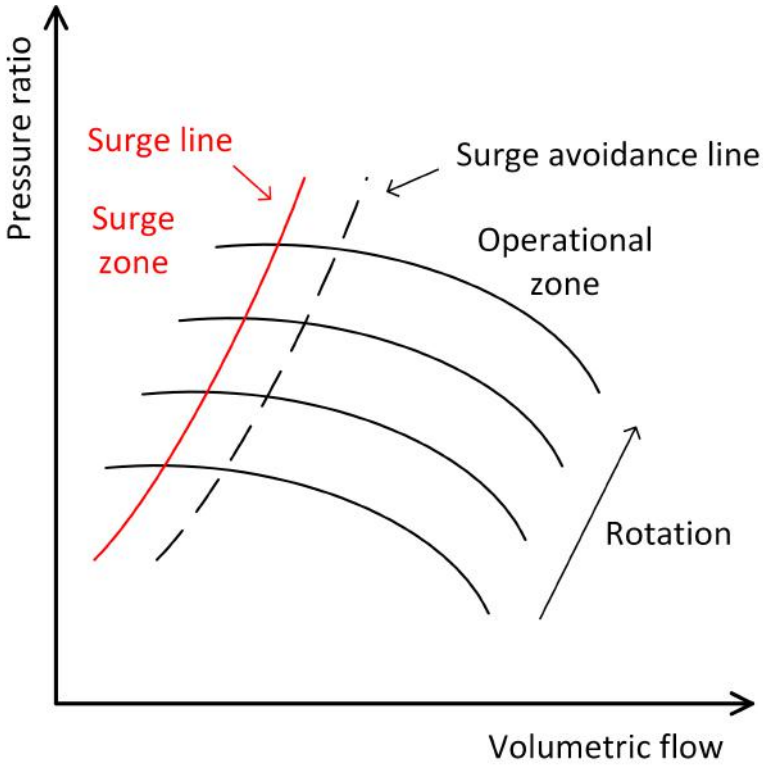

Figure 2.7: Compressor characteristic curve with a surge line delimiting transition between a stable and an unstable region. Adapted from GRAVDAHL & EGELAND (1999b)

One may think that it is desired to operate as far from the surge line as possible, due to risks associated with surge (GRAVDAHL & EGELAND, 1999b). However, high compressor performance and efficiency are obtained near surge line. One control strategy that is usually employed in industry is known as surge-avoidance (BUDINIS & THORNHILL, 2016). In this strategy, it is common to use a parallel safe surge line, which is draw in Figure 2.7.

PLUCENIO *et al.* (2016a) proposed in their work a surge indicator to monitor where the compressor is operating in relation to the surge line based on compressor and surge line volumetric flow rates. The surge index is defined in Equation 2.37.

$$I_s = \frac{q_{sl}}{q_{in}^{co}} \tag{2.37}$$

where I_s is the surge index; q_{sl} is the volumetric flow at the surge line; and q_{in}^{co} is the volumetric flow at the compressor inlet. Surge occurs when q_{in}^{co} is smaller than q_{sl}, the volumetric flow at the safe surge line. Therefore, change of compressor stability occurs when $I_s = 1$. If $I_s < 1$, the compressor is operating normally. If $I_s > 1$, it entered into surge.

Volumetric flow at the safe surge line and at surge line are correlated as stated

in Equation 2.38.

$$q_{ssl} = \frac{q_{sl}}{\delta_{ssl}} \tag{2.38}$$

where q_{ssl} is the volumetric flow at the safe surge line; q_{sl} is the volumetric flow at the surge line; and δ_{ssl} is the safe surge line margin. Consequently, when $I_s = \delta_{ssl}$, the compressor is operating in the safe surge line. If $I_s < \delta_{ssl}$, the compressor is operating under the safe surge line; and if $I_s > \delta_{ssl}$, it has passed through the safe surge line.

An alternative to surge avoidance has been investigated by several authors (EPSTEIN *et al.*, 1989; EVEKER & NETT, 1993; GRAVDAHL *et al.*, 2002). Active surge control is inherently different from surge avoidance. Instead of avoiding surge, active control seeks to stabilize the unstable equilibrium by actively suppressing surge with control actions. This technique broaden compressor's operation region and higher compression efficiency can be achieved, as the once before unstable behaviour can now stabilized GRAVDAHL & EGELAND (1999a). However, safety is a major concern as active surge control pushes operation towards an open-loop unstable region, which can lead to surge if any failure in such control occurs. This technique has been mainly implemented in university laboratories and has not yet found wide spread use in industry due to lack of reliability (UDDIN & GRAVDAHL, 2012a). Therefore, for surge prevention, this work mainly focuses on surge avoidance using deterministic and robust NMPC.

Chapter 3

Surge Avoidance in a Gas Compression System

3.1 Subsea Gas Compression

Seabed gas compression is a fast evolving technology that is used for boosting production. It can improve recovery and production rates from the reservoir by reducing backpressure on wells. Furthermore, it provides advantages in flow assurance risk management, such as slugging, to ensure that production can be maintained to deliver the full reservoir potential (KONDAPI *et al.*, 2017).

The profile production of a typical natural gas field is shown in Figure 3.1. After start up, production achieves its natural plateau (1-2). During this phase, the reservoir has high energy and its pressure is sufficient to drive the flow. Production rate is limited by topside or downstream processing facilities. Thus, production rate is almost constant during this period. With the reservoir depletion, natural pressure starts to decrease (2-3). This has an impact on production rate, as the reservoir does not have enough energy to drive the flow as before. At a certain point (3), economical aspects or physical limitations may force production to stop.

The benefit of boosting a natural gas field production is also shown in Figure 3.1. Subsea compression can keep field production rate for a longer time (2-2') by compensating for its natural pressure decrease. However, even with added compression power, production plateau can not be maintained due to field depletion (2'-3'). Production is finally abandoned (3') as exploration stopped to be economically viable or compressor cannot deliver the pressure increase needed.

Subsea compression technology has gained great attention from oil and gas industry. In 2015, Equinor, former Statoil, started-up two subsea compression systems developed to create value for Åsgard and Gullfaks brown fields (VINTERSTØ *et al.*, 2016). Based on these successful experiences, subsea gas compression technology can

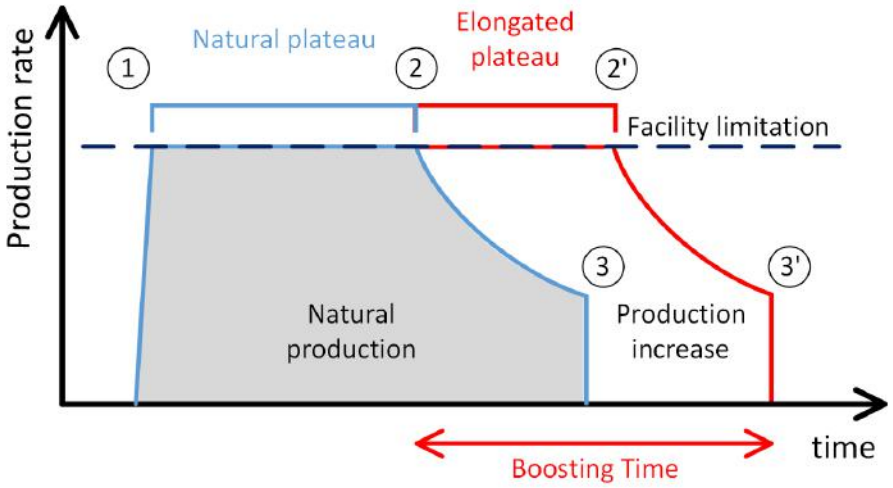

Figure 3.1: Production profile of a natural gas field with natural production and under boosting. Adapted from DETTWYLER *et al.* (2016).

be classified in two main concepts (TØNNESSEN *et al.*, 2017).

In single phase compression, gas/liquid separation is performed upstream the compressor to reduce Liquid Volume Fraction (LVF) in gas stream. This enables gas to be boosted by a "traditional" dry compressor, while the liquid is boosted by a pump. The term "traditional" is used in the sense that it has adopted some common principles and requirements from topside compression industry. This system is known for its high performance, efficiency and flexibility. However, it has some drawbacks related with utility supply for pump and compressor, and intervention cost due to its heavy structure.

In well-stream compression, well-stream is boosted directly through the multiphase wet compressor. Therefore, there is no need for a separation process upstream. Depending on the compressor type and flow characteristics, there might be needed a slug damper upstream the wet compressor. This system is attractive due to significant savings on cost, size and weight by avoiding separation and pumping. However, it cannot deliver comparable performance or operating envelop. According to GILARRANZ R. *et al.* (2010), available test data indicates that the power required to boost wet gas through a centrifugal compressor is higher than boosting liquid and gas separately. Also, there are some issues in predicting accurately the compressor performance under wet gas conditions, which has the potential to cause premature degradation of the machine components.

3.2 Åsgard Field

Åsgard production complex is located approximately 200 km west of the coast of mid Norway. It is being operated by Equinor Energy AS, former Statoil Petroleum

AS, in partnership with ENI Norge AS, ExxonMobil Exploration and Production Norway AS, Petoro AS and Total E&P Norge AS (STORSTENVIK, 2016).

Equinor started oil production during 1999 with the Floating Production Storage and Offloading (FPSO) Åsgard A. Meanwhile, gas production was initiated in later 2000 with the semi-submersible platform Åsgard B, where treatment of gas and stabilization of oil and condensates occur, and the storage ship for condensate Åsgard C. By that time, it was of knowledge from Equinor and its partners that production from Mikkel and Midgard fields would decrease with time, due to declining pressure. Therefore, to extend the life-time of both fields and increase gas recovery, additional compression would be needed (BECKMAN, 2015). However, lack of available space in Åsgard B posed a challenge, as a new compression system was needed. An obvious solution would be to construct a dedicated compression platform but it would be costly. Therefore, subsea compressions was recognized as a cost-effective alternative (VINTERSTØ *et al.*, 2016). Åsgard subsea compression project has started to be developed in 2005 to be the world's first subsea compression station (STORSTENVIK, 2016). Due to the large size of the field and great step-out distance from Mikkel and Midgard, single phase compression technology was selected for greater pressure boost (VINTERSTØ *et al.*, 2016).

The subsea compression station is installed at a water depth of 270 m and is comprised of two identical compressor trains that, at full production, produces a total of 21 MSm^3/d. Currently, it is one of the biggest subsea compression stations in the world, where each compressor has a total duty of 11.5 MW. Start-up occurred in 2015 and it is expected to secure production until 2032 with estimated recovery of further 306 million barrels of oil equivalent (VINTERSTØ *et al.*, 2016). Some technical aspects of Åsgard field are summarized in Table 3.1.

Table 3.1: Technical data for Åsgard (VINTERSTØ *et al.*, 2016).

Field	Åsgard
Start-up	16 September 2015
Design lifetime	30 years
Water depth	250-325 m
Gas Volume Fraction	97 vol %
Compression system structure size	75 x 45 x 20 m (LxWxH)
Compression system weights	4800 tonnes
Design gas flow rate	21 MSm3/d
Pressure boost (dP)	50 bar
Design pressure	210 bar
Liquids (max) into station	3 vol %
Max liquids into compressor	0.46 vol %
Step out	40 km
Additional gas recovery	306 million barrels of oil equivalent Recovery increase from 67 to 87% (Midgard) and 59 to 84% (Mikkel)
Power	2 x 11.5 MW centrifugal compressors (with upstream gas scrubbing)

3.2.1 Process and Control System

The main objective of the compression station process system is to rise the pressure of wellhead fluid to accelerate production and increase recovery while operating at a reduced wellhead pressure (STORSTENVIK, 2016). The compression station is comprised of two identical and independent compressor trains. Each train is composed of several modules, such as an inlet cooler module, separator module, pump module, compressor-module, discharge cooler module, transformer module and other smaller modules (KLEYNHANS *et al.*, 2016). In Figure 3.2 a simplified process flow diagram of one compression train is presented.

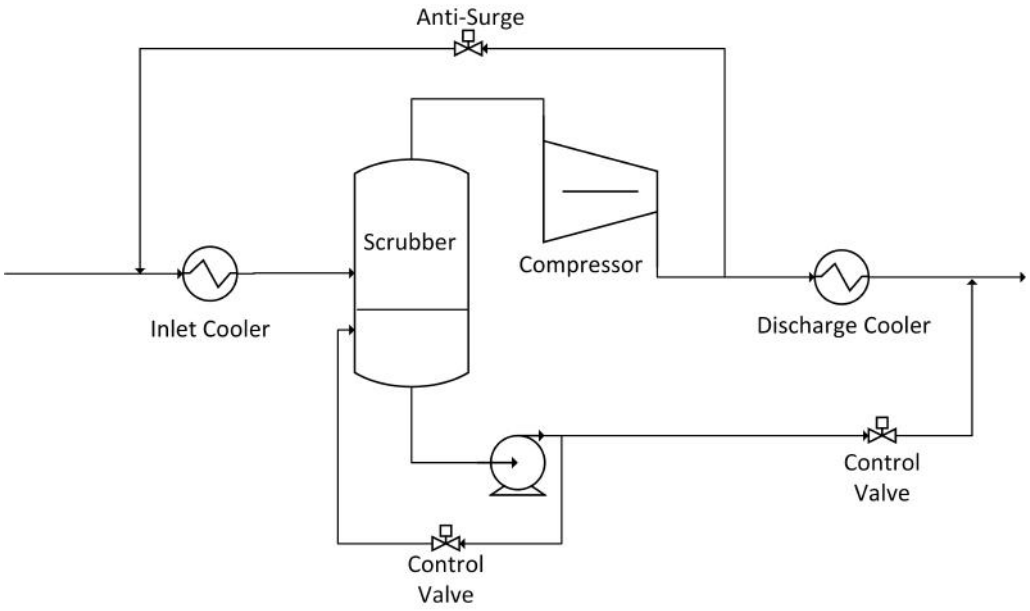

Figure 3.2: Representation of Åsgard dry gas compression system. Based in (STORSTENVIK, 2016).

The incoming well-fluid is cooled to achieve a desired process temperature. This is important, since compressor's efficiency may be affected by temperature changes (ALBUSAIDI & PILIDIS, 2015). Afterwards, the fluid is separated by a scrubber into gas and liquid stream to reduce liquid carry over through the gas phase. Then, the separated gas is pressurized by the centrifugal compressor while the separated liquid is compressed by a centrifugal pump. Before both phases are recombined, the compressed gas phase is cooled to avoid pipeline degradation, as maximum design temperature is lower in the pipelines than in compressor discharge. Finally, both phases are recombined and flow to topside as a multiphase stream (STORSTENVIK, 2016).

The newly developed centrifugal gas compressor is used for boosting the gas phase. Despite being a single phase compression, it must have certain liquid tolerance as the scrubber does not guarantee a perfect separation. Gas phase might contain liquid droplets, which affect compressor performance. Thus, an extensive technology qualification program was developed in which the centrifugal compressor has been qualified, designed and tested to operate with gas containing presence of free liquids such as water, hydrocarbon condensate and glycol. Its performance was monitored with gas containing from 0% to 30% of Liquid Mass Fraction (LMF) (KLEYNHANS *et al.*, 2016).

The subsea control system is entirely electrical-powered. It is based on a redundant configuration where systems A and B operate simultaneously. If a malfunction occurs in one of these systems, the other will continue to operate and the compressor system will not suffer any non-programmed stop. Three control valves are present in

the subsea process system, two of them are used to maintain the pump flow between a minimum and a maximum flow, while the other one is an anti-surge valve which is used to avoid surge operation, this strategy is known as surge avoidance. Most of these control logics are maintained in the topside process control system at Åsgard B. However, some close-loop systems need fast response. Therefore. anti-surge and magnetic bearing control loop are contained in the subsea system (KLEYNHANS *et al.*, 2016).

3.3 Compression System Case-Study

One of the most important aspects of subsea process installations is reliability. In compression systems, surge may reduce compressor's life-time or even damage the equipment, which may force unscheduled maintenance. To carry out major repairs in deep-water it is necessary to mobilize Remotely Operated Vehicles (ROV) from a floating deep-water drilling rig. Cost of subsea intervention in deep-water wells were estimated to be over $200,000 per day in the past years, as rig services are leased at daily rates (FANAILOO & ANDREASSEN, 2008). Therefore, a compression system case-study has been developed to analyse how deterministic and robust NMPC perform in a surge avoidance strategy.

For an online implementation of a NMPC, it is desired to solve the optimal control problem in a reasonable time. Therefore, simplified models must be developed. For that reason, the virtual plant model was based on PLUCENIO *et al.* (2016b). The process flow diagram can be seen in Figure 3.3. The subsea module consists of

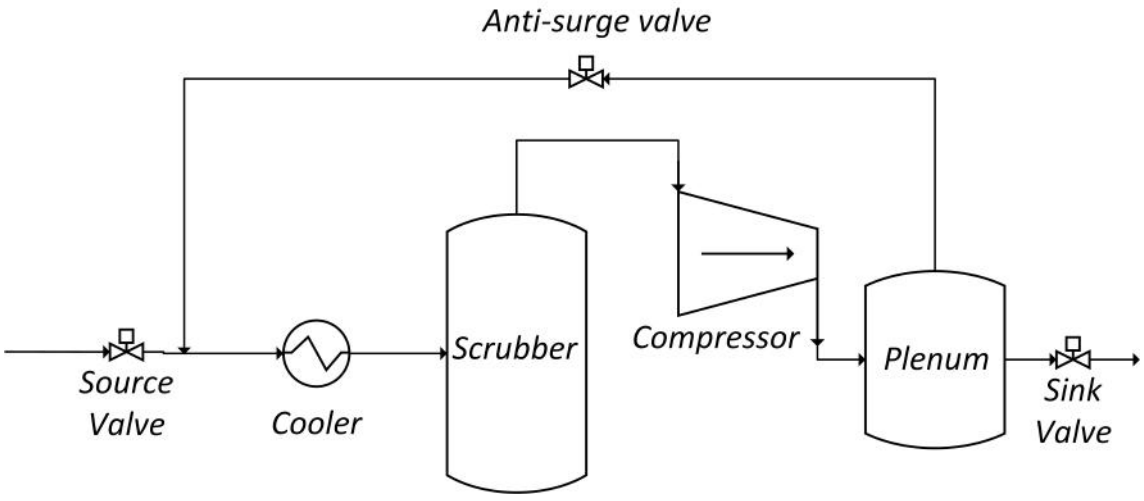

Figure 3.3: Process flow diagram of the case-study based on Åsgard dry compression system.

one source control valve, one inlet cooler, one anti-surge control valve, one compressor and one sink control valve. The general assumptions of this model are presented

as follows:

Assumption 1. Ideal gas behaviour is considered to be followed by the fluid, with deviations being corrected by introducing a given compressibility factor (Z) (black-oil);

Assumption 2. Valve formulation considers a compressible flow;

Assumption 3. Gas condensation does not occur after cooling;

Assumption 4. There is no mass exchange between gas and liquid phase in the scrubber;

Assumption 5. The plenum represents a hypothetical volume that comprehends compressor discharge and pipeline;

Assumption 6. Specific heat capacity (c_p, c_v) does not change with temperature;

Assumption 7. Gas compressibility (Z) does not change with pressure and temperature;

Assumption 8. The system is thermally isolated from the seawater and heat loss is not considered.

In the next sections, models for each system building-block are discussed. Also, for a better reading experience, several units were omitted. It is important to highlight that, for the system model, all variables and equations are in terms of the International System of Units (SI). However, for some figures present in this work, pressure conversion from pascal to bar was employed.

3.3.1 Control Valve

Control valves are automatic devices that modify fluid flow rate by changing its opening based on control decisions (EDGAR *et al.*, 2008). For topside applications, control valve technology is considered to be very mature. This is not the case for subsea control valve despite its evolution in recent years. Several subsea separation projects have decided to use pumps with Variable Speed Driver (VSD) as a final control element for level control, due to a lack of high capacity fast acting flow control valves, e.g. Troll/2001, Tordis/2007, BC-10/2009, Perdido/2010 (HAHEIM & GAILLARD, 2009). In 2011 Pazflor project it was decided to use topside control valves, whereas in 2013 Marlin project choke valves and pumps for level control were adopted. Recently, due to 2011 Ormen Lange and to 2015 Åsgard projects, it is believed that control valves have become sufficiently mature to be applied in subsea systems.

There are still some concerns regarding subsea control valves reliability and response time. However, it is feasible to assume that a commercial 15 second full-stroke time will be readily available in the near future (LI *et al.*, 2014). Therefore, for this case-study, a maximum change in valve opening was considered. The model for a control valve is shown in Equations 3.1a-3.1e (ISA, 2007). The superscript v is a reference to valve.

$$m_{in}^{v} = m_{out}^{v} \tag{3.1a}$$

$$m_{out}^{v} = K_{v}^{v} \phi^{v} P_{in}^{v} Y^{v} \sqrt{\left(\frac{P_{in}^{v} - P_{out}^{v}}{P_{in}^{v}}\right)\left(\frac{M_{w}}{T_{in}^{v} Z}\right)} \tag{3.1b}$$

$$Y^{v} = 1 - \left(\frac{1}{3F_{\gamma}^{v} x_{T}^{v}}\right)\left(\frac{P_{in}^{v} - P_{out}^{v}}{P_{in}^{v}}\right) \tag{3.1c}$$

$$F_{\gamma}^{v} = \frac{\gamma}{1.40} \tag{3.1d}$$

$$T_{in}^{v} = T_{out}^{v} \tag{3.1e}$$

where m_{in}^{v} is the inlet mass flow rate; m_{out}^{v} is outlet mass flow rate; K_{v}^{v} is the flow coefficient; ϕ^{v} is the valve opening percentage; P_{in}^{v} is the inlet pressure; Y^{v} is the expansion factor; x_{T}^{v} is the pressure differential ratio factor; M_{w} is the fluid molecular weight; T_{in}^{v} is the inlet temperature; Z is the compressibility factor; T_{out}^{v} is the outlet temperature; F_{γ}^{v} is the specific heat ratio factor; γ is the adiabatic index or specific heat ratio factor; and P_{out}^{v} is the outflow pressure.

3.3.2 Flow Mixer

The flow mixer has a simple model based on mass, energy balance and pressure equality. For the flow mixer present in the case-study, there are two inlets and one outlet streams. Therefore, the mixer model is given by Equations 3.2a-3.2c.The superscripts mix is a reference to mixer.

$$m_{out}^{mix} = m_{in,1}^{mix} + m_{in,2}^{mix} \tag{3.2a}$$

$$T_{out}^{mix} = \frac{m_{in,1}^{mix}\, T_{in,1}^{mix} + m_{in,2}^{mix}\, T_{in,2}^{mix}}{m_{out}^{mix}} \tag{3.2b}$$

$$P_{in,1}^{mix} = P_{in,2}^{mix} = P_{out}^{mix} \tag{3.2c}$$

where $m_{in,1}^{mix}$ and $m_{in,2}^{mix}$ are the inlet fluid mass flow rate; m_{out}^{mix} is the outlet mass flow rate; $T_{in,1}^{mix}$ and $T_{in,2}^{mix}$ are the inlet fluid temperature; T_{out}^{mix} is the outlet fluid temperature; $P_{in,1}^{mix}$ and $P_{in,2}^{mix}$ are the inlet fluid pressure; and P_{out}^{mix} is the outlet fluid pressure.

3.3.3 Cooler

For the inlet cooler model, the process fluid heat loss was simplified. Only the process fluid mass balance and energy balance were considered, and the pressure drop through the cooler was neglected. Therefore, its model can be represented by Equations 3.3a-3.3c. The superscript hx is a reference to cooler.

$$m_{in}^{hx} = m_{out}^{hx} \tag{3.3a}$$

$$Q^{hx} = m_{in}^{hx}\, c_p\, (T_{in}^{hx} - T_{out}^{hx}) \tag{3.3b}$$

$$P_{in}^{hx} = P_{out}^{hx} \tag{3.3c}$$

where m_{in}^{hx} is the inlet fluid mass flow rate; m_{out}^{hx} is the outlet mass flow rate; Q^{hx} is the heat rate removed from the inlet fluid; c_p is the specific heat capacity of the fluid at constant pressure; T_{in}^{hx} is the inlet fluid temperature; T_{out}^{hx} is the outlet fluid temperature; P_{in}^{hx} is the inlet fluid pressure; and P_{out}^{hx} is the outlet fluid pressure.

3.3.4 Scrubber

The scrubber is a vertical gas-liquid separator used to protect rotating equipments (e.g. centrifugal compressor). To perform that, it is usually required that scrubbers have different separation internals installed in series. In this way, scrubbers can have very high demisting efficiency and can deal with very small liquid droplets contained in a gas flow; consequently reducing carry over by the process gas (AUSTRHEIM, 2006).

Simplifications made due to **Assumption 4** led the scrubber to be modelled similarly to a vertical vessel in terms of mass and energy balance. Its model is described in Equations 3.4a-3.4d. The superscript sc is a reference to scrubber.

$$\frac{\mathrm{d}P^{sc}}{\mathrm{d}t} = \frac{R\, Z\, T_{out}^{sc}}{M_w\, V^{sc}} (m_{in}^{sc} - m_{out}^{sc}) \tag{3.4a}$$

$$\frac{\mathrm{d}T^{sc}}{\mathrm{d}t} = \frac{R\, Z\, T_{out}^{sc}}{M_w\, V^{sc}} \frac{m_{out}^{sc}}{P_{out}^{sc}} (T_{in}^{sc} - T_{out}^{sc}) \tag{3.4b}$$

$$P_{out}^{sc} = P^{sc} \tag{3.4c}$$

$$T_{out}^{sc} = T^{sc} \tag{3.4d}$$

where P^{sc} is the pressure in the scrubber; R is the ideal gas constant; Z is the compressibility factor; M_w is the molecular weight; V^{sc} is the scrubber volume; m_{in}^{sc} is the inlet fluid mass flow rate; m_{out}^{sc} is the outlet fluid mass flow rate; T_{in}^{sc} is the inlet fluid temperature; T_{out}^{sc} is the outlet fluid temperature; T^{sc} is the temperature in the scrubber; and P_{out}^{sc} is the outlet fluid pressure.

3.3.5 Centrifugal Compressor

For this work, the centrifugal compressor was modelled through a hybrid approach with the usage of first principle models, polytropic equations and compressor characteristic curves obtained from manufacturer data.

One of the major works regarding compressor models was developed by GREITZER (1976). In his work, a theoretical first principle was developed for an axial compressor. His lumped dynamic model was later shown to give a reasonable agreement between experimental and simulation results for a centrifugal compressor (HANSEN *et al.*, 1981). Greitzer-type models were further developed with slightly modifications, such as the ones by MACDOUGAL & ELDER (1983), GRAVDAHL & EGELAND (1999a) and BOINOV *et al.* (2006). A one-stage compressor with recycle is shown in Figure 3.4.

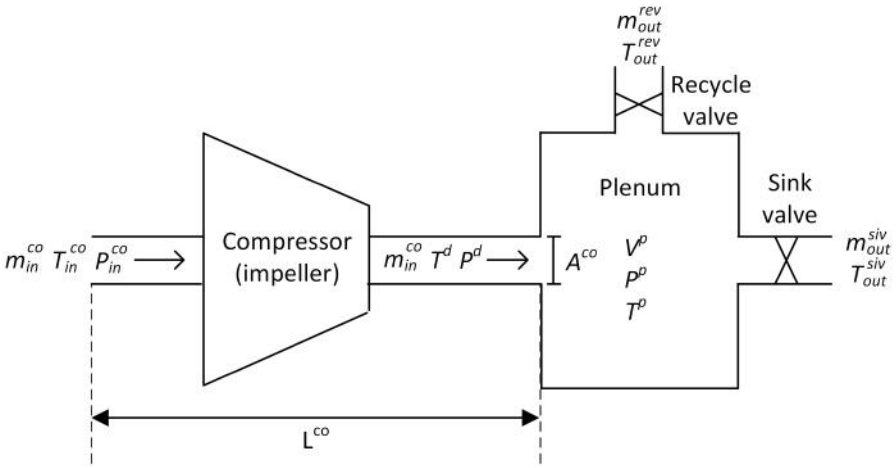

Figure 3.4: One-stage compression system with recycle line. Adapted from UDDIN & GRAVDAHL (2012b).

The first principle model is expressed as an algebraic differential system given by a plenum mass and energy balance, and a duct momentum balance. This model is represented in Equations 3.5a-3.5f. The superscripts *co*, *p*, *rev* and *siv* are references

to compressor, plenum, recycle valve and sink valve, respectively.

$$\frac{\mathrm{d}P^p}{\mathrm{d}t} = \frac{R\,Z\,T^p}{M_w\,V^p}(m^{co}_{in} - m^p_{out,1} - m^p_{out,2}) \tag{3.5a}$$

$$\frac{\mathrm{d}T^p}{\mathrm{d}t} = \frac{R\,Z\,T^p}{M_w\,V^p}\left(\frac{m^p_{out,1} + m^p_{out,2}}{P^p}\right)(T^{co}_d - T^p) \tag{3.5b}$$

$$\frac{\mathrm{d}m^{co}_{in}}{\mathrm{d}t} = \frac{A^{co}}{L^{co}}\,(P^{co}_d - P^p) \tag{3.5c}$$

$$\Psi^{co}(r^{co}, q^{co}_{in}) = \frac{P^{co}_d}{P^{co}_{in}} \tag{3.5d}$$

$$q^{co}_{in} = \frac{m^{co}_{in}}{\rho^{co}_{in}} \tag{3.5e}$$

$$\rho^{co}_{in} = \frac{P^{co}_{in} M_w}{R\,Z\,T^{co}_{in}} \tag{3.5f}$$

$$P^p_{out,1} = P^p_{out,2} = P^p \tag{3.5g}$$

$$T^p_{out,1} = T^p_{out,2} = T^p \tag{3.5h}$$

where P^p is the plenum pressure; R is the ideal gas constant; Z is the gas compressibility factor; T^p is the plenum temperature; M_w is the fluid molecular weight; V^p is the plenum volume; m^{co}_{in} is the compressor inlet mass flow rate; $m^p_{out,1}$ and $m^p_{out,2}$ are the plenum outlet mass flow rate; A^{co} is the compressor duct cross sectional area; L^{co} is the duct length; T^{co}_d is the discharge temperature; P^{co}_d is the discharge pressure; $\Psi_c(\cdot)$ is the compressor characteristic; r^{co} is the compressor angular speed or rotation; q^{co}_{in} is the compressor inlet volumetric flow rate; P^{co}_{in} is the compressor inlet pressure; ρ^{co}_{in} is the compressor inlet density; T^{co}_{in} is the compressor inlet temperature; $P^p_{out,1}$ and $P^p_{out,2}$ are the plenum outlet pressure; and $T^p_{out,1}$ and $T^p_{out,2}$ are the plenum outlet temperature.

SCHULTZ (1962) developed a polytropic model to predict the compressor performance based on real and ideal gas. In his analysis, a polytropic process is commonly defined by the path shown in Equation 3.6.

$$PV^\beta = constant \tag{3.6}$$

where β is the polytropic volume exponent; P is the pressure; and V is the volume.

For a more fundamental definition, Equation 3.7 is shown.

$$V\frac{\mathrm{d}P}{\mathrm{d}h} = \eta_p. \tag{3.7}$$

where h is the enthalpy; and η_p is the polytropic efficiency.

As the polytropic path shown by Equation 3.6 is constant, one may obtain Equa-

tion 3.8.

$$P_{in}(V_{in})^{\beta} = P_{out}(V_{out})^{\beta} \tag{3.8}$$

where P_{in} is the inlet pressure; V_{in} is the inlet volume; P_{out} is the outlet pressure; and V_{out} is the outlet volume.

To accommodate for non-ideal behaviour, Equation 3.9 is used.

$$Z \equiv \frac{PV}{RT} M_w \tag{3.9}$$

where Z is the compressibility factor.

Equation 3.10 is obtained by merging Equation 3.9 with Equation 3.8 using **Assumption 7**.

$$\frac{T_{in}}{T_{out}} = \left(\frac{P_{in}}{P_{out}}\right)^{\left(\frac{\beta-1}{\beta}\right)} \tag{3.10}$$

It is possible to correlate a polytropic process with an isentropic process. An isentropic analysis follows the path defined by Equation 3.11.

$$PV^{\gamma} = constant \tag{3.11}$$

where γ is the specific heat ratio given in Equation 3.12.

$$\gamma = \frac{c_p}{c_v} \tag{3.12}$$

where c_p is the specific heat capacity at constant pressure; and c_v is the specific heat capacity at constant volume.

One can merge Equation 3.11 and 3.9 using **Assumption 8**, obtaining Equation 3.13.

$$\frac{T_{in}}{T_{out}} = \left(\frac{P_{in}}{P_{out}}\right)^{\left(\frac{\gamma-1}{\gamma}\right)} \tag{3.13}$$

It is possible to see that Equations 3.6 and 3.11 are similar. A process needs to be reversible in order to be considered isentropic. In other words, in an isentropic process, the work done by compressing a gas can be completely recovered when decompression occurs. Although a compressor system realizes work in a fluid, it is not an isentropic process, as the fluid suffers from energy losses due to shock and friction (FERGUSON, 1963). Therefore, if $\beta = \gamma$ a polytropic process achieves its maximum efficiency. Therefore, polytropic efficiency can be written on the form of Equation 3.14.

$$\frac{\beta}{\beta - 1} = \eta_p \frac{\gamma}{\gamma - 1} \tag{3.14}$$

The energy per mass of fluid given to the system during a polytropic compression is termed as polytropic head. In Equation 3.15, a representation in terms of polytropic

volume exponent is shown.

$$H_p = \frac{\beta}{\beta - 1} \frac{ZRT_{in}}{M_w} \left[\left(\frac{P_{out}}{P_{in}} \right)^{\frac{\beta-1}{\beta}} - 1 \right] \tag{3.15}$$

where H_p is the polytropic head.

If β from Equation 3.14 is substituted in Equation 3.15, a representation in terms of polytropic efficiency (Equation 3.16) is obtained.

$$H_p = \eta_p \frac{\gamma}{\gamma - 1} \frac{ZRT_{in}}{M_w} \left[\left(\frac{P_{out}}{P_{in}} \right)^{\frac{\gamma-1}{\eta_p \gamma}} - 1 \right] \tag{3.16}$$

The system actual head and the power applied to the fluid by the compressor can be calculated, respectively, from Equation 3.17 and Equation 3.18.

$$H = \frac{H_p}{\eta_p} \tag{3.17}$$

$$W = H\, m_{in} \tag{3.18}$$

where H is the actual head; W is the power; and m_{in} is the inlet mass flow rate. Therefore, for the system shown in Figure 3.4, Equations 3.19a-3.19d were applied.

$$T_d^{co} = T_{in}^{co} \left(\frac{P_d^{co}}{P_{in}^{co}} \right)^{\left(\frac{\gamma-1}{\gamma}\right)} \tag{3.19a}$$

$$H_p^{co} = \eta_p^{co} \frac{\gamma}{\gamma - 1} \frac{ZRT_{in}^{co}}{M_w} \left[\left(\frac{P_d^{co}}{P_{in}^{co}} \right)^{\frac{\gamma-1}{\eta_p^{co}\gamma}} - 1 \right] \tag{3.19b}$$

$$H^{co} = \frac{H_p^{co}}{\eta_p^{co}} \tag{3.19c}$$

$$W^{co} = H^{co}\, m_{in}^{co} \tag{3.19d}$$

Where H_p^{co} is the compressor polytropic head; η_p^{co} is the compressor polytropic efficiency; H^{co} is the compressor actual head; and W^{co} is the compressor power.

The compressor's characteristic are usually provided by the manufacturers as curves of pressure ratio, compressor head and polytropic efficiency generally represented as a function of the compressor angular speed and mass flow rate or volumetric flow rate. From manufacturer data sheet, obtained experimentally in a controlled environment test rig, it is possible to derive polynomial correlations for these curves. A generic representation used by THOMAZ (2017) was employed for the pressure ratio, Ψ^{co} and polytropic efficiency, η_p^{co}. Nevertheless, a constant value of 60 was added to convert the inlet fluid volumetric flow rate unit from m^3/s to m^3/min.

Therefore, the generic representations are introduced in Equation 3.20a-3.20b.

$$\Psi^{co}(r_p^{co}, q_{in}^{co}) = a_0 + a_1\left(\frac{60\,q_{in}^{co}}{r_p^{co}}\right) + a_2 r_p^{co} + a_3\left(\frac{60\,q_{in}^{co}}{r_p^{co}}\right)^2 + a_4\,(60\,q_{in}^{co}) + a_5(r_p^{co})^2, \tag{3.20a}$$

$$\eta_p^{co}(r_p^{co}, q_{in}^{co}) = b_0 + b_1\left(\frac{60\,q_{in}^{co}}{r_p^{co}}\right) + b_2 r_p^{co} + b_3\left(\frac{60\,q_{in}^{co}}{r_p^{co}}\right)^2 + b_4\,(60\,q_{in}^{co}) + b_5(r_p^{co})^2, \tag{3.20b}$$

where r_p^{co} is the compressor rotation percentage; and q_{in}^{co} is the inlet fluid volumetric flow rate.

The surge line can be obtained from applying $\frac{\mathrm{d}\Psi^{co}}{\mathrm{d}q_{in}^{co}} = 0$ and is shown in Equation 3.21.

$$q_{sl}^{co} = \frac{1}{60}\left(-\frac{a_1}{2a_3} r_p^{co} + \frac{a_4}{2a_3} r_p^{co2}\right) \tag{3.21}$$

where the coefficients a and b are shown in Table 3.2.

Table 3.2: Pressure ratio and polytropic efficiency coefficients obtained for the polynomial approximation (THOMAZ, 2017).

Coefficients	Values	Coefficients	Values
a_0	-5,297	b_0	0.4146
a_1	0.2509	b_1	0..009058
a_2	-21.68	b_2	-0.09977
a_3	-0.0013	b_3	-0.0001147
a_4	-0.00723	b_4	0.01962
a_5	24.005	b_5	-1.310

The last part of the compressor model is the surge index, and a relation between the surge line and safe surge line volumetric flow rates. Both formulations have been discussed in a previous section, nevertheless they are shown in Equations 3.22-3.23.

$$I_s^{co} = \frac{q_{sl}^{co}}{q_{in}^{co}} \tag{3.22}$$

$$q_{ssl}^{co} = \frac{q_{sl}^{co}}{\delta_{ssl}^{co}} \tag{3.23}$$

where I_s^{co} is the surge index; q_{ssl}^{co} is the volumetric flow rate at the safe surge line; and δ_{ssl}^{co} is the safe surge line margin.

Chapter 4

Results and Discussion

4.1 Problem Description

The virtual plant model is defined as a semi-explicit index-1 differential-algebraic system, which is shown in Equations 4.1a-4.1b.

$$\dot{\mathbf{x}} = \mathbf{f}_c(\mathbf{x}, \mathbf{z}, \mathbf{u}, \mathbf{w}) \tag{4.1a}$$

$$0 = \mathbf{g}_c(\mathbf{x}, \mathbf{z}, \mathbf{u}, \mathbf{w}) \tag{4.1b}$$

Where $\mathbf{x}$ is the virtual plant state vector; $\mathbf{f}_c$ is the continuous differential equation vector; $\mathbf{z}$ is the virtual plant algebraic variable vector; $\mathbf{u}$ is the virtual plant control action vector; $\mathbf{w}$ is the virtual plant uncertainty vector; and $\mathbf{g}_c$ is the continuous algebraic equation vector. Figure 4.1 is used as reference to visually represent the relationship between functions and equipment.

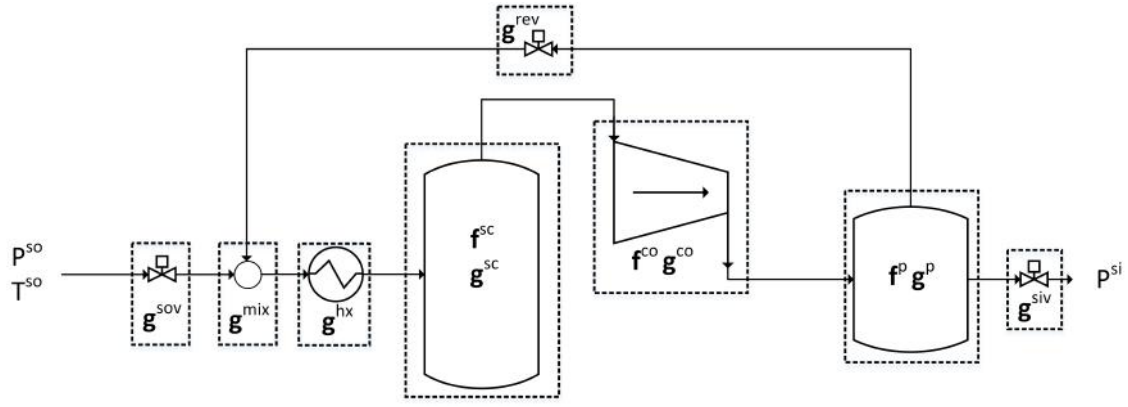

Figure 4.1: Virtual plant detailed functions, where P^{so}, T^{so} and P^{si} are the source pressure, source temperature and sink pressure, respectively. The superscripts *sov*, *mix*, *hx*, *sc*, *rev*, *co*, *p*, *siv* are reference to source valve, mixer, cooler, scrubber, compressor, plenum and sink valve, respectively.

The set of differential and algebraic equations are given by Equations 4.2a and

4.2b, respectively.

$$\mathbf{f}(\cdot) = \begin{bmatrix} \mathbf{f}^{sc}(\cdot)^T & \mathbf{f}^{co}(\cdot)^T & \mathbf{f}^{p}(\cdot)^T \end{bmatrix}^T \tag{4.2a}$$

$$\mathbf{g}(\cdot) = \begin{bmatrix} \mathbf{g}^{sov}(\cdot)^T & \mathbf{g}^{mix}(\cdot)^T & \mathbf{g}^{hx}(\cdot)^T & \mathbf{g}^{sc}(\cdot)^T & \mathbf{g}^{co}(\cdot)^T & \mathbf{g}^{rev}(\cdot)^T & \mathbf{g}^{siv}(\cdot)^T \end{bmatrix}^T \tag{4.2b}$$

Where $\mathbf{f}^{sc}(\cdot)$ is the set of differential equations for the scrubber; $\mathbf{f}^{co}(\cdot)$ is the set of differential equations for the compressor; $\mathbf{f}^{p}(\cdot)$ is the set of differential equations for the plenum; $\mathbf{g}^{sov}(\cdot)$ is the set of algebraic equations for the source valve; $\mathbf{g}^{mix}(\cdot)$ is the set of algebraic equations for the mixer; $\mathbf{g}^{hx}(\cdot)$ is the set of algebraic equations for the cooler; $\mathbf{g}^{sc}(\cdot)$ is the set of algebraic equations for the scrubber; $\mathbf{g}^{co}(\cdot)$ is the set of algebraic equations for the compressor; $\mathbf{g}^{rev}(\cdot)$ is the set of algebraic equations for the recycle valve; $\mathbf{g}^{siv}(\cdot)$ is the set of algebraic equations for the sink valve. Table 4.1 displays which set of differential and algebraic equations are part of each equipment model.

Table 4.1: Model equations used for each equipment in the virtual plant.

Equipment	Superscript	$\mathbf{f}(\mathbf{x}, \mathbf{z}, \mathbf{u}, \mathbf{p}, \mathbf{w})$	$\mathbf{g}(\mathbf{x}, \mathbf{z}, \mathbf{u}, \mathbf{p}, \mathbf{w})$
Source valve	sov	-	3.1a; 3.1b; 3.1c; 3.1d; 3.1e
Mixer	mix	-	3.2a; 3.2b; 3.2c
Cooler	hx	-	3.3a; 3.3b 3.3c
Scrubber	sc	3.4a; 3.4b	3.4c; 3.4d
Compressor	co	3.5c	3.5d; 3.5e; 3.5f; 3.19a; 3.19b; 3.19c; 3.19d; 3.20a 3.20b; 3.21; 3.22; 3.23
Plenum	p	3.5a; 3.5b	3.5g; 3.5h
Recycle valve	rev	-	3.1a; 3.1b; 3.1c; 3.1d; 3.1e
Sink valve	siv	-	3.1a; 3.1b; 3.1c; 3.1d; 3.1e

The virtual plant states $\mathbf{x}$, algebraic variables $\mathbf{z}$ and control actions $\mathbf{u}$ are given

in Equations 4.3a-4.3k.

$$\mathbf{x} = \begin{bmatrix} P^{sc} & T^{sc} & m_{in}^{co} & P^{p} & T^{p} \end{bmatrix}^T \tag{4.3a}$$

$$\mathbf{z} = \begin{bmatrix} \mathbf{z}^{sovT} & \mathbf{z}^{mixT} & \mathbf{z}^{hxT} & \mathbf{z}^{scT} & \mathbf{z}^{coT} & \mathbf{z}^{pT} & \mathbf{z}^{revT} & \mathbf{z}^{sivT} \end{bmatrix} \tag{4.3b}$$

$$\mathbf{z}^{sov} = \begin{bmatrix} m_{in}^{sov} & m_{out}^{sov} & P_{in}^{sov} & P_{out}^{sov} & T_{in}^{sov} & T_{out}^{sov} & Y^{sov} & F_{\gamma}^{sov} & x_T^{sov} \end{bmatrix}^T \tag{4.3c}$$

$$\mathbf{z}^{mix} = \begin{bmatrix} m_{in,1}^{mix} & m_{in,2}^{mix} & m_{out}^{mix} & T_{in,1}^{mix} & T_{in,2}^{mix} & T_{out}^{mix} & P_{in,1}^{mix} & P_{in,2}^{mix} & P_{out}^{mix} \end{bmatrix}^T \tag{4.3d}$$

$$\mathbf{z}^{hx} = \begin{bmatrix} m_{in}^{hx} & m_{out}^{hx} & T_{in}^{hx} & T_{out}^{hx} & P_{in}^{hx} & P_{out}^{hx} & Q^{hx} \end{bmatrix}^T \tag{4.3e}$$

$$\mathbf{z}^{sc} = \begin{bmatrix} m_{in}^{sc} & m_{out}^{sc} & T_{in}^{sc} & T_{out}^{sc} & P_{in}^{sc} & P_{out}^{sc} \end{bmatrix}^T \tag{4.3f}$$

$$\mathbf{z}^{co} = \begin{bmatrix} m_{in}^{co} & q_{in}^{co} & P_{in}^{co} & T_{in}^{co} & \rho_{in}^{co} & P_{d}^{co} & T_{d}^{co} & H_{p}^{co} & H^{co} & W^{co} & \eta_{p}^{co} & \Psi^{co} \\ q_{sl}^{co} & q_{ssl}^{co} & I_{s}^{co} \end{bmatrix}^T \tag{4.3g}$$

$$\mathbf{z}^{p} = \begin{bmatrix} m_{out,1}^{p} & m_{out,2}^{p} & P_{out,1}^{p} & P_{out,2}^{p} & T_{out,1}^{p} & T_{out,2}^{p} \end{bmatrix}^T \tag{4.3h}$$

$$\mathbf{z}^{rev} = \begin{bmatrix} m_{in}^{rev} & m_{out}^{rev} & P_{in}^{rev} & P_{out}^{rev} & T_{in}^{rev} & T_{out}^{rev} & Y^{rev} & F_{\gamma}^{rev} & x_T^{rev} \end{bmatrix}^T \tag{4.3i}$$

$$\mathbf{z}^{siv} = \begin{bmatrix} m_{in}^{siv} & m_{out}^{siv} & P_{in}^{siv} & P_{out}^{siv} & T_{in}^{siv} & T_{out}^{siv} & Y^{siv} & F_{\gamma}^{siv} & x_T^{siv} \end{bmatrix}^T \tag{4.3j}$$

$$\mathbf{u} = \begin{bmatrix} \phi^{rev} & r_{p}^{co} \end{bmatrix}^T \tag{4.3k}$$

Table 4.2 displays the parameter values used to simulate this system. These parameters were chosen based on technical data available from Åsgard subsea compression system presented in Table 3.1 and from STORSTENVIK (2016).

For this system, the uncertainty set is shown in Equation 4.4.

$$\mathbb{W} = \mathbb{E}(P^{so}) \pm \sigma_{P^{so}} \tag{4.4}$$

where $\mathbb{W}$ is the uncertainty set; $\mathbb{E}(P^{so})$ is the expected value of the source pressure; and $\sigma_{P^{so}}$ is the standard deviation of the source pressure.

The objective of this work was to evaluate closed-loop behaviour of a subsea compression system controlled by three distinct NMPC strategies, namely deterministic, offline min-max and multi-stage NMPC. Therefore, this chapter was divided into four parts. In the first study, open-loop simulations where step disturbances and changes in manipulation variable were performed with the intent to gather information about the system dynamics. For the second study, an oscillatory unknown disturbance was applied to the system and closed-loop behaviour was analysed. On the third study, open-loop predicted trajectories of the controllers at specific time samples were examined closely. For the last study, closed-loop controlled system performance was measured and evaluated by using indicators related with set-point

Table 4.2: Parameter values used in simulation.

Parameter	Units	Value	Comments
T^{so}	$[K]$	303.15	Source temperature
P^{si}	$[bar]$	125	Sink pressure
K_v^{sov}	$[kg/s]$	0.007	Source valve constant
ϕ^{sov}	$[dimensionless]$	0.5	Source valve opening
x_T^{sov}	$[dimensionless]$	0.7	Source valve pressure differential ratio factor
V^{sc}	$[m^3]$	4	Scrubber volume
V^{p}	$[m^3]$	1.5	Plenum volume
K_v^{rv}	$[kg/s]$	0.001	Recycle valve constant
x_T^{rv}	$[dimensionless]$	0.7	Recycle valve pressure differential ratio factor
K_v^{siv}	$[kg/s]$	0.007	Sink valve constant
ϕ^{siv}	$[dimensionless]$	0.5	Sink valve opening
x_T^{siv}	$[dimensionless]$	0.7	Sink valve pressure differential ratio factor
M_w	$[kg/mol]$	0.023	Fluid molecular weight
Z	$[dimensionless]$	0.95	Compressibility factor
γ	$[dimensionless]$	1.24	Adiabatic index
R	$[J/mol.K]$	8.31451	Gas constant

tracking, constraint handling, mass flow production, system power consumption and efficient production.

The NMPC formulations were expanded with the addition of stage difference cost, constraints for control input, stability ingredients, soft constraints and system discretization. For the deterministic approach, Equations 4.5a-4.5i display the optimal control problem based on OCP_N. The objective function is shown in Equation 4.5a, with its cost function present in Equation 4.6. As for the equality constraints in Equation 4.5b, they comprehend a discrete form of the model shown in Equations 4.1a and 4.1b. Recycle valve opening limitation during normal operation was added by the addition of a soft constraint in Equation 4.5c, where a_k is the slack variable and α_W, present in the cost function, is the slack variable weight. The lower and upper bound of states, inputs and inputs stage difference are shown in Equations 4.5d, 4.5e and 4.5f, respectively. Due to the usage of direct transcript, shooting gaps

constraints are added in Equation 4.5h. The initial state is given by Equation 4.5i.

$$\min_{\mathbf{u},\mathbf{a}} \quad \{V_N(x_0, \mathbf{u}, \mathbf{a})\} \tag{4.5a}$$

$$\text{s.t.} \quad \mathbf{0} = \mathbf{F}\left(\tilde{\mathbf{x}}^{\mathbf{u}}_{k,c}, \tilde{\mathbf{z}}^{\mathbf{u}}_{k,c}, \tilde{\mathbf{u}}_k, \tilde{\mathbf{w}}^{\mathbf{u}}_{\mathbb{E}}\right), \qquad \forall k \in \mathcal{K}, \forall c \in \mathcal{C}, \tag{4.5b}$$

$$\phi^{rev}_k \leq a_k \qquad \forall k \in \mathcal{K}\backslash N, \tag{4.5c}$$

$$\mathbf{x}^{\mathbf{u}}_{lb} \leq \tilde{\mathbf{x}}^{\mathbf{u}}_{k,c} \leq \mathbf{x}^{\mathbf{u}}_{ub}, \qquad \forall k \in \mathcal{K}, \forall c \in \mathcal{C}, \tag{4.5d}$$

$$\mathbf{z}^{\mathbf{u}}_{lb} \leq \tilde{\mathbf{z}}^{\mathbf{u}}_{k,c} \leq \mathbf{z}^{\mathbf{u}}_{ub}, \qquad \forall k \in \mathcal{K}, \forall c \in \mathcal{C}_{\neq 0}, \tag{4.5e}$$

$$\mathbf{u}_{lb} \leq \tilde{\mathbf{u}}_k \leq \mathbf{u}_{ub}, \qquad \forall k \in \mathcal{K}, \tag{4.5f}$$

$$\Delta\mathbf{u}_{lb} \leq \Delta\tilde{\mathbf{u}}_k \leq \Delta\mathbf{u}_{ub}, \qquad \forall k \in \mathcal{K}, \tag{4.5g}$$

$$\tilde{\mathbf{x}}^{\mathbf{u}}_{k,d} = \tilde{\mathbf{x}}^{\mathbf{u}}_{k+1,0}, \qquad \forall k \in \mathcal{K}\backslash N, \tag{4.5h}$$

$$\tilde{\mathbf{x}}^{\mathbf{u}}_{0,0} = \mathbf{x}_0, \tag{4.5i}$$

With,

$$\begin{aligned} V_N(x_0, \mathbf{u}, \mathbf{a}) &= \sum_{k=0}^{N-1}\left[\sum_{c=1}^{d}(A_{k,c-1}) + B_k\right] + C \\ A_{k,c-1} &= \|\tilde{\mathbf{x}}_{k,c-1}\|_{\mathbf{x}^*}{}^T Q_W \|\tilde{\mathbf{x}}_{k,c-1}\|_{\mathbf{x}^*} \\ B_k &= \|\tilde{\mathbf{u}}_k\|_{\mathbf{u}^*}{}^T R_W \|\tilde{\mathbf{u}}_k\|_{\mathbf{u}^*} + \Delta\tilde{\mathbf{u}}_k{}^T W_W \Delta\tilde{\mathbf{u}}_k + \alpha_W a_k \\ C &= \|\tilde{\mathbf{x}}_{N,0}\|_{\mathbf{x}^*}{}^T P_W \|\tilde{\mathbf{x}}_{N,0}\|_{\mathbf{x}^*} \end{aligned} \tag{4.6}$$

where $V_N(\cdot)$ is the finite horizon objective function; $\mathbf{F}$ is the discretized system; $\tilde{\mathbf{u}}$ is the control action sequence; $\tilde{\mathbf{x}}^{\mathbf{u}}_{k,c}$ is the predicted or open-loop state vector at stage k, collocation c; $\tilde{\mathbf{z}}^{\mathbf{u}}_{k,c}$ is the predicted or open-loop algebraic variable vector at stage k, collocation c; $\tilde{\mathbf{u}}_k$ is the control action vector at stage k; $\tilde{\mathbf{w}}^{\mathbf{u}}_{\mathbb{E}}$ is the open-loop uncertainty vector associated with the expected realization; ϕ^{rev}_k is the recycle valve opening at stage k; a_k is the slack variable at stage k; subscripts lb and ub represent the lower and upper bounds for $\tilde{\mathbf{x}}^{\mathbf{u}}_{k,c}$, $\tilde{\mathbf{z}}^{\mathbf{u}}_{k,c}$, $\tilde{\mathbf{u}}_k$ and $\Delta\tilde{\mathbf{u}}_k$; $\Delta\tilde{\mathbf{u}}_k$ is the control action changes vector at stage k; Q_W is the stage cost sate weight matrix; α_W is the slack variable weight; R_W is the stage cost input weight matrix; W_W is the stage cost input weight matrix; and P_W is the terminal cost weight matrix.

The offline min-max approach is based on OCP_Δ. However, since in this work it was considered that only the source pressure had uncertainty, the solution to its *max* counterpart can be known through simulations, thus offline. Consequently, the offline min-max is posed as Equations 4.5a-4.5i considering the open-loop uncertainty vector associated with the worst realization Δ^0 instead of the nominal realization. Therefore, Equation 4.5b is changed to Equation 4.7.

$$\mathbf{0} = \mathbf{F}\left(\tilde{\mathbf{x}}^{\mathbf{u}}_{k,c}, \tilde{\mathbf{z}}^{\mathbf{u}}_{k,c}, \tilde{\mathbf{u}}_k, \tilde{\mathbf{w}}^{\mathbf{u}}_{\Delta^0}\right), \forall k \in \mathcal{K}, c \in \mathcal{C} \tag{4.7}$$

where $\mathbf{w}^{\mathbf{u}}_{\Delta^0}$ is the open-loop uncertainty vector associated with the worst realization Δ^0.

For the multi-stage NMPC, the $\text{OCP}_{\mathcal{S}}$ is used as a basis. The optimal control problem is posed in Equations 4.8a-4.8j.

$$\min_{\mathbf{u},\mathbf{a}} \quad \{V_{\mathcal{S}}(x_0, \mathbf{u}, \mathbf{a})\} \tag{4.8a}$$

$$\text{s.t.} \quad \mathbf{0} = \mathbf{F}\left(\tilde{\mathbf{x}}^{\mathbf{u}}_{k,c,s}, \tilde{\mathbf{z}}^{\mathbf{u}}_{k,c,s}, \tilde{\mathbf{u}}_{k,s}, \tilde{\mathbf{w}}_{\Delta(k,s)}\right), \qquad \forall k \in \mathcal{K}, \forall c \in \mathcal{C}, \forall s \in \mathcal{S}, \tag{4.8b}$$

$$\phi^{rev}_{k,s} \leq a_{k,s} \qquad \forall k \in \mathcal{K}, \forall s \in \mathcal{S}, \tag{4.8c}$$

$$\mathbf{x}^{\mathbf{u}}_{lb} \leq \tilde{\mathbf{x}}^{\mathbf{u}}_{k,c,s} \leq \mathbf{x}^{\mathbf{u}}_{ub}, \qquad \forall k \in \mathcal{K}, \forall c \in \mathcal{C}, \forall s \in \mathcal{S}, \tag{4.8d}$$

$$\mathbf{z}^{\mathbf{u}}_{lb} \leq \tilde{\mathbf{z}}^{\mathbf{u}}_{k,c,s} \leq \mathbf{z}^{\mathbf{u}}_{ub}, \qquad \forall k \in \mathcal{K}, \forall c \in \mathcal{C}_{\neq 0}, \forall s \in \mathcal{S}, \tag{4.8e}$$

$$\mathbf{u}_{lb} \leq \tilde{\mathbf{u}}_{k,s} \leq \mathbf{u}_{ub}, \qquad \forall k \in \mathcal{K}, \forall s \in \mathcal{S}, \tag{4.8f}$$

$$\Delta\mathbf{u}_{lb} \leq \Delta\tilde{\mathbf{u}}_{k,s} \leq \Delta\mathbf{u}_{ub}, \qquad \forall k \in \mathcal{K}, \forall s \in \mathcal{S}, \tag{4.8g}$$

$$\tilde{\mathbf{x}}^{\mathbf{u}}_{k,d,s} = \tilde{\mathbf{x}}^{\mathbf{u}}_{k+1,0,s} \qquad \forall k \in \mathcal{K}\backslash N, \forall s \in \mathcal{S}, \tag{4.8h}$$

$$\tilde{\mathbf{x}}^{\mathbf{u}}_{k,0,s_1} = \tilde{\mathbf{x}}^{\mathbf{u}}_{k,0,s_2} \Rightarrow \tilde{\mathbf{u}}_{k,s_1} = \tilde{\mathbf{u}}_{k,s_2} \qquad \forall k \in \mathcal{K}, \forall s_1, s_2 \in \mathcal{S} \tag{4.8i}$$

$$\tilde{\mathbf{x}}^{\mathbf{u}}_{0,0,s} = \mathbf{x}_0, \qquad \forall s \in \mathcal{S} \tag{4.8j}$$

With,

$$V_{\mathcal{S}}(x_0, \mathbf{u}, \mathbf{a}) = \sum_{s=1}^{S_t} \omega_s V_{N_s}(x_0, \mathbf{u}, \mathbf{a}) \tag{4.9}$$

Where ω_s is the weight associated with each scenario or scenario likelihood; and V_{N_s} is the finite horizon objective function of scenario s.

The constraint added in Equation 4.8i is known as a non-anticipative constraint. It states that, for each stage, if two different scenarios have the same state, both control actions must be the same as a decision must be made before knowing the outcome. To illustrate this, consider a case with two uncertainty realizations and two robust horizon, which gives a total number of four scenarios. The initial condition is the same for all scenarios as it was stated in Equation 4.8j. Therefore, the control action at stage $k = 0$ must be the same for all scenarios as shown in Equation 4.10.

$$\tilde{\mathbf{x}}_{0,0,1} = \tilde{\mathbf{x}}_{0,0,2} = \tilde{\mathbf{x}}_{0,0,3} = \tilde{\mathbf{x}}_{0,0,4} = \mathbf{x}_0 \Rightarrow \tilde{\mathbf{u}}_{0,1} = \tilde{\mathbf{u}}_{0,2} = \tilde{\mathbf{u}}_{0,3} = \tilde{\mathbf{u}}_{0,4} \tag{4.10}$$

The scenario tree branching starts and, as two uncertainty realizations were considered, two states are obtained at stage $k = 1$. Due to branching, at stage $k = 1$, one state is the same for the first and second scenario, while the other is equal for the third and fourth scenario. Once again, as it was stated the non-anticipative constraint, the same control action must be employed for all scenarios with the same

state at a particular stage, which is evidenced in Equation 4.11.

$$\begin{aligned} \tilde{\mathbf{x}}_{1,0,1} = \tilde{\mathbf{x}}_{1,0,2} \Rightarrow \tilde{\mathbf{u}}_{1,1} = \tilde{\mathbf{u}}_{1,2} \\ \tilde{\mathbf{x}}_{1,0,3} = \tilde{\mathbf{x}}_{1,0,4} \Rightarrow \mathbf{u}_{1,3} = \tilde{\mathbf{u}}_{1,4} \end{aligned} \tag{4.11}$$

Another branching occurs due to uncertainty realization, giving four possible states at stage $k = 2$. Now, each scenario has as a different state and the criteria for employing non-anticipative constraint is not met. Therefore, each scenario has its own control action and no further branching occurs for $k \geq N_R$. Considering this example, open-loop state trajectory and control action are illustrated in Figure 4.2. For clarity, collocation points were suppressed.

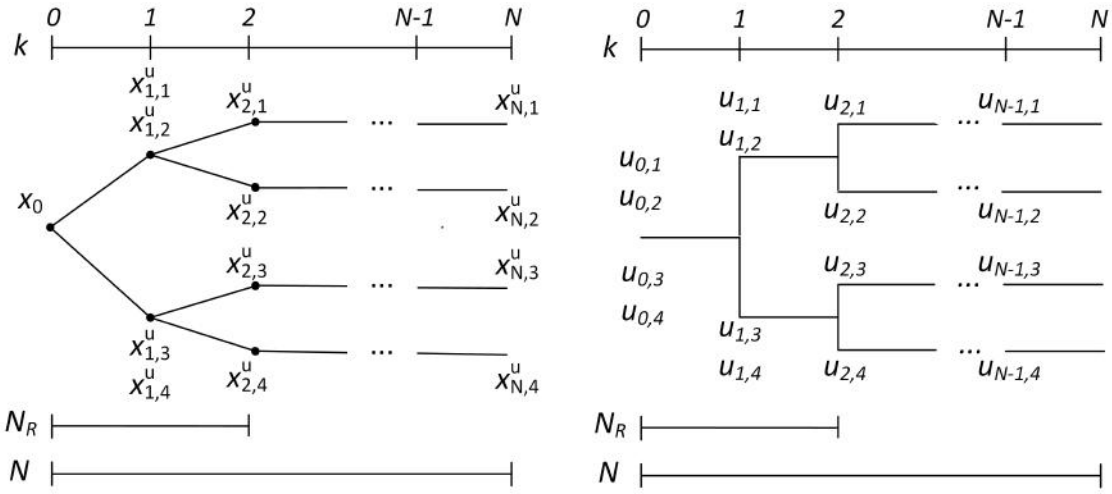

Figure 4.2: States and control actions when uncertainty realization and robust scenario are both equal to two.

The problem was implemented in CasADi Matlab Front-end. CasADi is a symbolic framework for algorithmic and numerical optimization. It was developed with the interest for dynamic optimization (ANDERSSON *et al.*, 2012). The system was scaled to adjust variables that were in different scales. IDAs algorithm was used to integrate the virtual plant, while IPOPT was employed to solve the large-scale NLP.

4.2 Open-loop Simulations Results

For each NMPC formulation it is important to tune some controller parameters, such as the sampling interval Δt, the prediction horizon N and the weights Q_W, R_W, W_W and α_W. According to HENSON (1998), the effect of these parameters in closed-loop performance is difficult to predict a priori. It is known that the sampling interval and prediction horizon have a great impact in computational effort and in the NMPC

performance. By decreasing the sampling interval, it is possible to obtain more details about faster dynamic behaviours due to an increase in the number of finite elements. However, in this case, it is also necessary to increase the prediction horizon to capture the full dynamic length. A few simulations were made to understand the virtual plant dynamic behaviour for better tuning.

The initial conditions for states, control inputs and uncertainty realization for the simulations are shown in Equation 4.12.

$$\mathbf{x}_0 = \begin{bmatrix} 65.0\,\text{bar} \\ 288.15\,\text{K} \\ 79.52\,\text{kg/s} \\ 130.80\,\text{bar} \\ 339.23\,\text{K} \end{bmatrix} \mathbf{u}_0 = \begin{bmatrix} 0.0 \\ 0.6892 \end{bmatrix} \mathbf{w}_0 = \begin{bmatrix} 75.0\,\text{bar} \end{bmatrix} \tag{4.12}$$

Where $\mathbf{x}_0$ is the virtual plant initial state vector; $\mathbf{m}_0$ is the virtual plant initial control action vector; and $\mathbf{w}_0$ is the virtual plant initial uncertainty vector.

4.2.1 Open-loop response for a source pressure disturbance

For the first test, disturbances were applied to the source pressure, P^{so}. From the initial conditions of 75 bar, a pulse with 8% magnitude, *i.e.* 6 bar, and duration of 30 seconds was applied to the system. After 70 seconds of simulation, a second pulse, now with a -8% magnitude, *i.e.* -6 bar, was applied to the system and was hold for 30 seconds. The disturbance profile is shown in Figure 4.3.

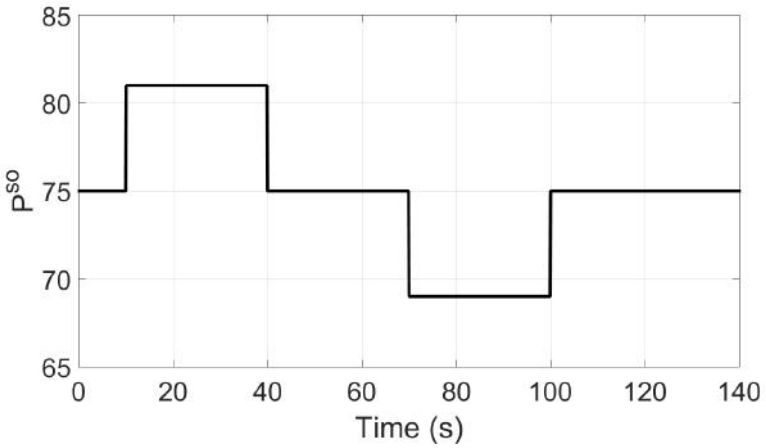

Figure 4.3: Disturbances applied to the source pressure (P^{so}) for dynamic behaviour study.

For the scrubber, the dynamic state response for such disturbance can be seen in Figures 4.4a and 4.4b. It can be observed that the scrubber pressure took approximately 5 seconds to achieve new steady states after disturbances were applied.

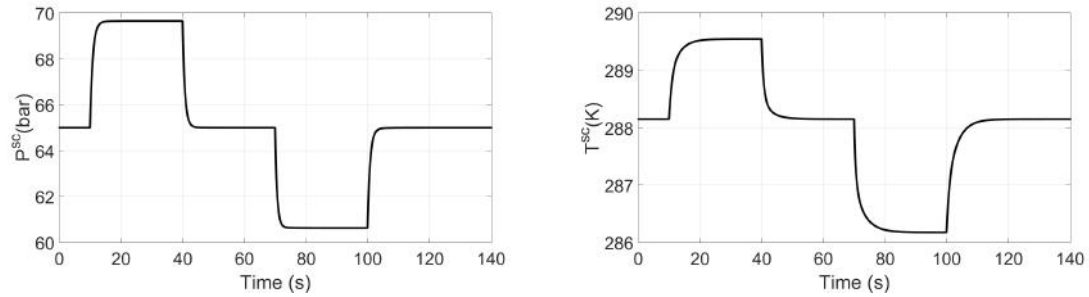

(a) (b)

Figure 4.4: Response of the scrubber states due to disturbances in the source pressure where: (a) is the scrubber pressure (P^{sc}); and (b) is the scrubber temperature (T^{sc}).

A slower dynamic can be seen for scrubber temperature. It took, approximately, 15 seconds for the steady states to be fully developed. Also, for the positive step disturbance, the new steady state was reached with scrubber pressure and temperature at 69.65 bar and 289.55 K, respectively. A negative step of 6 bar has reduced the scrubber pressure and temperature to 60.63 bar and 286.18 K, respectively. When comparing the achieved steady states, a slight disparity was detected for the scrubber pressure steady states gains, which represents a relative difference of 7.02%. As for the scrubber temperature, non-linearity was more accentuated as the steady state gain differ by 40.71%.

Disturbances to the source pressure have a direct impact in the mass flow rate entering the compressor, as is shown in Figure 4.5a. For the positive step distur-

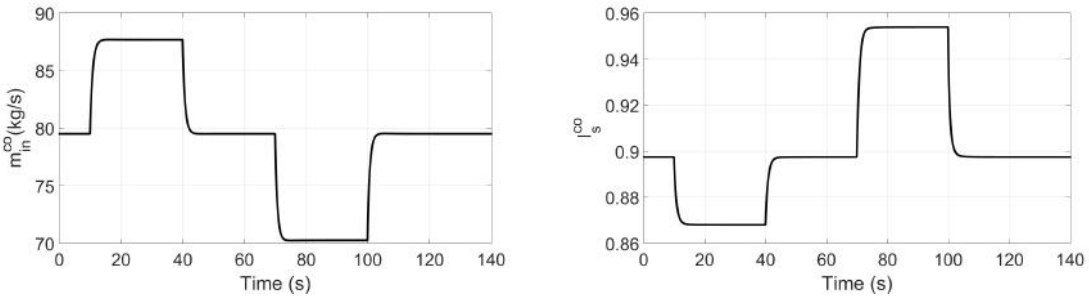

(a) (b)

Figure 4.5: Response of the compressor state and surge index due to disturbances in the source pressure where: (a) is the compressor inlet mass flow rate (m_{in}^{co}); and (b) is the surge index (I_s^{co}).

bance, the compressor mass flow rate increased from 79.518 kg/s to 87.691 kg/s, representing an 8.173 kg/s increase in the mass flow rate. For the negative step disturbance, mass flow rate was reduced from its initial value by 9.266 kg/s, reaching 70.252 kg/s. As for non-linearity, a relative difference between the steady state gains of 9.266% was obtained. In Figure 4.5b, the surge index trajectory started

by increasing the distance from surge region, going from 0.8975 to 0.8680. For the negative 6 bar step disturbance, the surge index increased from its initial value to 0.9539, indicating that operation almost reached surge. Also, steady state gains differ by 52.3%, representing the variable with the highest non-linearity for this particular disturbance. Both variables took approximately 5 seconds to reach steady state and their trajectories are shown in Figures 4.5a and 4.5b.

In Figures 4.6a and 4.6b, the plenum pressure and temperature responses are shown. For each state, a new steady state was reached in approximately 5 and

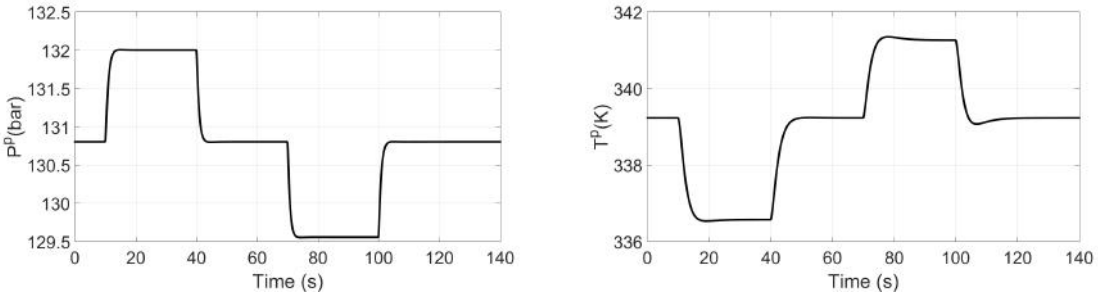

(a) (b)

Figure 4.6: Response of the plenum states due to disturbances in the source pressure where: (a) is the plenum pressure (P^p); and (b) is the plenum temperature (T^p).

15 seconds, respectively. For the positive step, the plenum pressure went from its initial value of 130.8 bar to 132.0 bar, representing an increase of 1.5 bar. After returning to its initial value, the negative step was responsible for decreasing the plenum pressure by 1.25 bar, reaching 129.55 bar. In addition, the relative difference between the steady states gains is 20.00% for the plenum pressure. A small overshoot can be seen in the plenum temperature response during its trajectory to reach steady state. For the same source disturbance, a initial temperature of 339.23 K reached steady state at 336.57 K and returned to its initial value afterwards. When the second disturbance occurred, a new steady state was obtained at 341.26 K. It can be observed that the steady state gains for the plenum temperature differs by 31.03%.

4.2.2 Open-loop response for a recycle valve manipulation

For the second test, recycle valve opening (ϕ^{rev}) was manipulated with the intent of analysing the system dynamic behaviour. After 10 seconds from the simulation beginning, a pulse was introduced in the recycle valve opening changing it from completely closed to fully opened. The pulse was hold for 30 seconds until resulting in completely closure of the recycle valve afterwards. This manipulation scheme is shown in Figure 4.7.

The scrubber dynamic states response can be seen in Figures 4.8a and 4.8b. Since

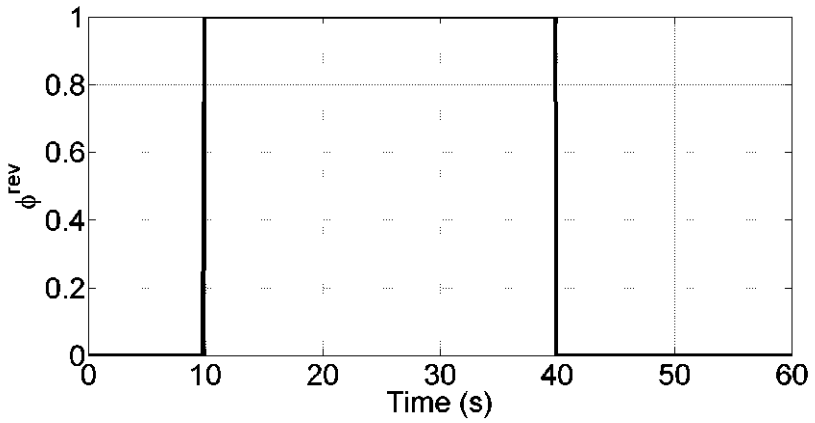

Figure 4.7: Recycle valve opening (ϕ^{rev}) pulse manipulation for dynamic behaviour study.

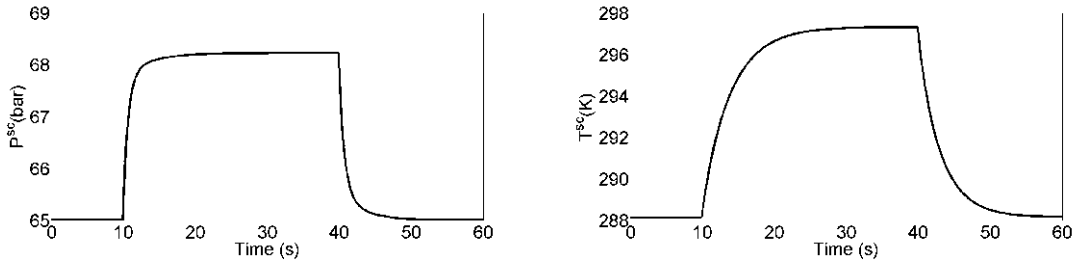

(a) (b)

Figure 4.8: Response of the scrubber states due to a pulse in the recycle valve opening where: (a) is the scrubber pressure (P^{sc}); and (b) is the scrubber temperature (T^{sc}).

the recycle valve was fully opened in simulation, new steady state for scrubber's pressure and temperature were achieved after approximately 20 and 25 seconds, respectively. The scrubber's pressure value started at 65 bar rising to 68.23 bar, which represents growth of 3.25 bar. As for the temperature, it went from 288.15 K to 297.32 K, which represents an increase of 9.17 K.

The main intent of opening the recycle valve is to increase compressor's inlet mass flow rate to steer away from surge region. It is possible to observe in Figure 4.9a that the inlet mass flow rate, which began at 79.52 kg/s, had a slight overshoot after the recycle valve was fully opened. Then, after 20 seconds, the steady state of 83.68 kg/s was achieved. As for the surge index shown in Figure 4.9b, its initial value decreased by 0.0298 reaching the steady state of 0.8677 after 20 seconds, approximately.

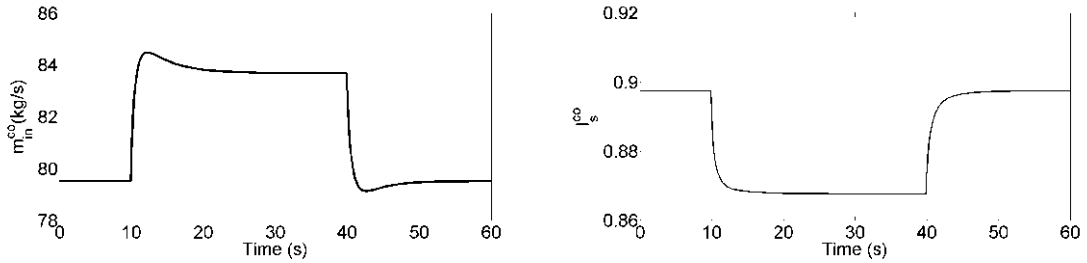

(a) (b)

Figure 4.9: Response of the compressor state and surge index due to a pulse in the recycle valve opening where: (a) is the compressor inlet mass flow rate (m_{in}^{co}); and (b) is the compressor surge index (I_s^{co}).

The plenum pressure and temperature also suffered changes when this test was applied. As it can been seen in Figure 4.10a, the plenum pressure decreased from its initial value of 130.80 bar as the recycle valve was opened. A slight overshoot occurred before the new steady state of 129.20 bar was reached after 5 seconds of transient operation. In Figure 4.10b, inverse response can be seen when changes occurred in the recycle valve opening. For the positive change, the plenum temperature decreased during a short time and, afterwards, increased from 339.23 K to 345.53 K, reaching this steady state after 30 seconds.

4.2.3 Open-loop response for compressor rotation manipulation

Compressor rotation is one of the process manipulated variables. Therefore, it is important to analyse how the compression system will behave when changes occur. The simulation started with a compressor rotation percentage equal to 68.92%. After 10 seconds, a pulse with 2% amplitude was introduced and hold for 30 seconds. At

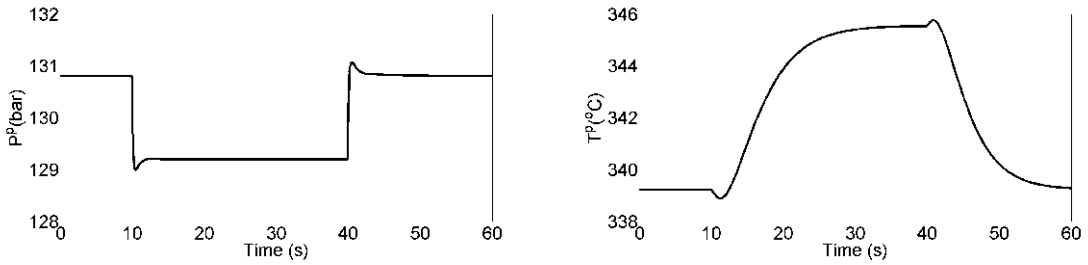

(a) (b)

Figure 4.10: Response of the plenum states due to a pulse in the recycle valve opening where: (a) is the plenum pressure (P^p); and (b) is the plenum temperature (T^p).

simulation time equal to 70 seconds, another pulse was applied to the compressor rotation. However, this time, the pulse had a -2% amplitude and was held for 30 seconds. Changes executed in the compressor rotation percentage can be seen in Figure 4.11.

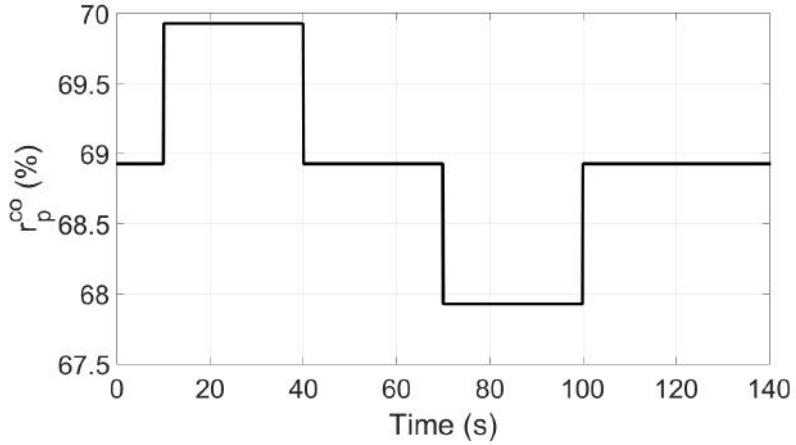

Figure 4.11: Compressor rotation percentage (r_p^{co}) pulse manipulation for dynamic behaviour study.

The influence on scrubber pressure and temperature due to changes in the compressor rotation percentage is shown in Figures 4.12a and 4.12b. Simulation started with scrubber pressure and temperature at its initial value, 65.0 bar and 288.15 K, respectively. As soon as the first pulse was introduced in the compressor rotation percentage, it took less than 5 and 15 seconds for the scrubber pressure and temperature to reach a new steady state with 64.32 bar and 288.55 K, respectively. For the scrubber pressure, an almost unnoticeable overshoot was detected. Afterwards, the system returned to its initial value and, due to another impulse manipulation in the compressor rotation percentage, a steady state was reached with scrubber pressure and temperature equal to 65.74 bar and 287.66 K. Regarding system dynamics, it seems that scrubber pressure and temperature behaves similar to a first-order sys-

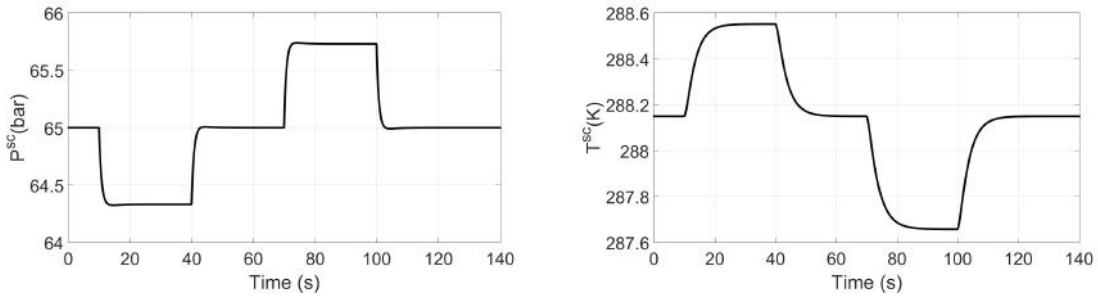

(a) (b)

Figure 4.12: Response of the scrubber states due to pulses in the compressor rotation percentage where: (a) is the scrubber pressure (P^{sc}); and (b) is the scrubber temperature (T^{sc}).

tem For both variables, the relative difference between their steady state gains were calculated and their values are 8.82% for the scrubber pressure and 18.37% for the scrubber temperature.

Compressor inlet mass flow rate and surge index transient behaviour can be observed in Figures 4.13a and 4.13b. For both variables, it was possible to notice

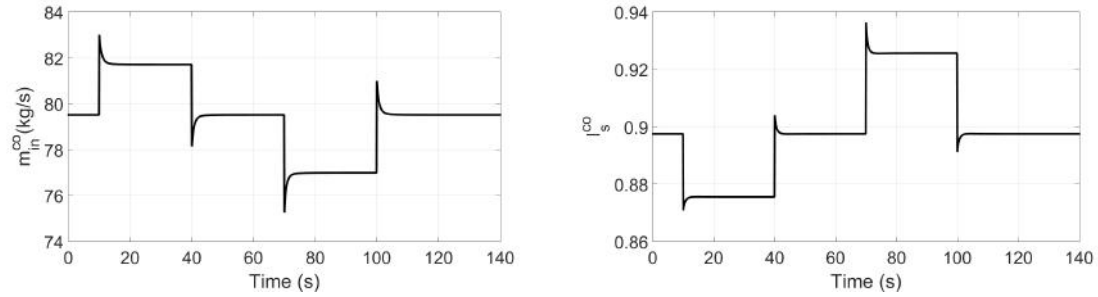

(a) (b)

Figure 4.13: Response of the compressor states and surge index due to pulses in the compressor rotation percentage where: (a) is the inlet mass flow rate (m_{in}^{co}); and (b) is the surge index (I_s^{co}).

that changes in compressor rotation percentage led to a quick overshoot that took less than 1 second to be fully developed. Also, it took approximately 4 seconds for the compressor inlet mass flow rate and surge index to reach a new steady state. The simulation started with an initial value of 79.52 kg/s for the compressor inlet mass flow rate and a surge index of 0.8975. From there, the first manipulation of compressor rotation percentage led those variables to a new steady state of 81.71 kg/s and 0.8755 surge index. After returning the system variables to its initial value, another change in the compressor inlet mass flow rate occurred. This time, both compressor inlet mass flow rate and surge index reached a steady state of 76.99 kg/s and 0.9256. Regarding non-linearities, the compressor inlet mass flow rate has a relative difference of 14.9% between its steady state gains. As for the

surge index its relative difference was 27.73%, which represents the highest value of relative difference due to compressor rotation manipulation. In Figures 4.14a and 4.14b it is possible to see the plenum pressure and temperature dynamic behaviour. Simulation started with an initial value of 130.80 bar and 339.23 K. Due to an

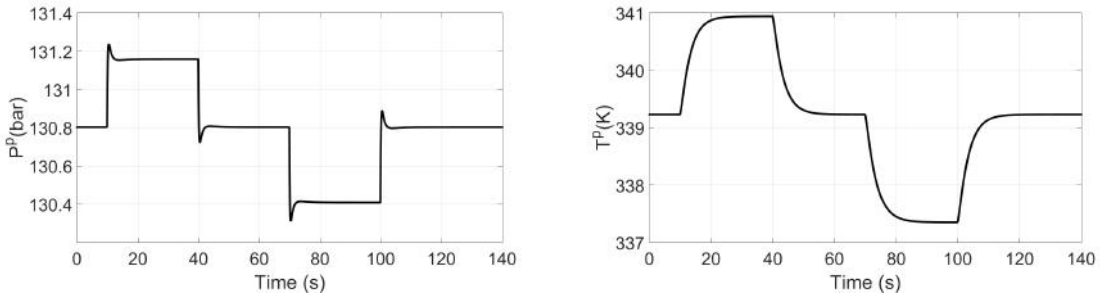

(a) (b)

Figure 4.14: Response of the plenum states due to pulses in the compressor rotation percentage where: (a) is the pressure (P^p); and (b) is the temperature (T^p).

increase in compressor percentage rotation velocity, a new steady state for plenum pressure and temperature at 131.15 bar and 340.94 K was reached. This steady state was kept until the compressor rotation percentage returned to its initial value and, consequently, both plenum pressure and temperature reached its initial value too. Afterwards, compressor rotation percentage was changed again. As a result, plenum temperature and pressure evolved towards steady state values equal to 130.41 bar and 337.38 K, until another change occurred and they returned to its initial value. For the plenum pressure, it was possible to perceive a slight overshoot that quickly disappeared, taking less than 5 seconds for a new steady state to be achieved. As for the plenum temperature, there was no sign of overshoot and it took approximately 15 seconds for another steady state to be reached. For both the plenum pressure and temperature, it was obtained a relative difference of 10.26% and 8.19% between its steady state gains, respectively.

4.2.4 Open-loop simulations remarks

A few observations are made regarding the results obtained until this point. It was seen from simulation that the surge index is highly sensitive to manipulation in the compressor rotation percentage and that some overshoots took less than 2 seconds to achieve its peak. Depending on the sampling time chosen for the NMPC, it is possible to predict the system behaviour without taking into account overshoots that occur in surge index due to changes in compressor rotation. This is highly undesirable, as the NMPC optimal solution may lead the virtual plant into surge. Therefore, to enable the NMPC to perceive this system behaviour, a small sampling

interval was chosen and is shown in Equation 4.13.

$$\Delta t = 1\,\mathrm{s} \tag{4.13}$$

Where Δt is the sampling interval in seconds.

When the simulation dynamics of all process variable were compared, it can be observed that some took at most 30 seconds until a new steady state was reached. In this way, the formulated NMPCs were tuned to predict no less than 30 seconds of simulation. Therefore, it is presented in Equation 4.14 the prediction horizon used in the NMPC formulations applied to this system.

$$N = 40 \tag{4.14}$$

Where N is the prediction horizon.

In the simulation results obtained from disturbances to the process source pressure, it is possible to infer which uncertainty value may eventually lead the system to violate its surge index boundary. In conclusion, the open-loop uncertainty vector associated with the worst realization Δ^0 is displayed in Equation 4.15.

$$\mathbf{w}^{\mathbf{u}}_{\Delta^0} = 69\,\mathrm{bar} \tag{4.15}$$

4.3 Closed-loop Simulations Results

Considering the compression system process, it is known that scrubber pressure and temperature are basically the same as those for compressor suction. The compressor performance map is obtained in a controlled environment, where suction temperature and pressure are fixed. Therefore, it is highly desirable to maintain these variables close to their set-point, as confidence in the map is reduced if the compression system operation deviates from it. For this work, it was considered that the scrubber temperature was perfectly controlled by a hierarchically lower control layer, such as a PI. Therefore, the NMPCs were designed to accomplish several objectives that are listed below in priority order:

1. Safety surge line constraint must be satisfied.
2. Scrubber pressure should stay as close as possible to its set-point.
3. Recycle valve should be closed during normal operation.
4. Changes in compressor rotation percentage should be penalized.

To fulfil these priorities, the regulatory control objectives and associated weights are introduced in Equations 4.16 and 4.17, respectively.

$$\mathbf{x}_* = \begin{bmatrix} 65\,\text{bar} \\ 288.15\,\text{K} \\ 79.52\,\text{kg/s} \\ 130.80\,\text{bar} \\ 339.23\,\text{K} \end{bmatrix} \quad \mathbf{u}_* = \begin{bmatrix} 0.0 \\ 0.6892 \end{bmatrix} \tag{4.16}$$

$$Q_W = \begin{bmatrix} 1 & 0 & 0 & 0 & 0 \\ 0 & 0 & 0 & 0 & 0 \\ 0 & 0 & 0 & 0 & 0 \\ 0 & 0 & 0 & 0 & 0 \\ 0 & 0 & 0 & 0 & 0 \end{bmatrix} P_W = \begin{bmatrix} 1 & 0 & 0 & 0 & 0 \\ 0 & 0 & 0 & 0 & 0 \\ 0 & 0 & 0 & 0 & 0 \\ 0 & 0 & 0 & 0 & 0 \\ 0 & 0 & 0 & 0 & 0 \end{bmatrix} R_W = \begin{bmatrix} 0 & 0 \\ 0 & 0 \end{bmatrix} W_W = \begin{bmatrix} 0 & 0 \\ 0 & 10 \end{bmatrix} \tag{4.17}$$

Where $\mathbf{x}_*$ is the state at set-point; $\mathbf{u}_*$ is the control value at set-point; Q_W is the stage cost state weight matrix; R_W is the stage cost input weight matrix; P_W is the terminal cost weight matrix; and W_W is the stage cost input change weight matrix.

Equation 4.18 sets the slack variable weight (α_W) that is associated with surge avoidance strategy implemented in the NMPC formulations.

$$\alpha_W = 1 \tag{4.18}$$

Regarding states, algebraic variables and input constraints, some observations are made. Almost all variables must have positive values and do not have an upper bound constraint. A few exceptions exist and are enlisted from Equation 4.19a to Equation 4.19e.

$$0 \leq I_s^{co} \leq \delta_{ssl}^{co} = 0.92 \tag{4.19a}$$

$$1.0 \leq \Psi^{co} \tag{4.19b}$$

$$0 \leq \phi^{rev} \leq a \tag{4.19c}$$

$$0 \leq r_p^{co} \leq 1.0 \tag{4.19d}$$

$$\Delta\phi^{rev} \leq \frac{1}{15} \tag{4.19e}$$

Where the surge line constraint is shown in Equation 4.19a; compressor pressure ratio lower bound is present in Equation 4.19b; recycle valve opening constraint associated with the slack variable (a) is seen in Equation 4.19c; compressor rotation percentage constraint is shown in Equation 4.19d; and, due to speed limitations of the control valve, Equation 4.19e is used to limit its opening rate at each stage.

The initial conditions for states, control inputs and uncertainty realization for the closed-loop simulation are shown in Equation 4.12.

To simulate an unknown disturbance in the closed-loop system, a fluctuation was introduced in the source pressure as a periodic function, which is shown in Equation 4.20.

$$P_k^{so} = P_0^{so}\left[1 + \theta(k-5)0.08\sin\left(\frac{k-5}{4}\right)\right], \quad \forall k \geq 1 \tag{4.20}$$

With the heaviside function given by Equation 4.21,

$$\theta(k-5) = \begin{cases} 0 & k < 5 \\ 1 & k \geq 5 \end{cases} \tag{4.21}$$

Where $\theta(\cdot)$ is the heaviside function.

The virtual plant uncertainty realization remained in its expected value of 75 bar during the first 5 seconds of simulation. Afterwards, a periodic oscillation is introduced with a time period of 25.13 seconds with maximum and minimum values of 81 bar and 69 bar, respectively. In Figure 4.15, the source pressure behaviour is shown for this study.

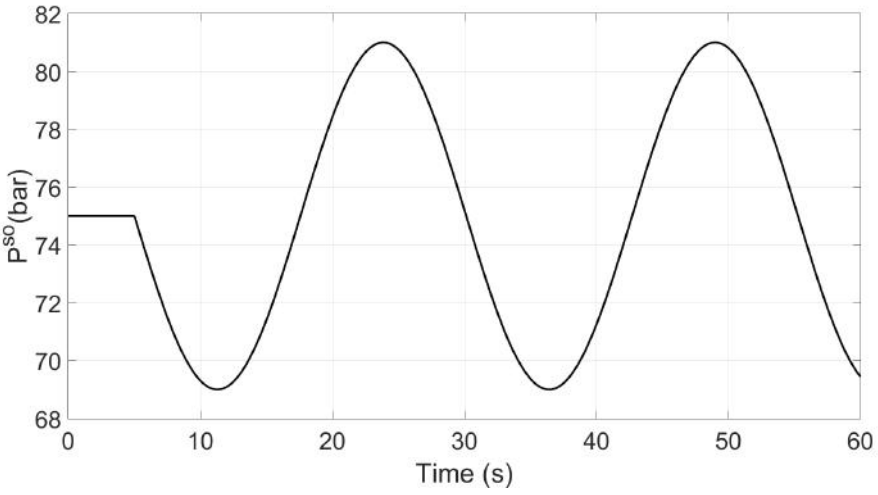

Figure 4.15: Oscillatory disturbance applied to the source pressure for unknown disturbance study.

As each controller deals with uncertainty differently, open-loop uncertainty realization are introduced in Equation 4.22.

$$\begin{aligned} \mathbf{w}_{\mathbb{E}}^{\mathbf{u}} &= \begin{bmatrix} 75\,\text{bar} \end{bmatrix} \\ \mathbf{w}_{\Delta 0}^{\mathbf{u}} &= \begin{bmatrix} 69\,\text{bar} \end{bmatrix} \\ \mathbf{w}_{\mathcal{S}}^{\mathbf{u}} &= \begin{bmatrix} 69\,\text{bar} & 75\,\text{bar} & 81\,\text{bar} \end{bmatrix}^T \end{aligned} \tag{4.22}$$

Where $\tilde{\mathbf{w}}^{\mathbf{u}}_{\mathbb{E}}$ is the open-loop uncertainty vector associated with the expected realization; $\mathbf{w}^{\mathbf{u}}_{\Delta}$ is the open-loop uncertainty vector associated with the worst realization Δ^0; and $\mathbf{w}^{\mathbf{u}}_{\mathcal{S}}$ is the multi-stage open-loop uncertainty vector. Robust horizon was set to $N_R = 1$ and the uncertainty set ($\mathbb{W}$) was discretized in three values ($N_\Delta = 3$), consequently the multi-stage NMPC tracks three different scenarios. The uncertainty trajectory of each scenario is shown in Equation 4.23.

$$\tilde{\mathbf{w}}^{\mathbf{u}}_{\mathbf{S_1}} = \begin{bmatrix} 69\,\text{bar} \\ 69\,\text{bar} \\ 69\,\text{bar} \end{bmatrix} \quad \tilde{\mathbf{w}}^{\mathbf{u}}_{\mathbf{S_2}} = \begin{bmatrix} 75\,\text{bar} \\ 75\,\text{bar} \\ 75\,\text{bar} \end{bmatrix} \quad \tilde{\mathbf{w}}^{\mathbf{u}}_{\mathbf{S_3}} = \begin{bmatrix} 81\,\text{bar} \\ 81\,\text{bar} \\ 81\,\text{bar} \end{bmatrix} \tag{4.23}$$

For the multi-stage NMPC formulation, it was considered a lack of information regarding likelihood of uncertainty. Therefore, scenario likelihood was set according to Equation 4.24.

$$\omega_s = \begin{bmatrix} 1 & 1 & 1 \end{bmatrix}^T \tag{4.24}$$

where ω_s is the weight associated with each scenario or scenario likelihood.

4.3.1 Virtual plant closed-loop behaviour

One of the controlling objectives is to keep the scrubber pressure at its set-point. Therefore, the closed-loop behaviour of the scrubber pressure is shown in Figure 4.16. In the first 5 seconds of simulation, it is possible to observe that the scrubber

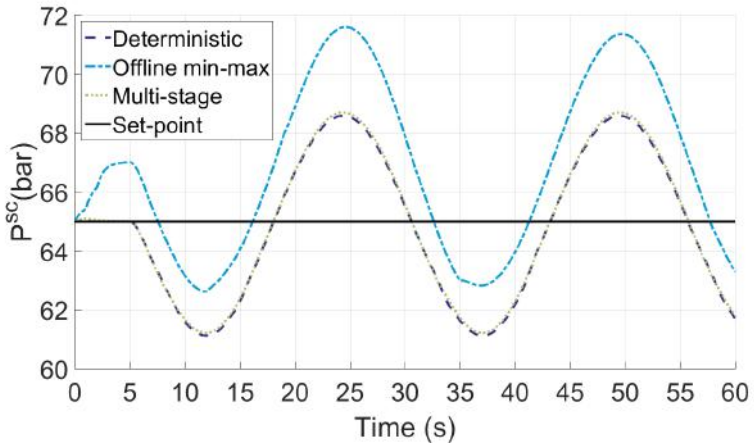

Figure 4.16: Closed-loop trajectory of the scrubber pressure (P^{sc}) considering an unknown oscillatory disturbance to the source pressure.

pressure was perfectly controlled by the deterministic NMPC as the system was not affected by any disturbances and the deterministic model matched exactly the virtual plant. During this time, a slight deviation can be seen when multi-stage NMPC was controlling the system. As for the offline min-max NMPC, a great deviation from

the set-point occurred in the first 5 seconds of simulation due to model mismatch. Afterwards, the periodic disturbance was introduced in the virtual plant and the three closed-loop trajectories of the scrubber pressure started to oscillate. Almost no difference can be perceived between the deterministic and multi-stage case. As for the offline min-max closed-loop trajectory, its is possible to observe that the scrubber pressure deviated less from its set-point when the virtual plant uncertainty assumed its lowest value, *i.e.*, its worst value, while a higher deviation was seen when the uncertainty assumed its highest value.

Another control objective is to keep the operation running without any surge line violation. Therefore, the closed-loop trajectory of the compressor surge index is shown in Figure 4.17. During the first 5 seconds of simulation it is possible

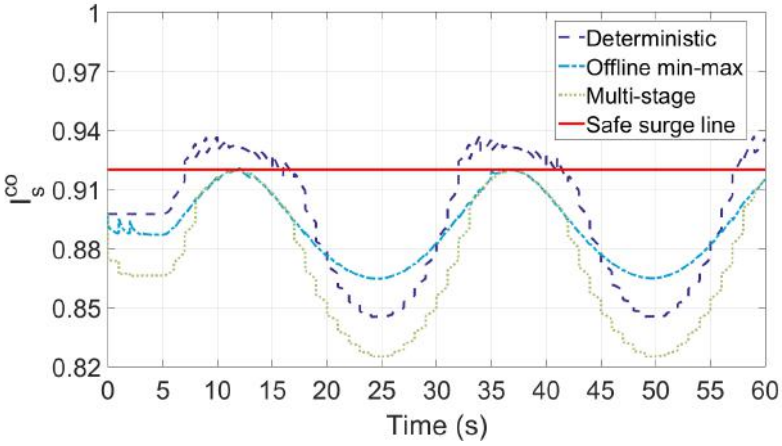

Figure 4.17: Closed-loop trajectory of the surge index (I_s^{co}) considering an unknown oscillatory disturbance to the source pressure.

to observe that all three controllers were capable of maintaining the closed-loop surge index below the safe surge line. However, as the source pressure started to oscillate, the deterministic NMPC led the actual system to violate the safe surge line constraint. The first violation occurred after 7.01 seconds of simulation and continued for 15.69 seconds. As for the second constraint violation, it occurred after 32.01 seconds of simulation and continued for 40.82 seconds. Finally, the third constraint violation was observed after 57.22 seconds had elapsed and continued until the end of simulation. Therefore, considering only the 50 seconds of simulation where source pressure oscillated, it can be concluded that deterministic NMPC maintained the safe surge line restriction satisfied during 59.48% of the time. This contrasts with both offline min-max and multi-stage NMPC, which were capable of maintaining the surge index closed-loop trajectory below safe surge line.

To achieve control objectives, anti-surge valve and compressor rotation were manipulated. The results can be observed in Figures 4.18 and 4.19. For the deterministic NMPC, the simulation began with the recycle valve closed and a steady

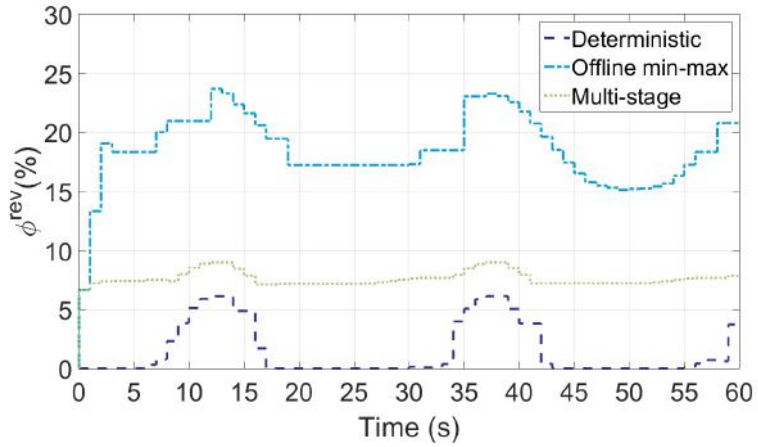

Figure 4.18: Anti-surge valve manipulation in a compression system under an unknown oscillatory disturbance to the source pressure. ϕ^{rev} is the recycle valve opening percentage.

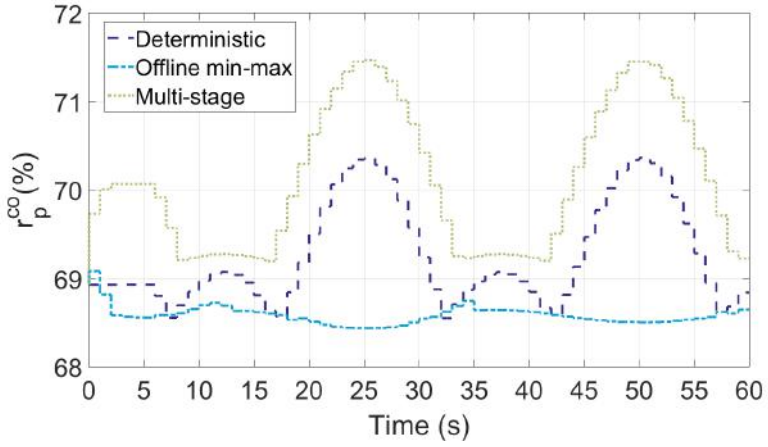

Figure 4.19: Compressor rotation percentage (r_p^{co}) manipulation in a compression system under an unknown oscillatory disturbance to the source pressure.

compressor rotation percentage. As source pressure decreased below its expected value, deterministic NMPC opened the recycle valve and performed small changes to the compressor rotation percentage. This behaviour occurred twice during the simulation window. Full valve closure can be seen when source pressure increased to a value above the expected. Moreover, compressor rotation percentage increased, adding more energy to the fluid and, consequently, increasing its volumetric flow rate as can be seen in Figure 4.20.

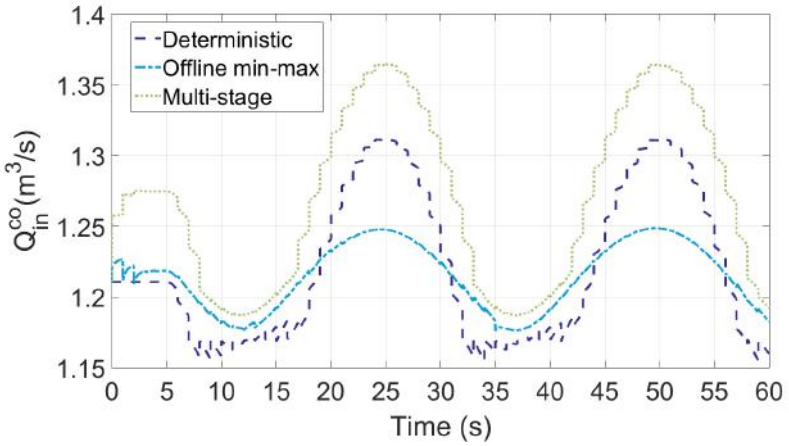

Figure 4.20: Closed-loop trajectory of the compressor inlet volumetric flow rate (Q_{in}^{co}) considering an unknown oscillatory disturbance to the source pressure.

For the offline min-max NMPC, the recycle valve was quickly opened during the initial part of simulation. Also, it was detected that when source pressure was lower than its expected value, recycle valve opening increased.

The multi-stage NMPC presented characteristics of both deterministic and offline min-max NMPC when manipulated variables were analysed. Despite keeping the recycle valve opened during the entire simulation, multi-stage NMPC opening percentage was usually 3 times less than offline min-max NMPC. Regarding compressor rotation percentage, a similar profile can be seen between deterministic and multi-stage NMPC after 8 seconds of simulation. However, multi-stage NMPC employs a higher rotation speed to the compressor.

For a better understanding of the decision making procedure taken by deterministic, offline min-max and multi-stage NMPC, some open-loop trajectories obtained at sampling times $t_k = \begin{bmatrix} 0 & 11 & 23 \end{bmatrix}$ seconds will be analysed in the next subsections. In Figure 4.21, the sampling times were highlighted to cover expected, low and high uncertainty realizations of the source pressure, respectively.

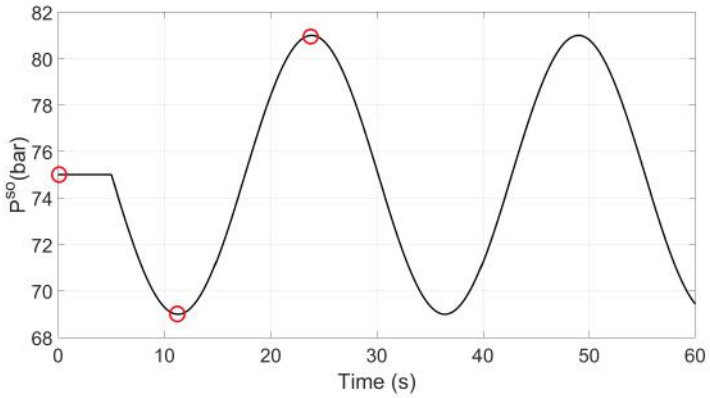

Figure 4.21: Oscillatory disturbance applied to the source pressure (P^{so}) for an unknown disturbance study with sampling times highlighted.

4.3.2 Deterministic NMPC open-loop decision making

Deterministic NMPC considered that source pressure assumes the expected value of 75 bar. Therefore, despite disturbances, the only information that controller had from the virtual plant was its current states.

Deterministic NMPC with sampling time $t_k = 0$ seconds was considered. Predicted trajectory for the scrubber pressure was kept in its set-point during the whole prediction horizon, as it can be seen in Figure 4.22. As for the surge line, the deter-

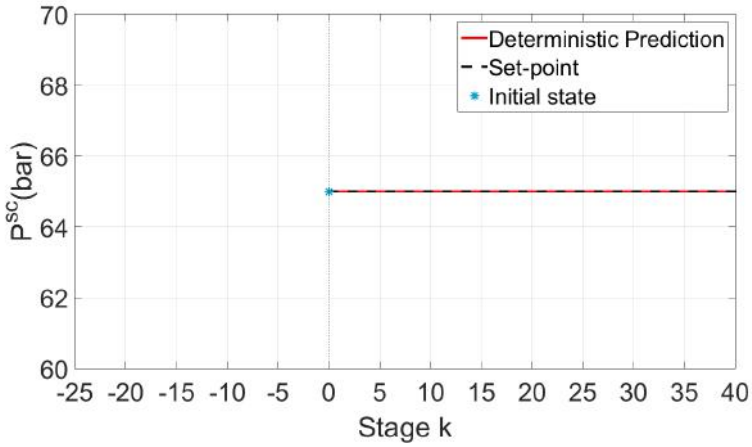

Figure 4.22: Predicted scrubber pressure (P^{sc}) for the deterministic NMPC at sampling time $t_k = 0$ seconds.

ministic prediction was far from violating this constraint, which can be observed in Figure 4.23. Therefore, no changes in the manipulated variable were necessary, as all objectives were accomplished and no model mismatch existed. In Figures 4.24 and 4.25, both the recycle valve opening and the compressor rotation percentage can be seen. In conclusion, as the source pressure of the virtual plant assumed its expected value, deterministic NMPC did not have any unexpected behaviour due

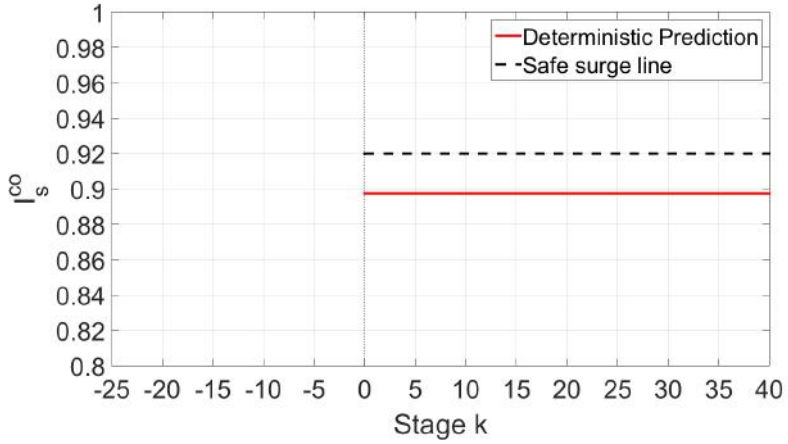

Figure 4.23: Predicted surge index (I_s^{co}) for the deterministic NMPC at sampling time $t_k = 0$ seconds.

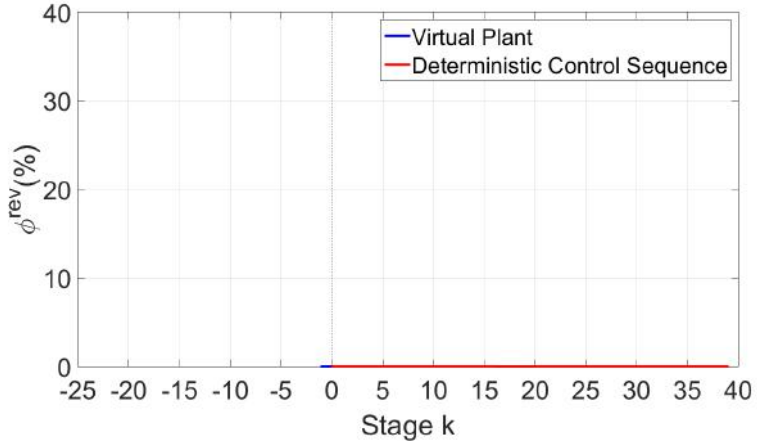

Figure 4.24: Optimal control sequence for the recycle valve opening (ϕ^{rev}) obtained by the deterministic NMPC at sampling time $t_k = 0$ seconds.

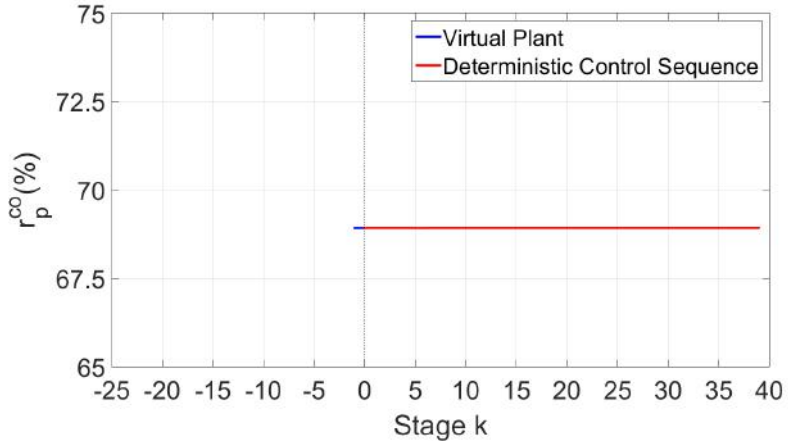

Figure 4.25: Optimal control sequence for the compressor rotation percentage (r_p^{co}) obtained by the deterministic NMPC at sampling time $t_k = 0$ seconds.

to a perfect match between the open-loop model considered in the NMPC and the virtual plant model.

The deterministic NMPC prediction at sampling time $t_k = 11$ seconds was also considered. It can be observerd in Figure 4.26 that the current initial state of the scrubber pressure is below its set-point. Also, deterministic NMPC predicted a tra-

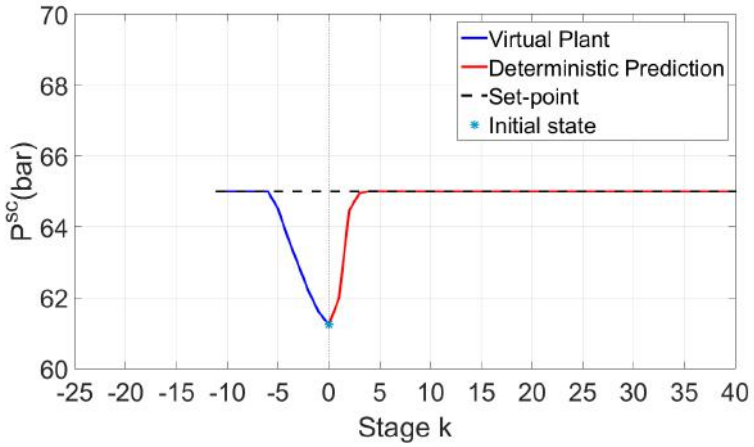

Figure 4.26: Predicted scrubber pressure (P^{sc}) for the deterministic NMPC sampling time $t_k = 11$ seconds.

jectory that reached the desired set-point in less than $k = 5$ stages. To perform that, deterministic NMPC computed an optimal control sequence for the recycle valve opening and the compressor rotation percentage. From the optimal control sequence shown in Figure 4.27, it can be observed that deterministic NMPC calculated a control sequence where the recycle valve was opened during the first stages and was closed thereafter. As for the compressor rotation percentage control sequence

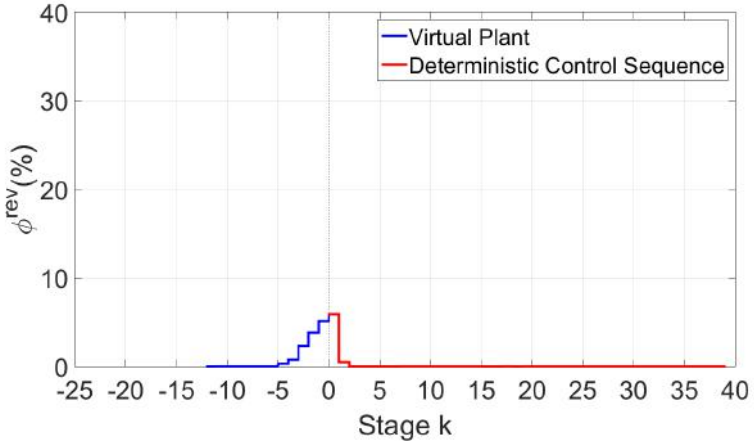

Figure 4.27: Optimal control sequence for the recycle valve opening (ϕ^{rev}) obtained by the deterministic NMPC at sampling time $t_k = 11$ seconds.

obtained by the deterministic NMPC, minor changes occurred until the scrubber pressure set-point was reached in the predicted trajectory and no further change in

rotation was needed. The control sequence for compressor rotation percentage can be seen in Figure 4.28.

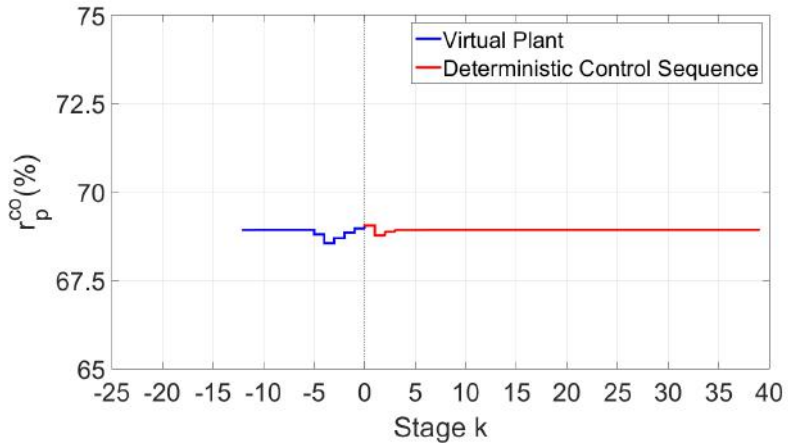

Figure 4.28: Optimal control sequence for the compressor rotation percentage (r_p^{co}) obtained by the deterministic NMPC at sampling time $t_k = 11$ seconds.

Through surge index behaviour in Figure 4.29, it is possible to comprehend the reason why the recycle valve was opened by deterministic NMPC. Violation of the

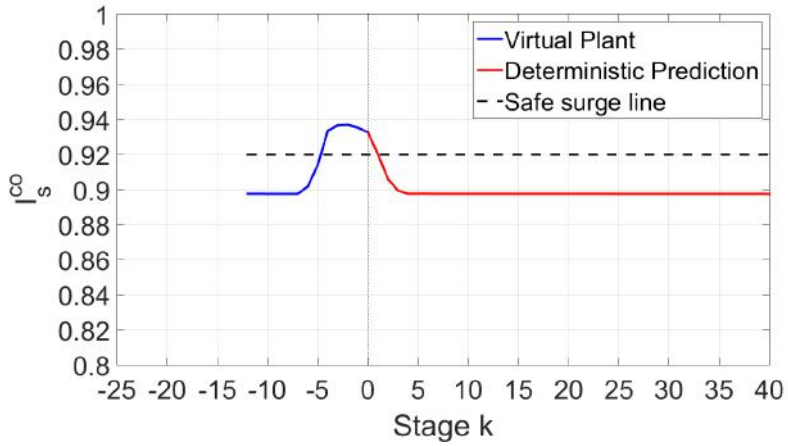

Figure 4.29: Predicted surge index (I_n^{co})for the deterministic NMPC at sampling time $t_k = 11$ seconds.

safe surge constraint occurred in the virtual plant, which means that surge index must be reduced for the current control inputs and initial dynamic states. During deterministic prediction, surge index decreased at the first stages until scrubber pressure prediction reached its set-point and no further control action was taken.

Finally, deterministic NMPC with sampling time $t_k = 23$ seconds was considered. The scrubber pressure prediction by the deterministic NMPC is shown in Figure 4.30. From this, it is possible to observe that scrubber pressure initial state was above the desired set-point. Despite that, deterministic NMPC prediction shows that it would be possible to achieve a scrubber pressure set-point in $k = 4$ stages.

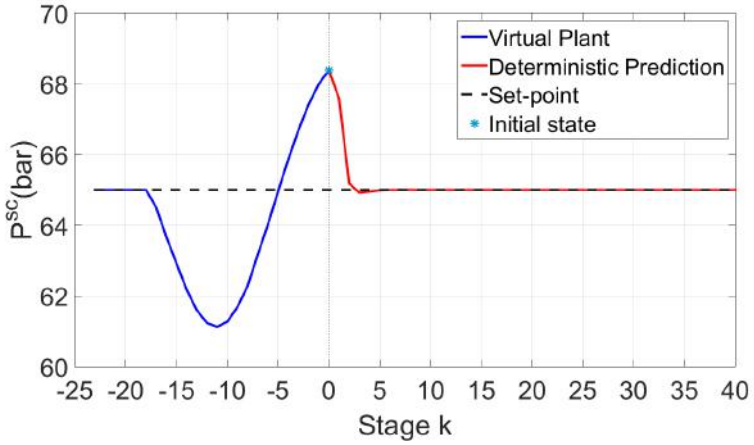

Figure 4.30: Predicted scrubber pressure (P^{sc}) for the deterministic NMPC at sampling time $t_k = 23$ seconds.

As for the surge index, Figure 4.31 shows that virtual plant surge index was below the safe surge constraint and, consequently, the constraint was satisfied for the entire prediction horizon.

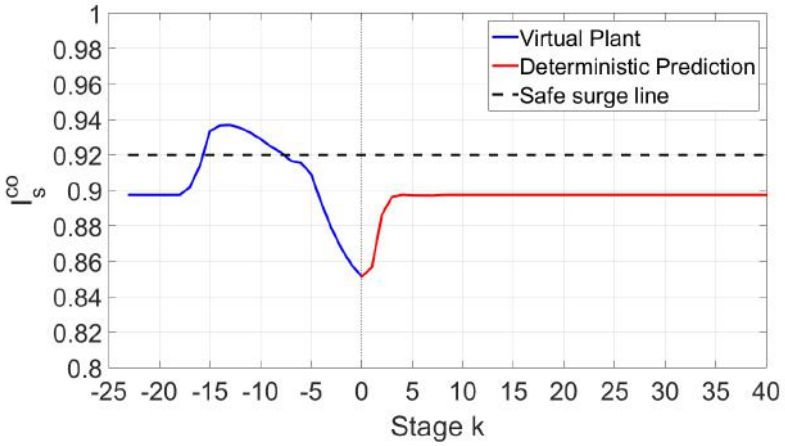

Figure 4.31: Predicted surge index (I_s^{co}) for the deterministic NMPC at sampling time $t_k = 23$ seconds.

No control action was performed to open the recycle valve as risk of constraint violation was not detected in deterministic NMPC open-loop prediction. Therefore, recycle valve was kept closed as shown in the control sequence present in Figure 4.32. Since the recycle valve was kept closed for the entire prediction horizon, changes in compressor rotation percentage were performed to reach the scrubber pressure set-point. Figure 4.33 displays the control sequence of the compressor rotation percentage.

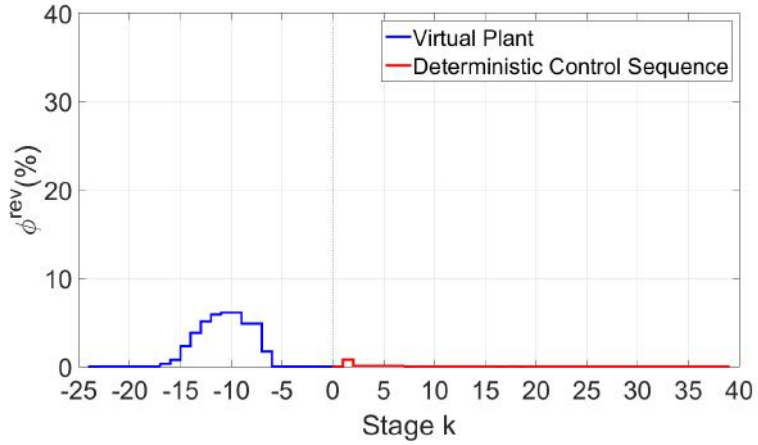

Figure 4.32: Optimal control sequence for the recycle valve opening (ϕ^{rev}) obtained by the deterministic NMPC at sampling time $t_k = 23$ seconds.

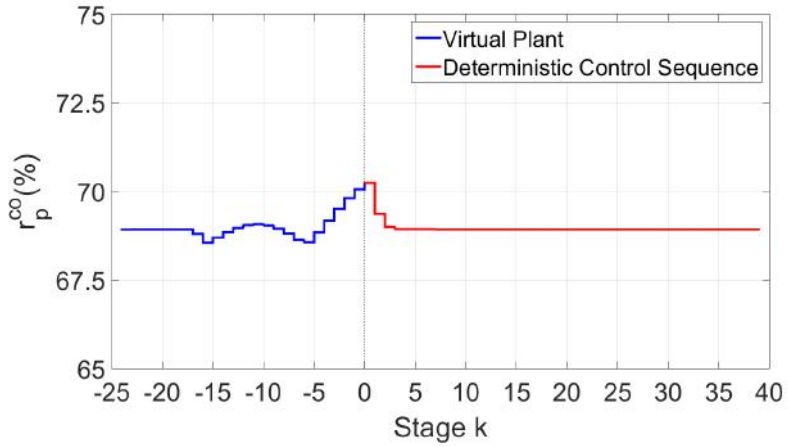

Figure 4.33: Optimal control sequence for the compressor rotation percentage (r_p^{co}) obtained by the deterministic NMPC at sampling time $t_k = 23$ seconds.

4.3.3 Offline min-max NMPC open-loop decision making

Offline min-max NMPC considered that source pressure assumed its lowest or worst value at 69 bar. Therefore, despite disturbances, the only information that the controller had from the virtual plant was its current states.

Offline min-max NMPC prediction at sampling time $t_k = 0$ seconds was considered. Figure 4.34 shows that the initial state of the scrubber pressure has the same value as the desired set-point and one would expect that offline min-max prediction trajectory would stay at the set-point. However, the scrubber pressure trajectory predicted by offline min-max NMPC was not asymptotically stable.

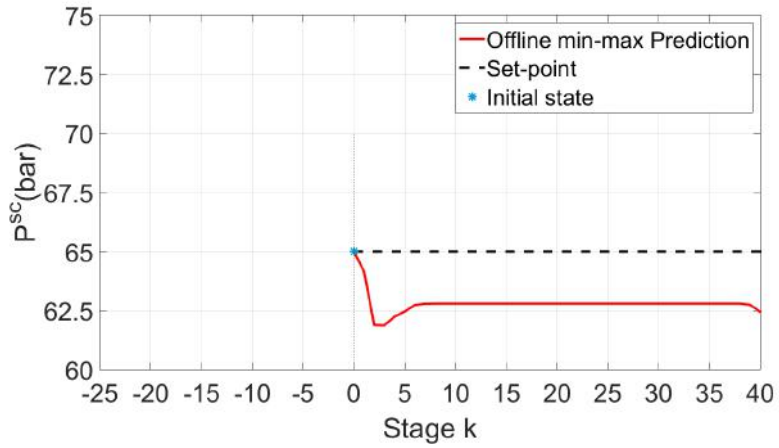

Figure 4.34: Predicted scrubber pressure (P^{sc}) for the offline min-max NMPC at sampling time $t_k = 0$ seconds.

To further investigate this behaviour, offline min-max predicted surge index trajectory was introduced in Figure 4.35. Controller prediction shows that the safe

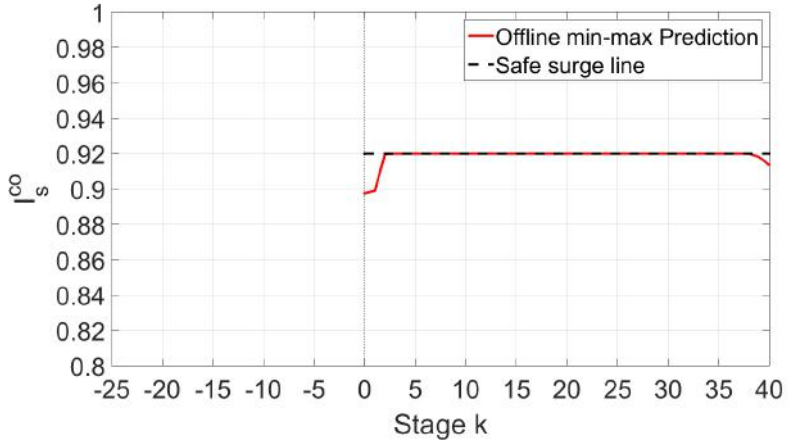

Figure 4.35: Predicted surge index (I_s^{co}) for the offline min-max NMPC at sampling time $t_k = 0$ seconds.

surge line constraint was active during a significant period of the prediction horizon.

This reduced the amount of degrees of freedom available to steer the scrubber pressure to its set-point. Optimal control sequence in Figure 4.36 shows that the recycle valve should be opened to avoid constraint violation by open-loop surge index. As

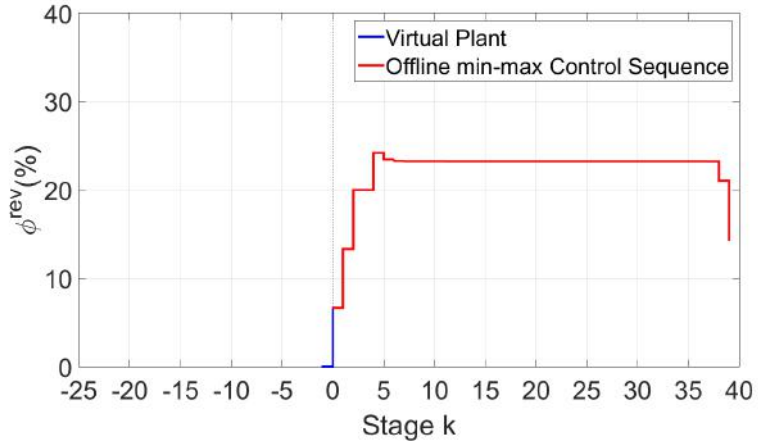

Figure 4.36: Optimal control sequence for the recycle valve opening (ϕ^{rev}) obtained by the offline min-max NMPC at sampling time $t_k = 0$ seconds.

changes in the compressor rotation may cause constraint violation, it is possible to observe in Figure 4.37 that after $k = 5$ stages, the compressor rotation percentage was kept constant.

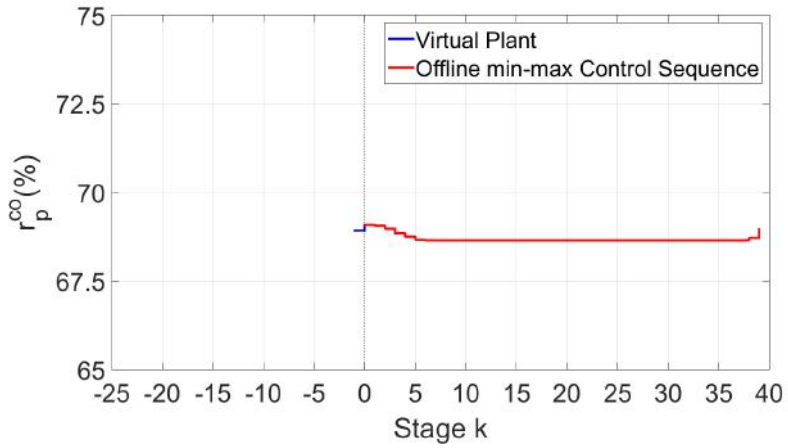

Figure 4.37: Optimal control sequence for the compressor rotation percentage (r_p^{co}) obtained by the offline min-max NMPC at sampling time $t_k = 0$ seconds.

The offline min-max NMPC at sampling time $t_k = 11$ seconds is also considered. For this case, source pressure assumes the lowest value of the uncertainty. Therefore, there was no mismatch between offline min-max open-loop model and virtual plant model. Figure 4.38 introduces the predicted trajectory for the scrubber pressure. Open-loop scrubber pressure stayed at the vicinity of its initial state value during the whole predicted trajectory, which is unfortunate since the desired set-point was not reached.

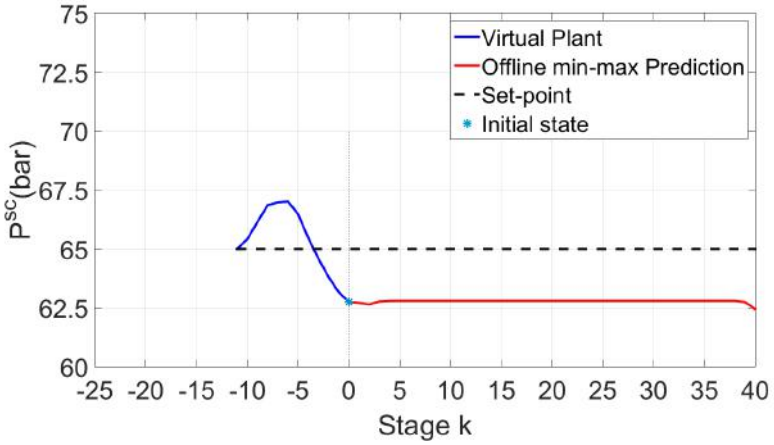

Figure 4.38: Predicted scrubber pressure (P^{sc}) for the offline min-max NMPC at sampling time $t_k = 11$ seconds.

Offline min-max prediction trajectory of the surge index is shown in Figure 4.39, where it can be seen that safe surge line was active in the current state of the virtual plant. Constraint activation was also perceived for the offline min-max prediction trajectory. To avoid constraint violation, an optimal control sequence where the recycle valve was maintained opened is shown in Figure 4.40.

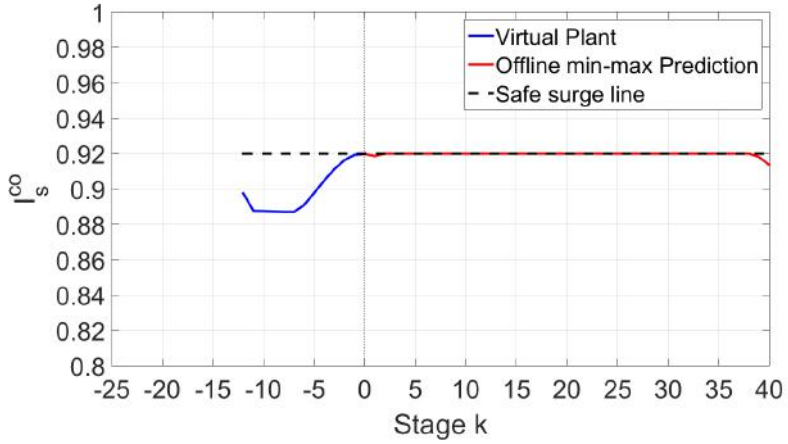

Figure 4.39: Predicted surge index for the offline min-max NMPC at sampling time $t_k = 11$ seconds.

For the compressor rotation percentage shown in Figure 4.41, it is possible to observe that almost no changes in rotation occurred in the predicted offline min-max optimal control sequence. Therefore, offline min-max NMPC showed that surge avoidance was handled by the recycle valve when it was mainly used to control surge index, while compressor rotation was maintained near its current value.

Offline min-max NMPC at sampling time $t_k = 23$ seconds is considered. In Figure 4.42 introduces the predicted trajectory of scrubber pressure by the offline min-max NMPC. Initial state of the open-loop trajectory presented a higher value

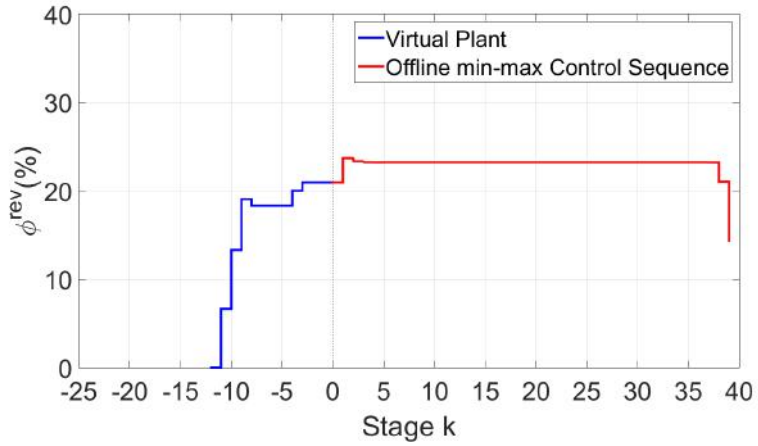

Figure 4.40: Optimal control sequence for the recycle valve opening (ϕ^{rev}) obtained by the offline min-max NMPC at sampling time $t_k = 11$ seconds.

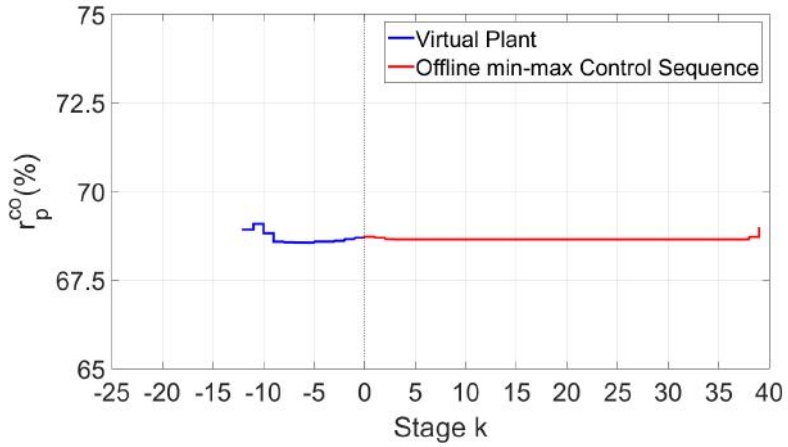

Figure 4.41: Optimal control sequence for the surge index (I_s^{co}) by the offline min-max NMPC at sampling time $t_k = 11$ seconds.

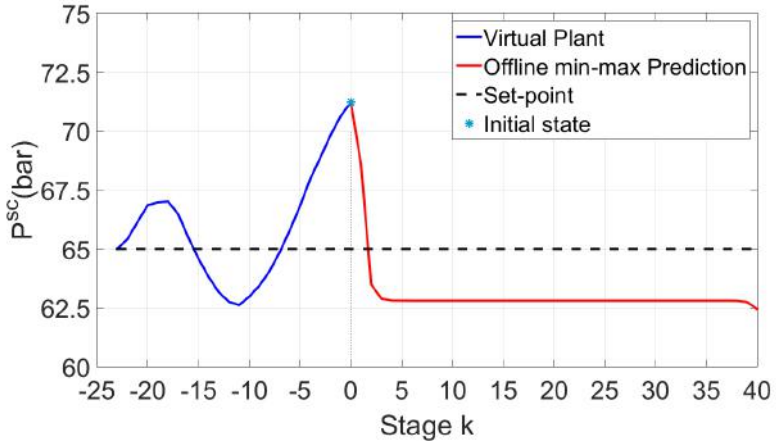

Figure 4.42: Predicted scrubber pressure (P^{sc}) for the offline min-max NMPC at sampling time $t_k = 23$ seconds.

than desired set-point, which indicates that scrubber pressure should be reduced to accomplish one of the controller objectives. Despite that, what was seen in the prediction trajectory was that the scrubber pressure crossed the set-point and steered away from it afterwards. In conclusion, offline min-max NMPC could not obtain optimal input values for the recycle valve opening and compressor rotation percentage, which led to an unfulfilled set-point tracking objective. Surge index predicted trajectory is shown in Figure 4.43. It can be seen that after a few stages safe surge line constraint became active, which means offline min-max NMPC took control decisions to avoid constraint violation.

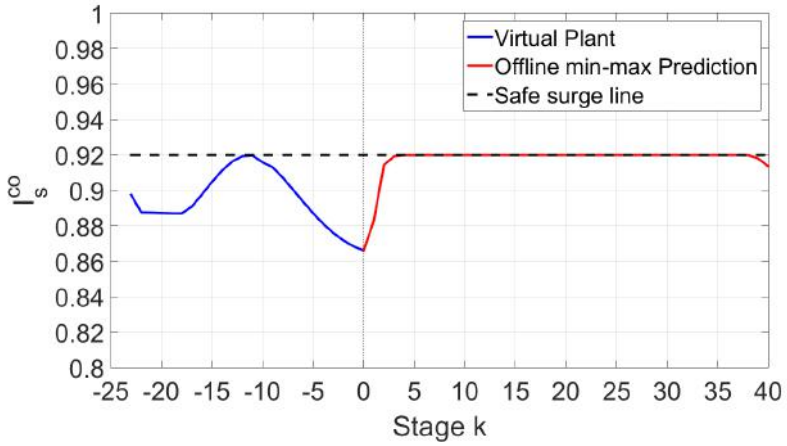

Figure 4.43: Predicted surge index (I_s^{co}) for the offline min-max NMPC at sampling time $t_k = 23$ seconds.

In Figures 4.44 and 4.45, both recycle valve and compressor rotation percentage optimal input values are shown. Recycle valve is maintained opened due to the risk of constraint violation detected by offline min-max NMPC. As for compressor rotation percentage, positive changes would decrease scrubber pressure, thus increasing distance from the set-point. On the other hand, negative changes would cause safe surge line constraint violation. Therefore, input values were kept constant for most part of the compressor percentage optimal control sequence.

4.3.4 Multi-stage NMPC open-loop decision making

Discretization of the uncertainty led multi-stage NMPC to consider three scenarios for the source pressure: high, expected and low realizations of 81, 75.0 and 69 bar, respectively. In this way, three distinct trajectories were predicted by the controller with the non-anticipative constraints being the common factor. Multi-stage NMPC formulation with robust horizon $N_R = 1$ implies that, due to the presence of non-anticipative constraints in the controller formulation, the first control action must be the same for all scenarios. Despite disturbances, the only information that the

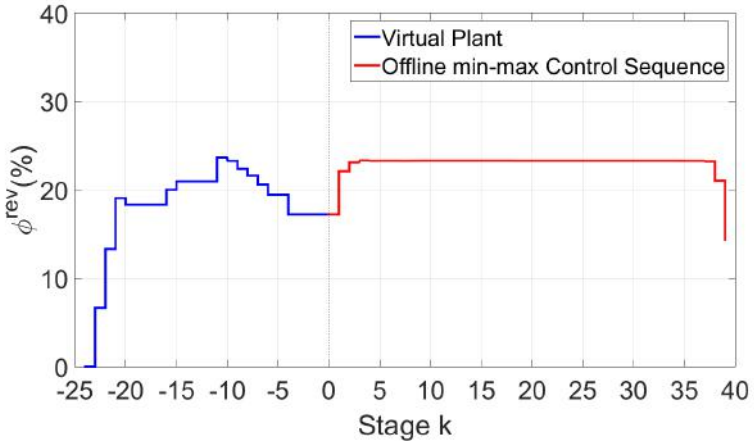

Figure 4.44: Optimal control sequence for the recycle valve opening (ϕ^{rev}) obtained by the offline min-max NMPC at sampling time $t_k = 23$ seconds.

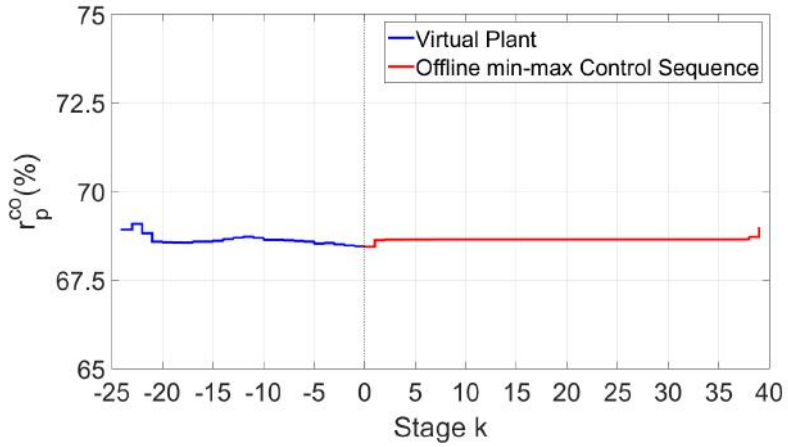

Figure 4.45: Optimal control sequence for the compressor rotation percentage (r_p^{co}) obtained by the offline min-max NMPC at sampling time $t_k = 23$ seconds.

controller had from the virtual plant was its current states.

NMPC prediction at sampling time $t_k = 0$ seconds is considered. Set-point tracking was one of the controller objectives. Hence, multi-stage NMPC prediction for the scrubber pressure is shown in Figure 4.46. During the initial stages, scrubber

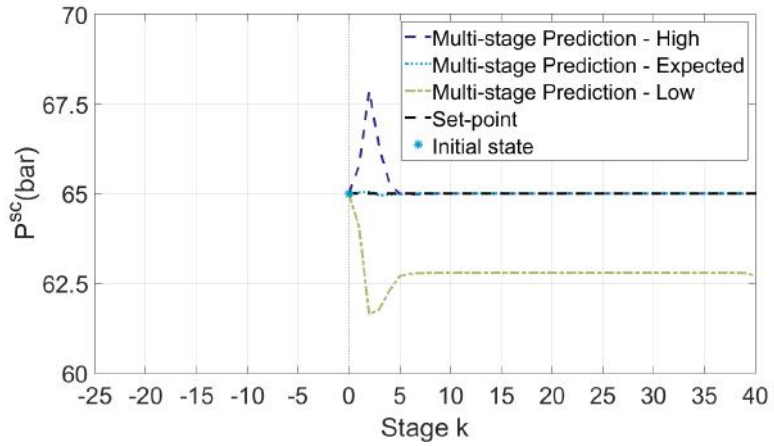

Figure 4.46: Predicted scrubber pressure (P^{sc}) for the multi-stage NMPC at sampling time $t_k = 0$ seconds.

pressure steered away from the desired set-point for both high and low uncertainty realizations, while for the expected source pressure value it was kept close to the set-point. From the three trajectories, both high and expected uncertainty realizations reached the desired set-point at a later stage. The sudden shift in the high uncertainty realization trajectory behaviour may be explained by the decreasing influence of non-anticipative constraints as stages move away from $k = 0$. For the low uncertainty realization, an offset was present.

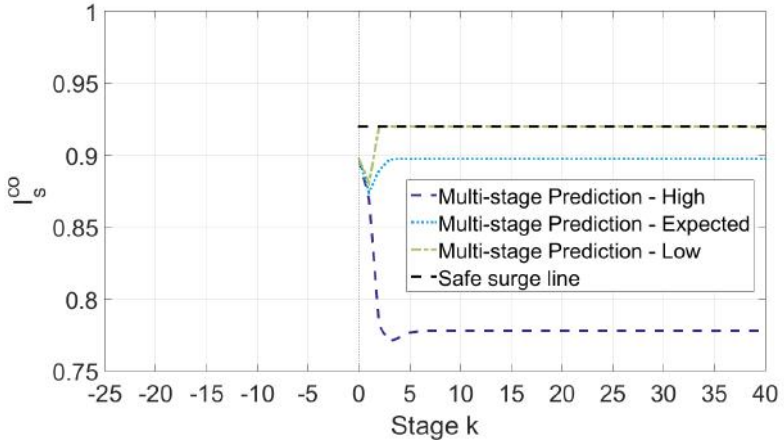

Figure 4.47: Predicted surge index (I_s^{co}) for the multi-stage NMPC at sampling time $t_k = 0$ seconds.

Surge index prediction trajectories can be seen in Figure 4.47. During the initial stages, surge index decreased for all uncertainty realizations and, consequently, safe

surge line constraint was inactive. However, as stages moved forward, constraint activation occurred only for the low uncertainty realization. Therefore, in order to satisfy the safe surge line constraint, a set-point of the pressure scrubber for low uncertainty realization was not reached.

In Figures 4.48 and 4.49, non-anticipative constraint as well as recycle valve opening and compressor rotation percentage optimal control sequences are shown. Analysing from the final stage to the first stage, multi-stage NMPC computed trajectories where the recycle valve stayed opened for the low uncertainty realization since a safe surge constraint violation was a concern for this particular scenario. For high and expected source pressures, recycle valve optimal control sequences were very similar, with full valve closure being considered. Despite having this similarity, the same cannot be said about compressor rotation percentage, as both high and expected uncertainty realization control sequences differ highly.

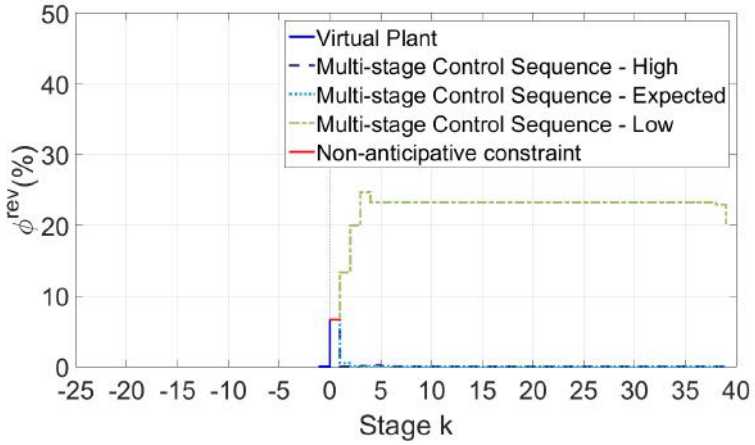

Figure 4.48: Optimal control sequences for the recycle valve opening (ϕ^{rev}) obtained by the multi-stage NMPC at sampling time $t_k = 0$ seconds.

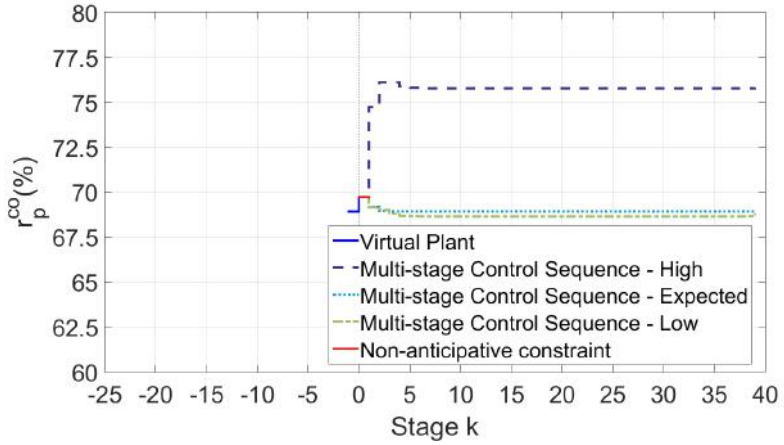

Figure 4.49: Optimal control sequences for the compressor rotation percentage (r_p^{co}) obtained by the multi-stage NMPC at sampling time $t_k = 0$ seconds.

Multi-stage NMPC prediction at sampling time $t_k = 11$ seconds is considered. One of the controller objectives is to reach pressure scrubber set-point. Figure 4.50 illustrate the open-loop trajectory obtained for each uncertainty realization. The scrubber pressure initial state is located below the desired set-point. From

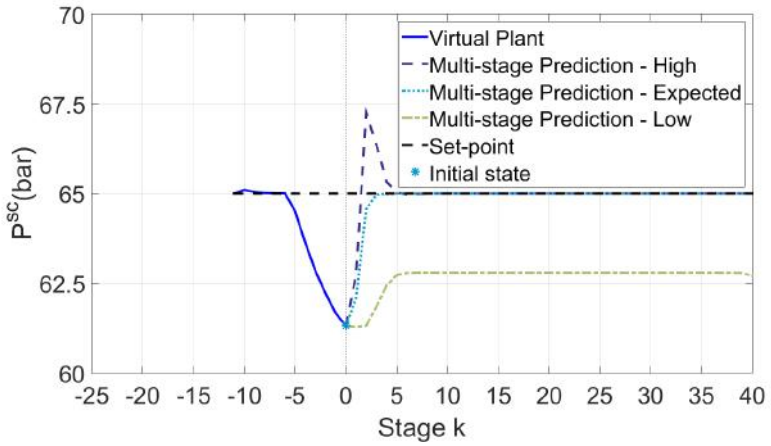

Figure 4.50: Predicted scrubber pressure (P^{sc}) for the multi-stage NMPC at sampling time $t_k = 11$ seconds.

the low uncertainty realization trajectory, there was a set-point offset that could not be reduced during the entire prediction horizon. In both high and expected uncertainty realization trajectories, set-point tracking objective was accomplished even if set-point deviation increased for high source pressure at the beginning of the predicted trajectory.

Multi-stage NMPC prediction trajectories are shown in Figure 4.51. All surge

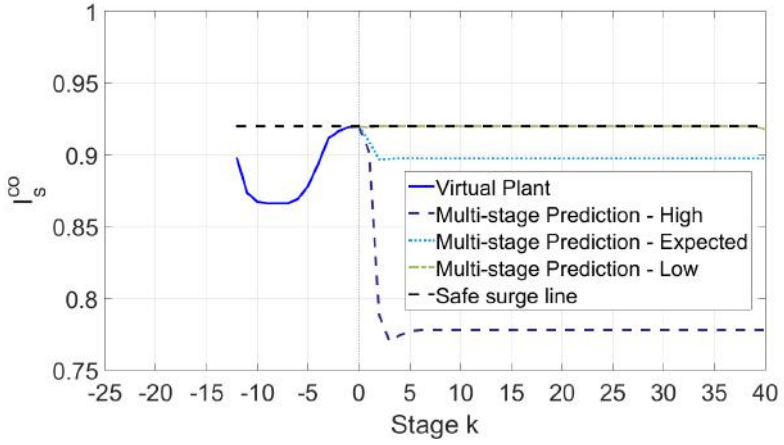

Figure 4.51: Predicted surge index (I_s^{co}) for the multi-stage NMPC at sampling time $t_k = 11$ seconds.

index trajectories started with the safe surge line constraint active. However, due to the decision making procedure, high and low uncertainty realization started to back-off from the constraint. As for the low uncertainty realization prediction, safe

surge constraint was kept active during the whole prediction horizon. Anti-surge valve optimal control sequences are shown in Figure 4.52, while compressor rotation percentage are present in Figure 4.53.

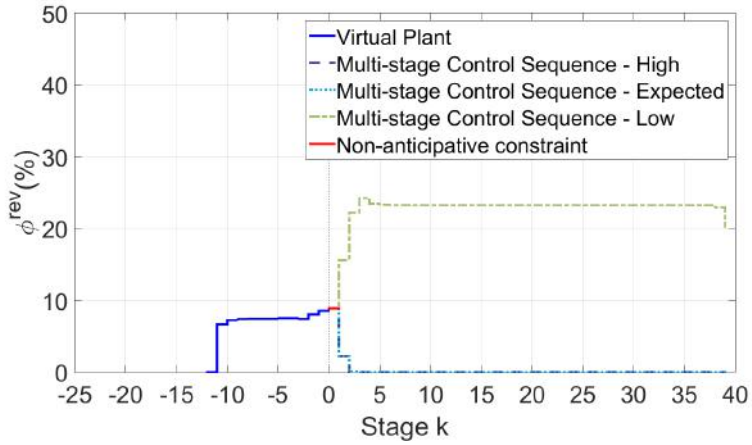

Figure 4.52: Optimal control sequences for the recycle valve opening (ϕ^{rev}) obtained by the multi-stage NMPC at sampling time $t_k = 11$ seconds.

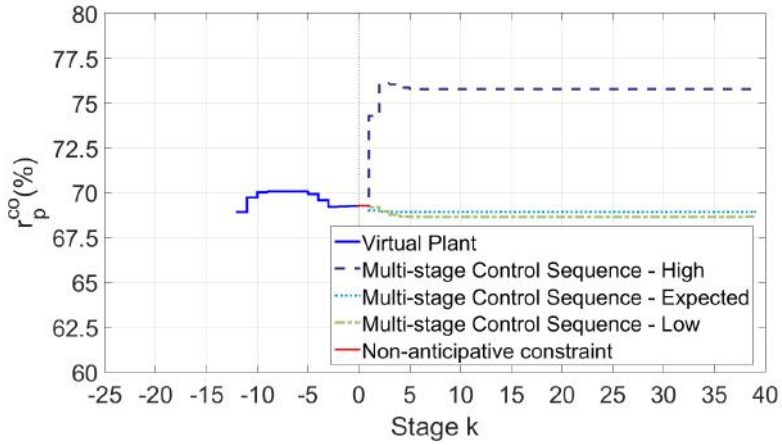

Figure 4.53: Optimal control sequences for the compressor rotation percentage (r_p^{co}) obtained by the multi-stage NMPC at sampling time $t_k = 11$ seconds.

At stage $k = 0$, non-anticipative constraint guarantees that the first control action will not lead to constraint violation considering all instances of uncertainty realizations. Therefore, the recycle valve must be opened due to a risk of constraint violation in the low uncertainty realization scenario. Thereafter, each multi-stage optimal control decision was chosen to accomplish their objectives. For the low uncertainty realization, recycle valve opening was increased, while compressor rotation percentage was slightly modified. In both high and expected uncertainty realizations, optimal control sequences showcased that recycle valve should be closed and maintained at this position after a few stages of the prediction horizon. As for the compressor rotation percentage, in order to accomplish each scenario objective,

multi-stage NMPC optimal control solution differs considerable for the high and expected uncertainty realizations.

Multi-stage NMPC prediction at sampling time $t_k = 23$ seconds is considered. From the scrubber pressure open-loop trajectories shown in Figure 4.54 it is possible to observe that the virtual plant current state is higher than the desired set-point. For both high and expected uncertainty realizations, predicted trajectories reached

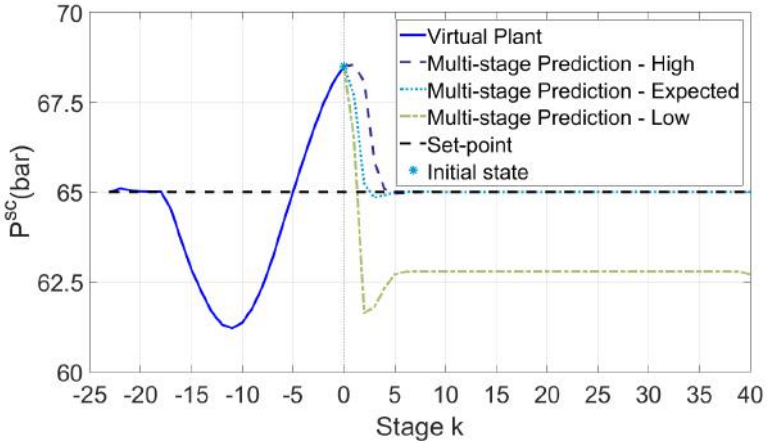

Figure 4.54: Predicted scrubber pressure (P^{sc}) for the multi-stage NMPC at sampling time $t_k = 23$ seconds.

the desired set-point after a few stages; whereas trajectory set-point was not achieved for the low uncertainty realization.

The surge index prediction is presented in Figure 4.55. Virtual plant surge index

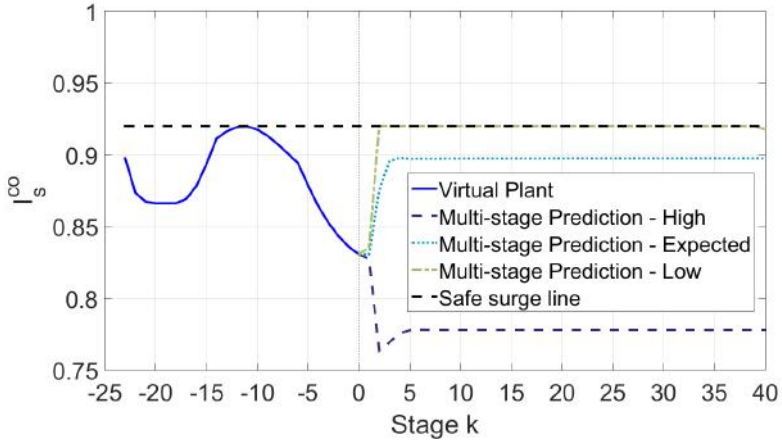

Figure 4.55: Predicted surge index (I_s^{co})for the multi-stage NMPC at sampling time $t_k = 23$ seconds.

trajectory shows that surge avoidance strategy has been successful in preventing safe surge line constraint violation. Also, current surge index evidenced how far the actual system is from constraint violation. At stage $k = 1$, a slight increase in the surge index for both low and expected uncertainty realizations occurred. On the

other hand, the surge index slightly decreased for high source pressure. Considering later stages of the prediction horizon, low uncertainty realization safe surge line was active, while this constraint remained inactive for both high and expected source pressure. For optimal control sequences of recycle valve opening and compressor rotation percentage, Figures 4.56 and 4.57 are referenced.

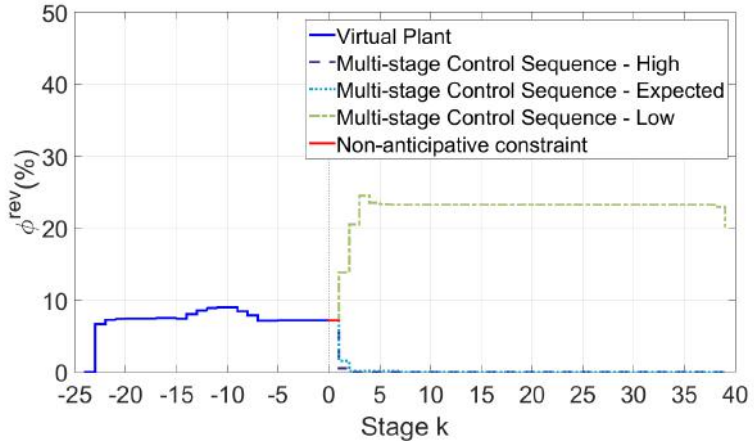

Figure 4.56: Optimal control sequences for the recycle valve opening (ϕ^{rev}) obtained by the multi-stage NMPC at sampling time $t_k = 23$ seconds.

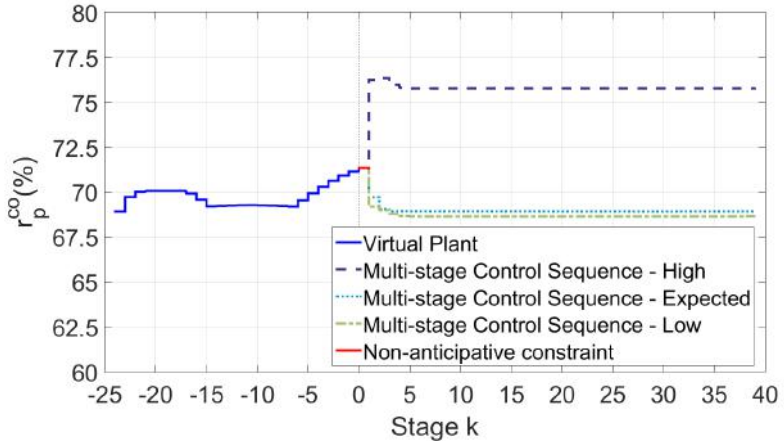

Figure 4.57: Optimal control sequences for the compressor rotation percentage (r_p^{co}) obtained by the multi-stage NMPC at sampling time $t_k = 23$ seconds.

The tendency for maintaining the recycle valve with the same opening value was confirmed by the control input at stage $k = 0$. Similarly to the other sampling times analysed previously, recycle valve was kept closed at later stages of high and expected uncertainty realizations. For the low value of source pressure, recycle valve was maintained opened for the entire optimal control sequence. Considering the compressor rotation percentage, the implemented control actions have been increasing from the moment the scrubber pressure values were higher than the desired set-point. This was an effort to reduce scrubber pressure as higher rotational speed

decreases compressor suction pressure. For later stages, optimal control sequences behaved differently, according to each scenario. Considering the high uncertainty realization optimal control sequence, compressor rotation percentage increased, which was necessary to achieve control objectives of the analysed scenario. As for expected and low uncertainty realizations, compressor rotation percentage was reduced with the intent to fulfil scenario objectives.

4.3.5 NMPC strategies evaluation

In order to estimate the closed-loop performance of deterministic, offline min-max and multi-stage NMPC, some performance indicators have been employed. The main aspects considered were set-point tracking, constraint violation, production, power consumption and efficient production. From the closed-loop simulations analysed, $t_f = 60$ seconds.

A performance indicator based on set-point tracking is defined. It was employed the integral square of the error as performance index to evaluate scrubber pressure set-point tracking. In Equation 4.25, the performance indicator is introduced.

$$ISE_p = \int_0^{t_f} \left(P^{sc}(t) - P_*^{sc}\right)^2 \, dt \tag{4.25}$$

where ISE_p is the integral square of the scrubber pressure error; t_f is the final time of simulation; P^{sc} is the scrubber pressure; and P_*^{sc} is the scrubber pressure set-point.

To evaluate if the controllers were capable of maintaining the closed-loop safe surge line constraint satisfied, the integral of the error between surge index and safe surge line was used. However, instead of considering the whole length of the simulation, this indicator only takes into account periods of time where constraint violation occurred. Values equal to 0 indicates that closed-loop safe surge line constraint was satisfied during the whole simulation. Whereas, positive values indicate that constraint violation occurred. Also, by using this index, the severity of constraint violation between controllers can be compared, with higher values indicating a worse performance. The integral of the surge index error can be seen in Equation 4.26.

$$IE_s = \int_0^{t_f} \theta\left(I_s(t) - \delta_{ssl}^{co}\right)\left(I_s(t) - \delta_{ssl}^{co}\right) \, dt \tag{4.26}$$

With the heaviside function given by Equation 4.27.

$$\theta\left(I_s(t) - \delta_{ssl}^{co}\right) = \begin{cases} 0 & I_s(t) < \delta_{ssl}^{co} \\ 1 & I_s(t) \geq \delta_{ssl}^{co} \end{cases} \tag{4.27}$$

where IE_s is the integral of the surge index error; I_s is the surge index; δ_{ssl}^{co} is the compressor safe surge margin; and $\theta(\cdot)$ is the heaviside step function.

Compression system production was evaluated in terms of a scaled mass flow, which calculates the amount of gas that passes through source valve over a time period divided by the steady state source mass flow considering a source pressure equal to its expected value of 75 bar. This index is introduced in Equation 4.28.

$$MFP = \frac{\frac{1}{t_f}\int_0^{t_f} m_{out}^{sov}(t)\,dt}{{}_{ss}m_{out}^{sov}} \tag{4.28}$$

where MFP is the mass flow production index; m_{out}^{sov} is the source valve outlet mass flow rate; and ${}_{ss}m_{out}^{sov}$ is the source valve outlet mass flow rate at steady state.

Compression system power consumption is an important matter when evaluating surge avoidance strategies. Therefore, a scaled index was considered comprising the work done by the compressor and heat rate exchanged by the cooler during a time period, which is divided by the steady-state compressor work and cooler removed heat rate.

$$CSPC = \frac{\frac{1}{t_f}\int_0^{t_f} \left[W^{co}(t) - Q^{hx}(t)\right] dt}{{}_{ss}W^{co} - {}_{ss}Q^{hx}} \tag{4.29}$$

where $CSPC$ is the compression system power consumption index; W^{co} is the compressor work; Q^{hx} is the cooler heat rate removed; ${}_{ss}W^{co}$ is the compressor work at steady state; and ${}_{ss}Q^{hx}$ is the cooler heat rate at steady state.

It was possible to evaluate how efficient system production was in relation with its energy consumption. To perform that, an indicator based on the ratio between MFP and $CSPC$ was used. Thus, efficient production index is introduced in Equation 4.30.

$$EP = \frac{MFP}{CSPC} \tag{4.30}$$

where EP is the efficient production index.

The results were summarised in Table 4.3, where performance indicators ISE_p, CV, MFP, CSPC and EP are shown for each NMPC strategy employed. From

Table 4.3: Performance indicators of the closed-loop system controlled by different NMPC strategies.

NMPC	ISE_p ($\text{bar}^2 s$)	IE_s	MFP	CSPC	EP
Deterministic	362.31	0.6225	0.9937	1.0161	0.9779
Offline min-max	709.48	0	0.8997	1.0594	0.8493
Multi-stage	363.93	0	0.9911	1.0854	0.9131

the scrubber pressure set-point performance, *i.e.* ISE_p, offline min-max NMPC has obtained the worst performance regarding set-point control objective. It was

seen previously from offline min-max open loop results that surge line constraint was always becoming active, independently of virtual plant uncertainty realization. Therefore, the main concern of offline min-max NMPC was to avoid constraint violation, which had a great impact in its set-point tracking performance. Deterministic and multi-stage NMPC had a similar ISE_p score with deterministic being slightly better.

Violation of safe surge line may be dangerous for operation, as the exact location where surge phenomena occurs is inaccurate. Changes in gas properties such as compressibility factor, molecular weight and/or heat ratio, or operational conditions like compressor inlet pressure and temperature may affect surge detection. Considering closed-loop simulation results, safe surge line violation only occurred during deterministic NMPC simulation as it can be seen by IE_s index. For the other controllers, *i.e.* offline min-max and multi-stage, safe surge line constraint has been satisfied during the whole simulation.

The compression system was designed to operate with a certain production or mass flow rate of gas. The MFP index compares production of each closed-loop trajectory with the designed one. Therefore, the closer it is to 1.0, the more similar production is with the designed value. Deterministic NMPC showed the highest MFP value, with a 0.63% loss of production, followed by multi-stage NMPC and offline min-max NMPC with a 0.89% and 1.03% loss of production, respectively.

CSPC index is related with power used for cooling and compression. In a compression system, the combination of a high compressor rotation with recycle valve usage has a great influence in energy consumption. From closed-loop simulation results, one may observe that multi-stage NMPC operated with higher values of nominal rotation manipulation when compared with other controllers. Also, by operating with an open recycle valve, recycled gas had to be cooled and boosted again. Due to these factors, multi-stage NMPC obtained the highest score of CSPC, spending 8.54 % more energy than designed operation. Offline min-max NMPC operates with a high value of recycle opening when compared with other controllers. However, when the same comparison is made regarding compressor rotation, offline min-max NMPC operated with the lowest value of compressor rotation. Therefore, it has expended 5.94% more energy than designed operation. The most economical in terms of power usage was the deterministic NMPC by expending 1.61% more energy than normal operation. This was due to the lack of recycle valve usage in comparison with other controllers. However, this behaviour led the closed-loop system to violate safe surge line constraint, which is a huge drawback.

The EP index is based on a ratio between MFP and CSPC. Therefore, it shows the mass production per system power consumption. A value o 1.0 for this indicator means that the relation between production and energy consumption is equal to

the designed compressor system, while lower values translates to a less efficient operation. Offline min-max closed-loop operation has attained the worst value with a decrease of 15.07% of EP in relation with the designed operation. This shows that, despite consuming less energy than multi-stage NMPC during operation, offline min-max NMPC has a worst performance when production is also taken into account. Therefore, multi-stage NMPC can be considered less conservative than offline min-max NMPC. When comparing EP index for the multi-stage NMPC and deterministic NMPC strategies, one may notice that multi-stage has an indicator which is 8.69% lower than designed operation, while deterministic attained a score of 2.21% lower than normal operation. Thus, deterministic NMPC can be considered a better solution. However, it is important to point out that this mark was only achieved in the expense of constraint violation. This in turn, shows that there exist a cost associated with robustness that must be paid to guarantee constraint satisfaction.

Chapter 5

Conclusions

In the present work, three NMPC strategies were implemented successfully in CasADi Matlab front-end to control a subsea compression system while accomplishing surge avoidance and set-point tracking. Due to measurement issues present in a subsea operation, disturbance was considered unknown. Indicators were developed and used to assess important aspects of closed-loop operation, which made possible to compare the performance of different control strategies.

Deterministic NMPC had the best results regarding set-point tracking objective and operational efficiency. However, constraint violation occurred during closed-loop simulations. This indicates the lack of robustness regarding constraints handling by deterministic NMPC strategy. For subsea systems, constraint robustness is a major aspect to consider when designing controllers specifically suited to operate in such environment, as constraint violation may lead to operation degradation, equipment failures or other catastrophic situation.

In the extreme opposite is offline min-max NMPC that showed the necessary capabilities to handle closed-loop constraint satisfaction. However, the cost of robustness was quite high as this solution decreased system efficiency by 15.07%, which is 6.82 times worst than deterministic NMPC with a decrease of 2.21% in efficiency. With the development of new greenfields in extreme locations and conditions, as well as brownfield revitalization, operational costs is a major concern. An inefficient operation may compromise a new field viability or a revitalization project.

Closed-loop system under multi-stage NMPC control did not violate any hard constraint during operation. This shows that, as offline min-max NMPC, Multi-stage strategy has the same advantage regarding constraint handling capabilities. However, closed-loop robustness has a cost associated with performance and computational burden. Multi-stage NMPC proved to be a less conservative solution, which is an improvement compared with offline min-max NMPC. As expected from a robust approach, the 8,69% decrease in performance for multi-stage NMPC was still 3.93 times worse than the 2,21% obtained from deterministic NMPC approach.

Chapter 6

Recommendation for Future Research

Multi-stage NMPC is a recent technology that has not been fully explored. Therefore, suggestions of future work are made bellow:

Likelihood of scenarios could be updated on-line. To do that, data acquired through plant measurement could be used to estimate likelihood weights, which would have an impact in scenario importance and improved closed-loop performance.

Asymptotically stability of multi-stage NMPC could be explored with newly developed ingredients or by adapting the ones that have been already used for nominal NMPC stability. Contribution for asymptotically stability under uncertainty may be found in GONÇALVES (2017).

Computational effort is an issue that needs to be solved. The time necessary to obtain a solution for multi-stage optimal control problem increases exponentially with the number of uncertainty realizations. This, in turn, limits implementation of this technology for bigger systems. A contribution for this area can be found in KRISHNAMOORTHY *et al.* (2018).

It is possible that deterministic NMPC could be more costly Measurement of compressor's degradation would provide valuable performance information as deterministic NMPC could potentially increase the risk of breakage. In this scenario, emergence maintenance would be needed and the cost associated with this strategy would increase. Therefore, development of tools to evaluate the impact of multi-stage NMPC in compressor's degradation considering a long term horizon should be investigated.

Bibliography

ALBUSAIDI, W., PILIDIS, P., 2015, "An iterative method to derive the equivalent centrifugal compressor performance at various operating conditions: Part I: Modelling of suction parameters impact", *Energies*, v. 8, n. 8, pp. 8497–8515. ISSN: 19961073. doi: 10.3390/en8088497.

ALLGÖWER, F., FINDEISEN, R., NAGY, Z. K., 2004, "Nonlinear model predictive control: From theory to application", *Journal of the Chinese Institute of Chemical Engineers*, v. 35, n. 3, pp. 299–315. ISSN: 03681653. Available at: <http://www.scopus.com/inward/record.url?eid=2-s2.0-3543101406{&}partnerID=tZOtx3y1>.

ANDERSSON, J., ÅKESSON, J., DIEHL, M., 2012, "CasADi: A symbolic package for automatic differentiation and optimal control". In: *Lecture Notes in Computational Science and Engineering*, v. 87 LNCSE, pp. 297–307. ISBN: 9783642300226. doi: 10.1007/978-3-642-30023-3_27.

AUSTRHEIM, T., 2006, *Experimental Characterization of High-Pressure Natural Gas Scrubbers*. Tese de Doutorado, University of Bergen.

BECKMAN, J., 2015, "Subsea compression prolongs gas production at Åsgard offshore Norway", *Offshore*, p. 1. Available at: <https://www.offshore-mag.com/articles/print/volume-75/issue-12/top-5-projects/subsea-compression-prolongs-gas-production-at-asgard-offshore-norway.html>.

BEMPORAD, A., 2006, "Model Predictive Control Design: New Trends and Tools", *Proceedings of the 45th IEEE Conference on Decision and Control*, , n. 1, pp. 6678–6683. ISSN: 0191-2216. doi: 10.1109/CDC.2006.377490. Available at: <http://ieeexplore.ieee.org/document/4178103/>.

BEN-TAL, A., NEMIROVSKI, A., 1999, "Robust solutions of uncertain linear programs", *Operations Research Letters*, v. 25, n. 1, pp. 1–13. ISSN: 01676377. doi: 10.1016/S0167-6377(99)00016-4.

BERTSIMAS, D., SIM, M., 2004, "The Price of Robustness", *Operations Research*, v. 52, n. 1, pp. 35–53. ISSN: 0030-364X. doi: 10.1287/opre.1030.0065. Available at: <http://pubsonline.informs.org/doi/abs/10.1287/opre.1030.0065>.

BIEGLER, L. T., 2012, *Nonlinear programming:concepts,algorithms,and applications to chemical processes*, v. XXXIII. ISBN: 9780874216561. doi: 10.1007/s13398-014-0173-7.2. Available at: <http://www.ncbi.nlm.nih.gov/pubmed/15003161{%}5Cnhttp://cid.oxfordjournals.org/lookup/doi/10.1093/cid/cir991{%}5Cnhttp://www.scielo.cl/pdf/udecada/v15n26/art06.pdf{%}5Cnhttp://www.scopus.com/inward/record.url?eid=2-s2.0-84861150233{&}partnerID=tZOtx3y1>.

BINDLISH, R., 2015, "Nonlinear model predictive control of an industrial polymerization process", *Computers & Chemical Engineering*, v. 73, pp. 43–48. ISSN: 00981354. doi: 10.1016/j.compchemeng.2014.11.001. Available at: <http://www.sciencedirect.com/science/article/pii/S0098135414003056>.

BITMEAD, R. R., GEVERS, M., WERTZ, V., et al., 1990, *Adaptive optimal control - The thinking's man GPC*. N. January. ISBN: 0130132772. doi: 10.1016/0005-1098(93)90079-9.

BOINOV, K. O., LOMONOVA, E. A., VANDENPUT, A. J. A., et al., 2006, "Surge control of the electrically driven centrifugal compressor", *IEEE Transactions on Industry Applications*, v. 42, n. 6, pp. 1523–1531. ISSN: 00939994. doi: 10.1109/TIA.2006.882683.

BUDINIS, S., THORNHILL, N. F., 2016, "Supercritical fluid recycle for surge control of CO2 centrifugal compressors", *Computers and Chemical Engineering*, v. 91, pp. 329–342. ISSN: 00981354. doi: 10.1016/j.compchemeng.2016.03.012. Available at: <http://dx.doi.org/10.1016/j.compchemeng.2016.03.012>.

CAMACHO, E. F., BORDONS, C., 2007, "Nonlinear Model Predictive Control: An Introductory Review". In: *Assessment and Future Directions of Nonlinear Model Predictive Control*, v. 358, pp. 1–16. ISBN: 978-3-540-72698-2. doi: 10.1007/978-3-540-72699-9_1. Available at: <http://www.springerlink.com/content/q76n6x44r7327218>.

CHISCI, L., LOMBARDI, A., MOSCA, E., 1996, "Dual-receding horizon control of constrained discrete time systems", *European Journal of Control*, v. 2, n. 4, pp. 278–285. ISSN: 09473580. doi: 10.1016/S0947-3580(96)70052-3.

DARLINGTON, J., PANTELIDES, C. C., RUSTEM, B., et al., 2000, "Decreasing the sensitivity of open-loop optimal solutions in decision making under uncertainty", *European Journal of Operational Research*, v. 121, n. 2, pp. 343–362. ISSN: 03772217. doi: 10.1016/S0377-2217(99)00034-X.

DETTWYLER, M., BÜCHE, D., BAUMANN, U., 2016, "Subsea Compression – Current Technology and its Use to Maximize Late Life Production", *45th Turbomachinery & 32nd Pump Symposia*, pp. 1–17. doi: https://doi.org/10.21423/R1Z593. Available at: <http://hdl.handle.net/1969.1/159799>.

EDGAR, T. F., SMITH, C. L., SHINSKEY, F. G., et al., 2008, *Process Control*. ISBN: 0071542159. doi: 10.1036/0071511318.

EPSTEIN, A. H., FFOWCS WILLIAMS, J. E., GREITZER, E. M., 1989, "Active suppression of aerodynamic instabilities in turbomachines", *Journal of Propulsion and Power*. ISSN: 0748-4658. doi: 10.2514/3.23137.

EVEKER, K. M., NETT, C. N., 1993, "Control of Compression System Surge and Rotating Stall: A Laboratory-Based "Hands-On" Introduction", *1993 American Control Conference*.

FANAILOO, P., ANDREASSEN, G., 2008, "Improving Reliability and Reducing Intervention Costs of Ultradeep Subsea Technology at the Design Stage". In: *Offshore Technology Conference*, pp. 1–9. Offshore Technology Conference, apr. doi: 10.4043/19539-MS. Available at: <http://www.onepetro.org/doi/10.4043/19539-MS>.

FERGUSON, T., 1963, *The centrifugal compressor stage*. London : Butterworths. doi: https://doi.org/10.1017/S0001924000061431. Available at: <http://books.google.com/books?id=k{_}JSAAAAMAAJ.>.

GILARRANZ R., J. L., KIDD, H. A., CHOCHUA, G., et al., 2010, "An Approach to Compact, Wet Gas Compression". In: *Volume 5: Industrial and Cogeneration; Microturbines and Small Turbomachinery; Oil and Gas Applications; Wind Turbine Technology*, pp. 765–776. ASME. ISBN: 978-0-7918-4400-7. doi: 10.1115/GT2010-23447. Available at: <http://proceedings.asmedigitalcollection.asme.org/proceeding.aspx?articleid=1609263>.

GONÇALVES, G. A. D. A., 2017, *On-line process model update in discrete-time predictive controllers: a Robust approach*. Tese de Doutorado, Universidade Federal do Rio de Janeiro.

GRAVDAHL, J. T., EGELAND, O., 1999a, "Centrifugal compressor surge and speed control", *IEEE Transactions on Control Systems Technology*, v. 7, n. 5, pp. 567–579. ISSN: 10636536. doi: 10.1109/87.784420.

GRAVDAHL, J. T., EGELAND, O., 1999b, *Compressor Surge and Rotating Stall*. Advances in Industrial Control. London, Springer London. ISBN: 978-1-4471-1211-2. doi: 10.1007/978-1-4471-0827-6. Available at: <http://scholar.google.com/scholar?hl=en{&}btnG=Search{&}q=intitle:Advances+in+Industrial+Control{#}0http://link.springer.com/10.1007/978-1-4471-0827-6>.

GRAVDAHL, J. T., EGELAND, O., VATLAND, S. O., 2002, "Drive torque actuation in active surge control of centrifugal compressors", *Automatica*, v. 38, n. 11, pp. 1881–1893. ISSN: 00051098. doi: 10.1016/S0005-1098(02)00113-9.

GREITZER, E. M., 1980, "Review - Axial compressor stall phenomena", *Journal of Fluids Engineering*, v. 102, n. 2, pp. 134–151. ISSN: 00982202. doi: 10.1115/1.3240634.

GREITZER, E. M., 1976, "Surge and Rotating Stall in Axial Flow Compressors—Part I: Theoretical Compression System Model", *Journal of Engineering for Power*, v. 98, n. 2, pp. 190. ISSN: 00220825. doi: 10.1115/1.3446138.

GRÜNE, L., PANNEK, J., 2011, *Nonlinear Model Predictive Control*, v. 152. ISBN: 9783319460239. doi: 10.1007/978-0-85729-501-9_3. Available at: <http://digital-library.theiet.org/content/journals/10.1049/ip-cta{_}20059060{%}0Ahttp://link.springer.com/10.1007/978-0-85729-501-9{_}3>.

HAHEIM, S., GAILLARD, X., 2009, "A Simplified Subsea Separation and Pumping System". In: *SPE Annual Technical Conference and Exhibition*, n. October, pp. 4–7. Society of Petroleum Engineers, apr. ISBN: 9781555632632. doi: 10.2118/124560-MS. Available at: <http://www.onepetro.org/mslib/app/Preview.do?paperNumber=SPE-124560-MS{&}societyCode=SPEhttp://www.onepetro.org/doi/10.2118/124560-MS>.

HANSEN, K. E., JØRGENSEN, P., LARSEN, P. S., 1981, "Experimental and Theoretical Study of Surge in a Small Centrifugal Compressor", *Journal of Fluids Engineering*, v. 103, n. 3, pp. 391–395. ISSN: 0098-2202.

doi: 10.1115/1.3240796. Available at: <http://dx.doi.org/10.1115/1.3240796>.

HENSON, M. A., 1998, "Nonlinear model predictive control: current status and future directions", *Computers & Chemical Engineering*, v. 23, n. 2, pp. 187–202. ISSN: 00981354. doi: 10.1016/S0098-1354(98)00260-9. Available at: <http://linkinghub.elsevier.com/retrieve/pii/S0098135498002609>.

ISA, 2007, *Flow Equations for Sizing Control Valves*, v. ISA-75.01. International Society for Automation. ISBN: 0876648995. Available at: <https://www.isa.org/pdfs/microsites121/isa-750101-spbd/>.

JOHANSEN, T. A., 2011, "Introduction to nonlinear model predictive control and moving horizon estimation", *... Topics on Constrained and Nonlinear Control*, , n. 1, pp. 1–53. Available at: <https://iam.chtf.stuba.sk/{~}fikar/nil11/nil-tbook-p.pdf{#}page=201>.

KEERTHI, S. S., GILBERT, E. G., 1988, "Optimal infinite-horizon feedback laws for a general class of constrained discrete-time systems: Stability and moving-horizon approximations", *Journal of Optimization Theory and Applications*, v. 57, n. 2, pp. 265–293. ISSN: 00223239. doi: 10.1007/BF00938540.

KLEYNHANS, G., BRENNE, L., KIBSGAARD, S., et al., 2016, "Development and Qualification of a Subsea Compressor", *Offshore Technology Conference*. ISSN: 01603663. doi: 10.4043/27160-MS. Available at: <http://www.onepetro.org/doi/10.4043/27160-MS>.

KONDAPI, P. B., CHIN, D., SRIVASTAVA, A., et al., 2017, "How Will Subsea Processing and Pumping Technologies Enable Future Deepwater Field Developments?" *Offshore Techonolgy coference*. ISSN: 01603663.

KRISHNAMOORTHY, D., FOSS, B., SKOGESTAD, S., 2016, "Real-Time Optimization under Uncertainty Applied to a Gas Lifted Well Network", *Processes*, v. 4, n. 4, pp. 52. ISSN: 2227-9717. doi: 10.3390/pr4040052. Available at: <http://www.mdpi.com/2227-9717/4/4/52>.

KRISHNAMOORTHY, D., SUWARTADI, E., FOSS, B., et al., 2018, "Improving Scenario Decomposition for Multistage MPC Using a Sensitivity-Based Path-Following Algorithm", *IEEE Control Systems Letters*, v. 2, n. 4, pp. 581–586. ISSN: 2475-1456. doi: 10.1109/LCSYS.2018.2845108. Available at: <https://ieeexplore.ieee.org/document/8374815/>.

LEE, E. B., MARKUS, L., 1968, *{F}oundations of {O}ptimal {C}ontrol {T}heory*. New York, John Wiley & Sons, Ltd.

LI, Z., OLSON, M., RAYACHOTI, V., et al., 2014, "Subsea Compact Separation: Control System Design". In: *Offshore Technology Conference*, n. May, pp. 5–8. Offshore Technology Conference, may. ISBN: 9781632665287. doi: 10.4043/25299-MS. Available at: <http://www.onepetro.org/doi/10.4043/25299-MS>.

LUCIA, S., FINKLER, T., ENGELL, S., 2013, "Multi-stage nonlinear model predictive control applied to a semi-batch polymerization reactor under uncertainty", *Journal of Process Control*, v. 23, n. 9, pp. 1306–1319. ISSN: 09591524. doi: 10.1016/j.jprocont.2013.08.008. Available at: <http://dx.doi.org/10.1016/j.jprocont.2013.08.008>.

LUCIA, S., ANDERSSON, J. A., BRANDT, H., et al., 2014a, "Handling uncertainty in economic nonlinear model predictive control: A comparative case study", *Journal of Process Control*, v. 24, n. 8, pp. 1247–1259. ISSN: 09591524. doi: 10.1016/j.jprocont.2014.05.008. Available at: <http://dx.doi.org/10.1016/j.jprocont.2014.05.008>.

LUCIA, S., PAULEN, R., ENGELL, S., 2014b, "Multi-stage Nonlinear Model Predictive Control with verified robust constraint satisfaction". In: *53rd IEEE Conference on Decision and Control*, v. 23, pp. 2816–2821. IEEE, decb. ISBN: 978-1-4673-6090-6. doi: 10.1109/CDC.2014.7039821. Available at: <http://ieeexplore.ieee.org/document/7039821/>.

MACDOUGAL, I., ELDER, R. L., 1983, "Simulation of centrifugal compressor transient performance for process plant applications", *Journal of Engineering for Power OCTOBER*, v. 105, n. October 1983, pp. 885.

MARRUEDO, D., ALAMO, T., CAMACHO, E., 2002, "Input-to-state stable MPC for constrained discrete-time nonlinear systems with bounded additive uncertainties", *Proceedings of the 41st IEEE Conference on Decision and Control, 2002.*, v. 4, n. December, pp. 4619–4624. ISSN: 0191-2216. doi: 10.1109/CDC.2002.1185106. Available at: <http://ieeexplore.ieee.org/document/1185106/>.

MAYNE, D. Q., RAWLINGS, J., 2000, "Constrained model predictive control: stability and optimality", *Automatica*, v. 36, n. 6, pp. 789–814.

MAYNE, D. Q., 2014, "Model predictive control: Recent developments and future promise", *Automatica*, v. 50, n. 12, pp. 2967–2986. ISSN: 00051098. doi:

10.1016/j.automatica.2014.10.128. Available at: <http://dx.doi.org/10.1016/j.automatica.2014.10.128>.

MAYNE, D., MICHALSKA, H., 1990, "Receding horizon control of nonlinear systems", *IEEE Transactions on Automatic Control*, v. 35, n. 7, pp. 814 – 824. ISSN: 0018-9286. doi: 10.1109/9.57020.

MICHALSKA, H., MAYNE, D. Q., 1993, "Robust Receding Horizon Control of Constrained Nonlinear-Systems", *Ieee Transactions on Automatic Control*, v. 38, n. 11, pp. 1623–1633. ISSN: 0018-9286. doi: Doi10.1109/9.262032.

MORARI, M., H. LEE, J., 1999, "Model predictive control: past, present and future", *Computers & Chemical Engineering*, v. 23, n. 4, pp. 667–682. ISSN: 00981354. doi: 10.1016/S0098-1354(98)00301-9.

PLUCENIO, A., VETTORAZZO, C., CAMPOS, M., et al., 2016a, "ADVANCED CONTROL APPLIED TO A GAS COMPRESSION STATION OF A PRODUCTION PLATFORM", *CBA*, , n. October.

PLUCENIO, A., VETTORAZZO, C., PICON YANG, B. B., et al., 2016b, "Modeling and Control of an Oil Platform Gas Compression Station", *Cba*, , n. 2, pp. 304–307.

PLUYMERS, B., LUDLAGE, J., ARIAANS, L., et al., 2008, "An industrial implementation of a generic NMPC controller with application to a batch process". In: *IFAC Proceedings Volumes (IFAC-PapersOnline)*, v. 17. ISBN: 9783902661005. doi: 10.3182/20080706-5-KR-1001.3842.

QIN, S. J., BADGWELL, T. A., 1997, "An overview of industrial model predictive control technology", *Automatica*, v. 93, n. 316, pp. 232–256. doi: 10.1.1.52.8909. Available at: <http://citeseerx.ist.psu.edu/viewdoc/summary?doi=10.1.1.52.8909>.

QIN, S. J., BADGWELL, T. A., 2000, "An Overview of Nonlinear Model Predictive Control Applications". In: *Nonlinear Model Predictive Control*, Birkhäuser Basel, pp. 369–392, Basel. ISBN: 3-7643-6297-9. doi: 10.1007/978-3-0348-8407-5_21. Available at: <http://link.springer.com/10.1007/978-3-0348-8407-5{_}21>.

RAWLINGS, J. B., MAYNE, D. Q., 2015, *Model Predictive Control: Theory and Design*. ISBN: 9780975937709. doi: 10.1109/TBME.2009.2039571.

RAWLINGS, J., MEADOWS, E., MUSKE, K., 1994, "Nonlinear Model Predictive Control: A Tutorial and Survey", *IFAC Proceedings Volumes*, v. 27, n. 2,

pp. 185–197. ISSN: 14746670. doi: 10.1016/S1474-6670(17)48151-1. Available at: <http://dx.doi.org/10.1016/S1474-6670(17)48151-1http://linkinghub.elsevier.com/retrieve/pii/S1474667017481511>.

SCHULTZ, J. M., 1962, "The Polytropic Analysis of Centrifugal", *Journal of Engineering for Power*, v. 84, n. 1, pp. 69–82. ISSN: 00220825. doi: 10.1115/1.3673381.

SCOKAERT, P. O. M., MAYNE, D. Q., RAWLINGS, J. B., 1999, "Suboptimal model predictive control (feasibility implies stability)", *IEEE Transactions on Automatic Control*, v. 44, n. 3, pp. 648–654. ISSN: 00189286. doi: 10.1109/9.751369.

SCOKAERT, P., MAYNE, D., 1998, "Min-max feedback model predictive control for constrained linear systems", *IEEE Transactions on Automatic Control*, v. 43, n. 8, pp. 1136–1142. ISSN: 00189286. doi: 10.1109/9.704989. Available at: <http://ieeexplore.ieee.org/document/704989/>.

SPANGELO, I., EGELAND, O., 1994, "Trajectory Planning and Collision Avoidance for Underwater Vehicles Using Optimal Control", *IEEE Journal of Oceanic Engineering*, v. 19, n. 4, pp. 502–511. ISSN: 15581691. doi: 10.1109/48.338386.

STORSTENVIK, A., 2016, "Subsea Compression - Designing and Building a Subsea Compressor Station". In: *Offshore Technology Conference*. Offshore Technology Conference, may. ISBN: 9781510824294. doi: 10.4043/27197-MS. Available at: <http://www.onepetro.org/doi/10.4043/27197-MS>.

THOMAZ, D. M., 2017, *Estratégia de controle preditivo multivariável para um sistema de compressão de gás de plataforma do pré-sal*. Tese de Doutorado, Universidade Federal do Rio de Janeiro.

TOMASGARD, A., SU, Z., EGGING, R., et al., 2016, *A multi-stage multi-horizon stochastic equilibrium model of multi-fuel energy markets*. ISBN: 9788293198154.

TØNNESSEN, L. A., KONGSBERG, F. M. C., AS, S., et al., 2017, "Future Subsea Compression", .

UDDIN, N., GRAVDAHL, J. T., 2012a, "Introducing back-up to active compressor surge control system", *IFAC Proceedings Volumes (IFAC-PapersOnline)*, v. 1, n. PART 1, pp. 263–268. ISSN: 14746670. doi: 10.3182/20120531-2-NO-4020.00053.

UDDIN, N., GRAVDAHL, J. T., 2012b, "A Compressor Surge Control System: Combination Active Surge Control System and Surge Avoidance System", *ISUAAAT Scientific Committee with JSASS Publication*. doi: https://doi.org/10.3182/20120531-2-NO-4020.00053.

VADA, J., SLUPPHAUG, O., FOSS, B. A., 1999, "Infeasibility handling in linear MPC subject to prioritized constraints", *IFAC Proceedings Volumes*, v. 32, n. 2 (jul), pp. 6763–6768. ISSN: 14746670. doi: 10.1016/S1474-6670(17)57155-4. Available at: <http://www.itk.ntnu.no/databaser/artikler/vedlegg/189{_}pdf.pdfhttp://linkinghub.elsevier.com/retrieve/pii/S1474667017571554>.

VERHEYLEWEGHEN, A., JÄSCHKE, J., 2016, "Health-aware operation of subsea gas compression system under uncertainty", *NTNU publication*.

VINTERSTØ, T., BIRKELAND, B., RAMBERG, R. M., et al., 2016, "Subsea Compression – Project Overview", *Offshore Technology Conference*, , n. May, pp. 2–5. ISSN: 01603663.

WU, X., BABATOLA, F., JIANG, L., et al., 2016, "Applying Subsea Fluid-Processing Technologies for Deepwater Operations", *Oil and Gas Facilities*, v. 5, n. 04, pp. 1–10. ISSN: 2224-4514. doi: 10.2118/181749-PA. Available at: <http://www.onepetro.org/doi/10.2118/181749-PA>.

YOON, S. Y., LIN, Z., ALLAIRE, P. E., 2013, *Control of Surge in Centrifugal Compressors by Active Magnetic Bearings*. ISBN: 978-1-4471-4239-3. doi: 10.1007/978-1-4471-4240-9. Available at: <http://link.springer.com/10.1007/978-1-4471-4240-9>.

ZHENG, A., MORARI, M., 1995, "Stability of model predictive control with mixed constraints", *Automatic Control, IEEE Transactions on*, v. 40, n. 10, pp. 1818–1823. ISSN: 0018-9286. Available at: <http://ieeexplore.ieee.org/xpls/abs{_}all.jsp?arnumber=467664>.